INTERFEROMETRIC STUDIES ON THE GROWTH FEATURES OF QUARTZ CRYSTALS.

Thesis submitted to the
University of London
for the Degree of
Doctor of Philosophy

by

B. T. M. Willis

March 1952

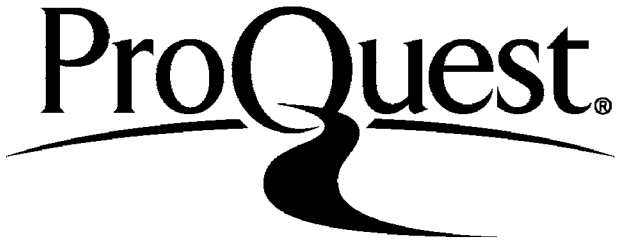

ABSTRACT.

Multiple-beam interferometry has been applied to the study of the surface topography of natural and synthetic quartz crystals. It is shown that the principal habit faces (major rhombohedron R, minor rhombohedron r, and prism m) consist of a number of 'growth pyramids', which are produced by the spreading of multimolecular growth sheets in succession from several initiating centres.

A description is given of the properties of these sheets (height, edge structure etc.) on the R faces, and of the vicinal faces constituting the sides of the growth pyramids. There are two respects in which the vicinal faces depart from the condition of being strictly plane. - They possess a cylindrical curvature with a radius of several metres, and their inclination to the close-packed plane increases towards the summit of the growth pyramid. From the interpretation of the results the mechanism of growth of the R faces is determined, and estimates are obtained of the mean distance of diffusion of adsorbed molecules and of the size of the theoretical two-dimensional nucleus.

The general features of the minor rhombohedral faces are similar to those of the R faces. Differences arise due to the greater irregularity of the growth fronts of the r faces, and this is probably connected with their greater rate of spreading.

The topography of natural prism faces is briefly described, and the origin of the striations on these faces discussed.

Two types of synthetic crystal have been studied; seeds with a thin layer (order of one wavelength) of synthetic growth, and crystals with a cm. or more of synthetic growth. The observations on these crystals indicate that growth initially takes place from a large number of growth nuclei, of the order of 10^4/sq.cm.; but that as growth proceeds, most of these nuclei becoms inactive and ultimately growth takes place from relatively few dominant centres.

Evidence is given for the existence of screw dislocations in quartz; and from the observations on natural and synthetic crystals it is concluded that fresh sheets are initiated by screw dislocations, by the re-entrant angles associated with twinned faces and, possibly, by foreign particles.

C O N T E N T S

Chapter I.

THE STUDY OF CRYSTAL SURFACES.

THE study of crystal growth has in recent years become important in both theoretical and experimental physics, and has been stimulated by the need for growing high quality synthetic crystals (e.g. quartz) of economic importance. Information concerning the way in which crystals grow can be obtained by studying crystal surfaces. In the words of Rowland, concluding the 1949 Faraday Society Discussion on "Crystal Growth": "... the theoretical physicist will only have a chance of getting to grips with the problem [of crystal growth] when the experimentalist has revealed what its essentials are. It is suggested that the best line of approach is to begin with a systematic study of crystal surfaces."

The aim of the work to be described in this thesis was, to study the surfaces of natural and synthetic quartz crystals, with a view to determining the mechanism and conditions of growth. Before describing the experimental techniques and the results, past work on the study of crystal surfaces will be reviewed.

With the development of the reflecting goniometer

by Wollaston, Mitscherlich, and others, it was realised that crystal surfaces only approximately obey the law of simple rational indices. From one crystal to another of the same substance small variations of interfacial angle were found to occur, and these variations even occurred between faces yielding single, sharp signals in the goniometer. Pfaff(1) made a carfeul investigation of the interfacial angles of several cubic crystals, and compared them with the theoretical angles, calculated by assuming the law of rational indices. He found that the observed angles differed from the theoretical angles by one minute to thirty minutes of arc. Similar results were obtained by Brauns(2) on octahedra of lead nitrate. Brauns attempted to explain his results on the basis of the distorting effect of gravity during the crystallisation process. The main conclusion to be drawn from the work of Pfaff and Brauns is that many habit faces make a very small and variable angle with the low-index plane, i.e. they are 'vicinal' faces.

The nature of the vicinal faces on a growing crystal was studied by Sir Henry Miers(3), who published his results in 1903 and 1904. Miers constructed a special goniometer, which enabled him to measure the interfacial

angles to within one minute of arc on a crystal while it was still growing in aqueous solution. He found that the goniometer reflection from each octahedral face of potassium alum consisted of three closely spaced images, whose positions were between one minute and twenty minutes of arc from the [111] direction. During growth the multiple images were repeatedly replaced by other images lying in definite zones. The transition was not gradual, but by steps, and often occurred after an interim period of confused signals. The experiments were extended to several other cubic crystals (including ammonium alum, sodium chlorate and zinc sulphate) and similar results were obtained. The discontinuous replacement of vicinal faces during growth was believed to indicate that the indices of the vicinal faces, however large, were rational. But subsequent work by Hedges[4], using the same kind of goniometer as Miers, has shown that the replacement of vicinal faces is gradual on crystals of Epsom salt and Rochelle salt, and therefore the vicinal faces of these crystals at least must lack rational indices. Miers' most important discovery was that the vicinal faces corresponding to any single habit face frequently produce low pyramids, or 'growth pyramids'. The angles between the individual vicinal faces of any one growth pyramid and the underlying low-index plane was constant to within a few minutes of arc.

In order to explain the occurrence of vicinal faces

in preference to simple forms Miers argued as follows. If the crystallising material descends directly on a low-index plane, there will be a considerable discontinuity in density of material at the growing crystal surface, as the packing in the crystal is much closer than in the solution. But if the material is deposited on vicinal planes parallel to lattice planes of low reticular density, this abrupt change in packing is appreciably reduced. It is reduced even further if the crystallising material is ordered in planes parallel to the vicinal planes immediately before deposition, and the solution in contact with the growing face should in this case exhibit double refraction. Miers was unable to detect this doubly refracting layer experimentally.

The goniometric study of vicinal faces was extended by Kalb(5) to non-cubic minerals, including quartz and topaz. Kalb demonstrated that the vicinal faces of these crystals can only occur along certain well-defined zones, and that in order to determine the exact positions of the low-index planes it is necessary to determine the points of intersection of these zones.

Schubnikow and Brunowsky(6) studied the properties of vicinal faces by X-ray and goniometric methods, and concluded that, to within the accuracy of their measurements,

vicinal faces are truly plane surfaces. Tolansky[7], however, has reported recently that, by using the more sensitive technique of multiple-beam interferometry, the vicinal faces on a major rhombohedral face of quartz were found to possess a very small cylindrical curvature. Tolansky's work is discussed more fully in Chapter 5.

We have seen that Miers believed that vicinal faces are produced by the laying down of molecular planes of solute parallel to high-index planes of the lattice. He was supported in this view by Kalb (loc.cit.), although there was no direct experimental evidence in favour of it. But there is the alternative explanation that vicinal faces consist of a series of uniformly spaced steps, which arise from a system of growth layers parallel to the low-index plane[8]. If successive layer edges cannot be individually resolved by the microscope, the vicinal face will give a sharp signal in the goniometer. But before considering this further the evidence that crystals grow by the successive deposition of layers will be reviewed, as this concept is of fundamental importance in the interpretation of the topography of the crystals.

The first definite indication of growth by layer deposition was reported in a posthumous publication of R. Marcelin[9] in 1918. Marcelin studied the growth from

alcoholic solution of thin plates of p-toluidine. The plates were sufficiently thin to exhibit Newton's colours in reflection, so that growth in depth and surface area could be simultaneously observed. It was found that, as growth proceeded, uniformly coloured bands with precise geometrical limits were formed and spread across the face at a regular speed. They were succeeded by other bands exhibiting different colours on the Newton scale. Thus at any given time the surface contained a series of coloured bands, regularly spaced and with parallel edges. The colour of each band remained constant as it spread across the whole face, and the difference in tint between adjacent bands corresponded, in one case, to a layer only three molecules thick. Marcelin concluded that the crystals grew by the deposition and spreading of successive layers, whose thicknesses approached molecular dimensions.

These experiments were extended by Kowarski(10) to the growth of p-toluidine crystals from the vapour. It was found in this case that the layers were usually initiated at the edge of the face, and particularly at the point of intersection of the edge with a neighbouring crystal. The layer edges were initially circular, but as they spread across the face they became irregular and lacked any precise geometrical shape. The thinner layers were in general propagated more quickly than the thicker ones, which were

occasionally overtaken by the thinner layers following behind.

A. Marcelin and Bondin[11] observed layer formation on naphthalene and several other organic crystals; and evidence for the growth of diamond by layer deposition has been produced by Tolansky and Wilcock[12] by means of their crossed fringe multiple-beam technique. It is well known that some crystals of diamond have their surfaces marked with pits in the form of equilateral triangles of various sizes. Tolansky demonstrated that these pits are probably formed by the intersection of growth sheets advancing across the crystal surface in three directions inclined at 60 degrees to each other.

An extensive survey of layer formation on crystals of many different substances, both ionic and non-polar, was undertaken by Bunn and Emmett[8]. Their experimental method consisted of placing a drop of warm saturated solution on a warm microscope slide, covering with a thin cover-slip, and observing under the microscope while the solution cooled. The minimum height of the growth sheet edges which could be seen by this method was of the order of 1000Å. The main conclusions emerging from these experiments were as follows:
(1) The growth sheets spread in general not from the edges or corners but from the centres of the faces.

(2) The thickness of the sheets increased as they spread away from their points of initiation.

(3) The growth fronts were often irregular, particularly when the growth was rapid; but as the growth rate decreased the fronts tended to be more regular and to conform to the symmetry of the face.

(4) Growth sheets were only visible on ionic crystals. Some twenty or more organic crystals were studied, but, under the conditions of observation, no growth sheets could be detected on their surfaces, unless the crystals contained ~~organic~~ ionic groups.

Bunn suggested an explanation for the formation of thick layers, based on the morphological principle of low rational indices. A series of uniformly spaced molecular layers constitutes a high-index surface; but if the layers are split up into several groups, each group forming a thick layer, the new layers will be predominantly of low-index, and the surface energy per unit height of layer will be reduced.

The concept of growth by the successive deposition of layers has been incorporated in the theory of growth of a perfect crystal from the vapour. The main principles underlying this theory were first laid down by Gibbs[13] and Volmer[14], and subsequently developed in quantitative detail by Kaischew and Stranski[15] and Becker and Doring[16].

The theory assumes that the growth of a perfect crystal from the vapour at low supersaturations takes place by the initiation and subsequent spreading of molecular layers. Each layer originates from a two-dimensional nucleus, which, once it has attained a critical size, rapidly spreads across the whole surface. The rate of growth of the crystal depends on the rate of formation of critical nuclei, and not on their rate of spreading, which is a comparatively rapid process. The theory explains why a crystal assumes a regular shape with plane habit faces, even when it grows under non-uniform conditions. A simple quantitative treatment of it is given in the next chapter.

For a long time it was believed that the two-dimensional nucleation theory applied satisfactorily to the growth of real crystals, and even now this belief is firmly held by Buckley(17) and others. But according to the observations of Marcelin, Kowarski and Bunn a large number of growth fronts can be seen at any one time spreading across the crystal surface; whereas theory indicated that the growth sheets will spread at a much greater rate than they are initiated, so that one layer will be completed before the initiation of the next. The experiments suggested the interpretation of vicinal faces as a succession of uniformly spaced growth fronts. But this interpretation is not possible on the nucleation theory, and we have already seen that there

is little evidence in support of the alternative interpretation of Miers (loc.cit.).

Further, Stranski[18] calculated that the positions of greatest molecular binding energy in ionic crystals with the sodium chloride structure are at the edges and corners of the faces, so that it is here that two-dimensional nuclei are most likely to be initiated. But Bunn observed that the initiation of layers in ionic crystals (including sodium chloride) almost invariably took place towards the centres of the faces. This observation cannot be explained on the basis of a non-uniform supersaturation over the face, as Bunn showed by an interferometric method that the supersaturation is higher at the centre of the face than at the edges and corners. [Berg[19] and Humphreys-Owen[20] discovered in the same way that in the case of growth of sodium chlorate crystals from solution the supersaturation of the solution in contact with the crystal is highest at the face centres.] It is perhaps possible to explain Bunn's results as being due to small amounts of impurity adsorbed near the centre of the face, although there appears to be no reason why the impurity should avoid the face edges.

It was only recently pointed out by Burton, Cabrera and Frank[21] that the observations of Volmer and Schultze in 1931 on the growth of iodine crystals from the vapour could

not be interpreted by the nucleation theory. Volmer and Schultze[22] showed that iodine crystals grow at a supersaturation, σ, as low as 0.01. Substituting this value of σ in the formula giving the rate of formation of two-dimensional nuclei as a function of σ, Burton found that the theoretical rate of nucleation is smaller than the observed rate by the enormous factor of exp(3,600).

It was therefore evident that there were serious discrepancies between theory and experiment, particularly as regards the interpretation of vicinal faces and the experiments of Volmer and Schultze; and accordingly Burton and Cabrera[23] decided to re-examine in detail the bases of the nucleation theory. They refined it to incorporate the concept of Frenkel[24] that the boundary of the nucleus is not exactly rectilinear at finite temperatures owing to the presence of thermal (or 'Frenkel') kinks; and considered the effects of the surface diffusion of adsorbed molecules, and the change in shape of the nucleus in various stages of its growth. (Becker and Doring restricted their attention to square nuclei.) Burton and Cabrera concluded that the formulae developed by Becker and Doring[16] were correct apart from the omission of relatively unimportant numerical factors, and that the discrepancy between the theory and the experimental results of Volmer and Schultze was still enormous.

An explanation of the discrepancy was suggested by Frank[21], who showed that the results were in much closer accord with the theoretical rate of growth of iodine crystals containing a particular type of lattice imperfection (screw dislocation). He pointed out that the two-dimensional nucleation theory applied to the growth of perfect crystals, but there is strong evidence that real crystals possess an imperfect lattice structure. The intensities of X-ray reflections indicate a mosaic structure of crystals, and the mechanical strength of real crystals is only a small fraction of the theoretical strength of perfect crystals. Frank suggested that the rate of growth of a crystal is similarly structure-sensitive, and showed that the presence of screw dislocations in the lattice enables a crystal to grow at much lower supersaturations than are permitted on the two-dimensional nucleation theory. If a screw dislocation terminates on a crystal face, a molecular ledge runs along the surface from the point of emergence of the dislocation to a neighbouring screw dislocation of opposite hand, or to the edge of the face. Growth can take place by the deposition of molecules along this ledge, provided its length is greater than the critical size of the two-dimensional nucleus, without the formation of a two-dimensional nucleus. Moreover, the molecular ledge will persist and never 'grow out', as will a molecular ledge on a perfect face. Frank[23] calculated the geometrical form of the growth fronts

terminating on screw dislocations, and found that this form is in general a spiral. A crucial point of difference between the growth of perfect crystals containing screw dislocations is therefore the geometrical form of the growth fronts. In particular, spiral fronts can only occur on imperfect crystals.

In the majority of crystals it is not possible to observe the molecular growth fronts, owing to the difficulties of resolution with an optical or electron microscope. (The growth fronts are generally too closely spaced to be laterally resolved with an optical microscope, and too small in vertical height to be detected with an electron microscope.) But molecular steps have been observed on a small number of exceptionally well-developed crystals: By Griffin[25] on a mineral crystal of beryl, Verma[26] and Amelinckx[27] on synthetic crystals of silicon carbide, and Dawson and Vand[28] on certain paraffins of relatively high molecular weight. In all these cases it was found that the growth fronts were frequently of spiral form - thus providing direct evidence in favour of Frank's theory. It is interesting to note that the presence of spiral growth fronts on silicon carbide was first reported by Menzies and Sloat[29] in 1929; but this observation exited little interest at the time.

Bunn[8] observed that the growth fronts on the crystals which he studied were invariably closed; but this is

hardly an argument against a dislocation mechanism of growth, as the growth fronts were not unimolecular, but several hundred molecules high. And further, Forty[30] has very recently shown that cadmium iodide crystals (which were amongst those studied by Bunn) occasionally develop spiral polymolecular growth fronts.

We have already seen that the two-dimensional nucleation theory fails to explain the universal presence of vicinal faces. On Frank's theory however, vicinal faces receive a natural interpretation, for each growth spiral gives rise to a low growth pyramid centred on an 'active' dislocation group. The successive branches of the spiral are uniformly spaced and if the spiral is polygonal, rather than circular, each side of the polygon will give rise to a vicinal face. But there is little experimetnal evidence in favour of this interpretation, as the growth spirals were polygonal only on the paraffin crystals studied by Dawson and Vand.

The topography of only a few crystals has been studied on the molecular scale, and the bulk of the available evidence has favoured the dislocation rather than the nucleation mechanism of growth. But neither theory can explain many features connected with crystal habit and habit modification[31] and oriented overgrowth[32]. Hence in the interpretation of the results on the topography of quarts, given in Parts III and IV of this thesis, an open mind must be kept as regards the applicability of any particular theory of growth.

Chapter II

THEORIES OF CRYSTAL GROWTH

Brief quantitative treatments of the theories of growth of perfect and imperfect crystals from the vapour will now be given. Several of the formulae derived in this chapter will be considered later in relation to quartz.

1. Growth of a Perfect Crystal.

The experiments of Cockroft[33] and Volmer and Estermann[34] have indicated that appreciable surface migration of the adsorbed molecules occurs during growth, before they return to the vapour phase or become incorporated in the lattice. The growth of a molecular layer will therefore take place primarily by the diffusion of adsorbed molecules towards its edge. The direct current of molecules to the edge from the vapour is relatively unimportant, and will be ignored in the following treatment. This treatment is mainly due to Mott[35]

Let PQRS (Fig.1) represent the growing crystal face, and N the nucleus, assumed circular, from which the next molecular layer spreads. The over-riding factor which determines the rate of growth of the crystal is the difficulty of formation of fresh nuclei such as N. When the radius of the nucleus is less than a critical value r_o, the nucleus is unstable and tends to shrink; when its radius is greater than r_o, the

nucleus is still unstable but tends to grow and to spread rapidly over the surface. In order to calculate the rate of growth of the crystal we must therefore find the probability of formation of nuclei of size r_0.

If the radius of the nucleus N is r, its free energy F is given by:

$$F = -\pi r^2 \epsilon + 2\pi r \sigma \quad , \qquad (2.1)$$

where ϵ is the free energy gained per unit area when an adsorbed molecule becomes attached to the nucleus, and σ is the free energy per unit length of the step at the boundary of the nucleus. F is plotted as a function of r in Fig.2. At first F increases as the size of the nucleus increases, and reaches a maximum, F_0, at $r = r_0$. For r greater than r_0, F decreases with increasing r. It is clear that when $r = r_0$ the nucleus is in unstable equilibrium with the supersaturated vapour, and has reached the minimum size for which it will tend to grow. Differentiation of formula (2.1) with respect to r gives:

$$F_0 = \frac{\pi\sigma^2}{\epsilon} \quad , \quad r_0 = \frac{\sigma}{\epsilon} \quad . \qquad (2.2)$$

It remains to estimate ϵ in terms of the given conditions of growth, i.e. temperature and supersaturation. If a^2 is the area of the surface occupied by a single adsorbed molecule, the change of free energy of the nucleus when it incorporates an adsorbed molecule is ϵa^2. This change

is equivalent to the change of free energy of the total adsorbed molecules for the same process. The free energy F' of n isolated adsorbed molecules is:

$$F' = U - TS = n\omega' - kT \ln \left\{ \frac{N!}{n!\,(N-n)!} \right\} .$$

Here ω' is the energy required to transport a single molecule from the nucleus to an adsorbed site, N is the total number of available adsorbed sites, k is Boltzmann's constant and T the absolute temperature. The change in F' when n changes by unity is therefore:

$$\Delta F' = \epsilon a^2 = \omega' + kT \ln \left\{ \frac{n}{N-n} \right\} . \qquad (2.3)$$

The vapour is in equilibrium with the crystal when $\Delta F' = 0$. Let n_o be the value of n at equilibrium. Then from (2.3):

$$0 = \omega' + kT \ln \left\{ \frac{n_o}{N-n_o} \right\} ; \qquad (2.4)$$

and from (2.3) and (2.4), assuming $n_o \ll N$:

$$\epsilon a^2 = kT \ln (n/n_o) .$$

The saturation ratio α is defined as the ratio of the vapour pressure p of the vapour to the equilibrium vapour pressure p_o of the saturated vapour. Hence:

$$\alpha = p/p_o = n/n_o ,$$

and $$\epsilon a^2 = kT \ln \alpha .$$

Substituting this value of ϵ in (2.2) we obtain:

$$F_0 = \frac{\pi \phi^2}{kT \ln \alpha}, \qquad (2.5)$$

and

$$r_0 = \frac{a\phi}{kT \ln \alpha}, \qquad (2.6)$$

where $\phi = \sigma a$ is the nearest-neighbour binding energy.

Rigorous analysis[16] shows that formula (2.5) should include an additional small numerical factor. The two formulae (2.5) and (2.6) are the expressions for the activation energy for growth (F_0) and the radius of the critical nucleus (r_0) in terms of the temperature and supersaturation of the vapour.

2. Rate of Advance of a Straight Step.

We now require to derive a formula for the rate of advance of a straight monomolecular step as a function of the temperature and supersaturation. Such a step is approximately represented in practice by the boundary of a two-dimensional nucleus after it has attained a size many times the critical size, r_0.

The concentration of the vapour at large distances from the growing step is n, where $n = n_0 \alpha$, and α is the supersaturation. We will assume that the concentration at the

step itself is the equilibrium concentration n_0. A reasonable estimate of the smallest distance from the step, measured along the surface, at which the concentration is n is the mean distance of diffusion x_s of adsorbed molecules. In this case the concentration gradient at the step is $(n_0\alpha - n_0) \div x_s$; and as molecules diffuse in both directions towards the step, the velocity v_∞ of the straight step is given by:

$$v_\infty = a^2 \times \text{(number of molecules diffusing towards 1cm. of step per second)}$$

$$= 2D \frac{(n_0\alpha - n_0)}{x_s} a^2 , \qquad (2.7)$$

where D is the surface diffusion coefficient.

x_s is given by the well-known Einstein formula for Brownian motion:

$$x_s^2 = D\tau_s , \qquad (2.8)$$

where τ_s is the mean time that an adsorbed molecule remains on the surface; and Frenkel[36] has shown that:

$$\tau_s = \frac{1}{\nu} \exp\left(\frac{A}{kT}\right) , \qquad (2.9)$$

where ν is a frequency factor and A is the evaporation energy of a single adsorbed molecule.

Thus from (2.8) and (2.9):

$$D = x_s^2 \nu \exp\left(-\frac{A}{kT}\right) .$$

Substituting this expression and the expression

$$n_0 = \frac{1}{a^2} \exp\left(-\frac{W_s}{kT}\right),$$

(where W_s is the evaporation energy from the step to the surface), in formula (2.7), we finally obtain:

$$v_\infty = 2(\alpha-1)x_s \nu \exp\left(-\frac{W}{kT}\right). \quad (2.10)$$

Here $W(= W_s+A)$ is the total evaporation energy from the step to the vapour.

In formula (2.10) the quantities on the right-hand side are all independent of crystallographic orientation. But observation shows that growth fronts are either circular or polygonal, corresponding to v_∞ being independent or dependent on the orientation. In order to account for the polygonal case it is assumed[23] that $x_0 > x_s$, where x_0 is the mean distance between Frenkel kinks. The adsorbed molecules which are within a distance x_s of the kinks will be incorporated in the step, but those which are within a distance x_s of the step but greater than this distance from the nearest kink will not be incorporated. Hence, as x_0 varies with orientation, being a maximum for the close-packed directions of the step, v_∞ will also be dependent on the orientation. In this case formula (2.10) must be multiplied by the factor $C_0 < 1$, given by[23]:

$$C_0 = \frac{\pi x_s}{x_0 \ln(1{\cdot}12\, x_s/a)}.$$

In practice a growth front, whether the boundary of a circular or polygonal sheet, will possess, at least, a small degree of curvature. It is therefore necessary to extend the above argument for a straight step to the case of a curved step.

3. Rate of Advance of a Curved Step.

A step of radius of curvature r will advance slower than a straight step under the same conditions, owing to the greater rate of evaporation from the curved edge to the adsorption space on the crystal surface. In fact we have already seen that this rate of evaporation exactly balances the rate of incorporation of adsorbed molecules when $r = r_o$, and the velocity of the step is then zero. The complete calculation of the rate of advance v_r as a function of r is rather complicated[23]; but the result is expressed simply by the formula:

$$v_r = v_\infty \left(1 - \frac{r_o}{r}\right), \qquad (2.11)$$

where v_∞ is given by (2.10). (2.11) is valid for $r \geqslant r_o$ and provided that $r_o > x_s$. For a polygonal growth front r_o refers to the normal distance from the edge of the nucleus to its centre, and r to the normal distance p from the growth front to the centre of the nucleus.

4. Curvature of Polygonal Growth Fronts.

It can be shown theoretically that the boundary of a polygonal growth sheet possesses a slight degree of curvature. The radius of curvature ρ is given by the formula:

$$\frac{\rho}{p} = 1 + \frac{1}{4} \exp\left(\frac{2\omega}{kT}\right), \qquad (2.12)$$

where ω is the energy of evaporation from a Frenkel kink to the adsorbed state. The rigorous derivation of (2.12) is rather lengthy[23], but a simple geometrical proof is as follows.

In Fig.3 let AB, A'B' represent the positions of a growth front at times t, t+dt respectively. O is the centre of the nucleus from which the growth front has spread, OP is the normal to AB from O, and ψ is the orientation with respect to the OP direction of the element CD, length ds. The kink density n_ψ varies with ψ according to the formula[23]:

$$n_\psi = n_0 \left[1 + \frac{1}{8} \psi^2 \exp\left(\frac{2\omega}{kT}\right)\right],$$

where n_0 is the kink density of the close-packed element normal to OP. The rate of advance v_ψ of the element CD is proportional to n_ψ, so that:

$$v_\psi = v_0 \left[1 + \frac{1}{8} \psi^2 \exp\left(\frac{2\omega}{kT}\right)\right], \qquad (2.13)$$

where v_0 is the velocity of advance of the close-packed element. If CD moves to C'D' in time dt:

$$DD' - CC' = \left[v_{\psi + \frac{\partial \psi}{\partial s} ds} - v_\psi\right] dt \quad ; \qquad (2.14)$$

and the element ds rotates through an angle

$$d\psi = \frac{DD' - CC'}{ds}$$

which from (2.13) and (2.14) becomes:

$$d\psi = \frac{v_0\, dt}{4\rho}\,\psi \exp\left(\frac{2w}{kT}\right), \qquad (2.15)$$

where ρ is the radius of curvature of the element. By geometry we have from Fig.3, as $\psi \to 0$:

$$RS:\ d\psi = \rho + d\rho : \psi \qquad (2.16)$$

and

$$\rho + d\rho = \rho + RS + v_0\, dt. \qquad (2.17)$$

Combining (2.15), (2.16), (2.17) :

$$\frac{d\rho}{dp} = 1 + \frac{1}{4}\exp\left(\frac{2w}{kT}\right)$$

or

$$\rho/p = 1 + \frac{1}{4}\exp\left(\frac{2w}{kT}\right) \qquad (2.11)$$

as $\rho = 0$ for $p = 0$.

In order to determine the order of magnitude of ρ/p consider a face-centred cubic crystal and assume nearest-neighbour interaction only. Then $2w = \phi$, where ϕ is the nearest-neighbour interaction energy, and for the typical value $\phi/kT = 4$, $\rho/p = 15$. Thus the curvature of the growth fronts is small except in the region of the origin.

5. Growth of a Crystal with Screw Dislocations.

Frank (21) has shown that the Becker-Döring theory requires a degree of supersaturation of the order of 50 % for the growth of perfect crystals. But crystals containing screw dislocations can grow at much lower supersaturations, for the molecular ledge

connecting the point of emergence of the screw dislocation with the edge of the face can never 'grow out', and therefore growth can take place at this ledge without the necessity for two-dimensional nucleation. According to Burton (23) the activation energy for growth from the ledge terminating on a screw dislocation is virtually zero, provided that the dislocation is greater than a distance r_o from the edge of the face.

In general growth will take place from a number of dislocation groups, but let us first consider the special case of growth from a single dislocation. The step terminating on the dislocation will rapidly wind itself up into the form of a spiral, whose hand is determined by the sign of the dislocation. Each element of the spiral will advance at a rate given by equation (2.11);

$$v_r = v_0 \left(1 - \frac{r_0}{r}\right) , \qquad (23)$$

where r is the radius of curvature of the element. Frank has shown that for $r \gg r_o$ a good approximation to the equation of the spiral in polar coordinates (r, θ) is :

$$r = 2 r_0 \theta .$$

The distance y_o between successive turns of the spiral is constant for sufficiently large r and will be given by:

$$y_0 = \Delta r = 2 r_0 . 2\pi ,$$

or

$$y_0 = 4 \pi r_0 .$$

The next simplest case to consider is that of two dislocations of the same sign. If they are separated by a

by a distance l greater than $2\pi r_0$ they will each give rise independently to a growth spiral; but if they are closer than this distance apart, the individual spirals 'co-operate', and wind up inside each other producing a single doubly-branched spiral. In this case the dislocations are located at the centre of each branch, and as the spiral rotates during growth there is an exchange of centres at each half-turn. This exchange of centres imposes a slight delay on the rate of rotation of the spiral, which is negligible for $l \ll 2\pi r_0$. The equation for y_0 in the case of two dislocations of the same sign is thus:

$$y_0 = \frac{4\pi r_0}{\epsilon} ,$$

where $\epsilon = 1$ for $l \gg 2\pi r_0$

$= 2$ for $l \ll 2\pi r_0$

and $1 < \epsilon < 2$ for intermediate values of l.

In the general case of S dislocations of the same sign, each dislocation will produce its own independent growth spiral (with $y_0 = 4\pi r_0$) when the distance between adjacent dislocations is greater than $2\pi r_0$. But if l is less than $2\pi r_0$ co-operation between the spirals takes place and the equation for y_0 (23) becomes

$$y_0 = \frac{4\pi r_0}{S}\left(1 + \frac{L}{2\pi r_0}\right), \qquad (8.18)$$

where L is the length of the line of dislocations.

Strictly speaking, the theories outlined in this chapter only apply to the growth of crystals from the vapour. But it is clear that they will apply in principle to growth from solution. The main difference is that we expect in general that the distance x_o between Frenkel kinks is less than x_s (distance from diffusion of adsorbed molecules) for growth from the vapour, and greater than x_s for growth from solution. For this reason formulae (2.5) and (2.9) are only qualitatively correct for growth from solution; but formulae (2.6), (2.11), and (2.12) still apply exactly. It is mainly these last three formulae which will be required in Parts III and IV, in discussing the growth of quartz from solution. Finally it may be mentioned in support of these remarks that the experiments of Griffin[25] have indicated that the theory of growth of an imperfect crystal from the vapour applies quantitatively, as well as qualitatively, to the growth of beryl crystals from solution.

Chapter III.

MULTIPLE - BEAM INTERFEROMETRY.

1. General Considerations.

The position of each point on the surface of a crystal is defined by three rectangular co-ordinates, x, y, z. The ordinary microscope can be used to determine two of these co-ordinates, viz. x and y lying in the plane which is normal to the axis of the microscope. But for topographical studies it is essential to determine the third co-ordinate z, and to a much greater degree of accuracy than is necessary for x and y. For only by determining z down to molecular dimensions is it possible to observe the behaviour of the successive molecular layers, and hence to deduce the fundamental mechanism of growth.

To determine z to this order of accuracy on quartz crystals two experimental techniques are available - electron microscopy and multiple-beam interferometry. A third technique - phase-contrast microscopy - has been used with success by Griffin[25] and Verma[26] in observing molecular growth fronts on beryl and carborundum. These authors assumed that each growth front was of equal height (single molecule), so that the z co-ordinate was given by the number of molecular steps counted from a given reference point. But we will see later (Parts III and IV) that the growth fronts on quartz vary considerably in height over the same crystal surface. At a few isolated points they are of molecular height, but elsewhere

they possess any height up to 5000Å. Thus, although phase-contrast microscopy has been used extensively in the work on quartz, it was imperative to use another technique to determine z. The technique used was multiple-beam interferometry.

The theory and practice of multiple-beam interferometry has been fully described by Tolansky[37] in his book "Multiple-beam Interferometry of Surfaces and Films", and in original papers by Tolansky[38], Brossel[39], Barakat[40], and Holden[41]. The studies on quartz were mainly carried out using 'Fizeau' fringes of the reflected system. Fringes of equal chromatic order were occasionally used to study the topography of selected regions of a face and to measure surface angles (see section 3). The reflected system was used in preference to the transmitted system, as, in general, it was only possible to study the whole of a face with reflection fringes. Transmission fringes required a parallel beam of light to be passed through the crystal, and the width of this beam was limited by reflection at the different faces. This difficulty can be overcome by immersing the crystal in clear oil of the same refractive index (e.g. Canada balsam); but the procedure is troublesome, as the oil must be prevented from touching the silvered face underneath. Alternatively, the crystal can be cut parallel to the face to be studied, and a cover slip attached to the cut surface with a drop of Canada balsam. This rather drastic procedure was carried out on several small and less precious specimens,

including several that were subsequently used as seeds for experiments on synthetic growth.

It is only possible to use light of one wavelength with reflection fringes, although Bruce[42] has recently overcome this disadvantage by the elimination of all rays reflected externally at the front surface of the interferometer.

The optimum conditions for multiple-beam interferometry are those which lead to the production of the sharpest possible fringes at a reasonably good contrast. It will be convenient to consider separately the conditions necessary for sharpness and contrast, although it will be seen that the separate conditions are to a certain extent incompatible, and it is necessary to seek a compromise.

The sharpness of the fringes increases with R, where R is the geometric mean ($\sqrt{R_1 R_2}$) of the reflectivities, R_1 and R_2, of the front and back surfaces of the interferometer. An approximate formula for the fringe half-width δ as a function of R is[37]:

$$\delta = \frac{1-R}{\sqrt{R}} \qquad (3.1)$$

This formula shows that δ is particularly sensitive to changes of R, when R is in the neighbourhood of unity. δ is a minimum when R is a maximum, and for R a maximum it is essential to reduce the absorption coefficient A as much as possible.

Formula (3.1) is derived from the Airy formula for the intensity distribution of Fabry-Perot fringes. For Fizeau fringes δ will be larger than (3.1) indicates, unless special attention is paid to certain factors which tend to reduce the number of co-operating multiple-beams in the image plane of the objective.

These factors are summarised from (a) - (c):

(a) The presence of a wedge angle θ between the two interferometer surfaces produces an unequal path difference between successive beams. The path difference between the first and the n^{th} beams is $2nt - \frac{4}{3} n^3\theta^2 t$, where t is the thickness of the wedge at the place considered. If $\frac{4}{3} n^3\theta^2 t = \frac{\lambda}{2}$, the first and n^{th} beams are exactly out of phase, and fringe broadening results. The broadening effect is made negligible by reducing t, so that $\frac{4}{3} n^3\theta^2 t \ll \frac{\lambda}{2}$. In practice this means that t can rarely be more than 15 wavelengths.

(b) The linear displacement of the successive beams, which again arises from the presence of the wedge angle θ, must be kept within the lateral resolving limit of the objective. On this account t must again be reduced as much as possible, and it is preferable to use normal incidence of illumination. Further the numerical aperture of the objective must be large enough to collect a sufficient number of beams: for normal incidence a numerical aperture of 0.1 is adequate.

0·15

(c) Fringe broadening arises from the slight angular spread of the incident beam, and from the finite line width of the monochromatic source.

These spurious broadening effects were eliminated in practice by restricting t to a maximum value of 10^{-3}cms., by using as source a slightly underrun high-pressure mercury arc, and by limiting the diameter of the source iris to 2mms. The iris was used in conjunction with a collimating lens of 10cms. focal length.

The contrast (or visibility) of the transmitted fringes is not seriously affected by a change of the absorption coefficient A, when R is in the neighbourhood of unity. Thus for a silver film of R = 94% extremely sharp transmitted fringes can be readily seen, and their visibility remains good several hours after the preparation of the film, when the film normally tends to deteriorate and acquire a higher absorption.

On the other hand, the contrast of the fringes in the reflected system is very sensitive to a change of the absorption coefficient A_1 of the front reflecting surface of the interferometer. For a film of reflectivity R_1 = 90%, a slight increase of A_1, due to exposure of the film to the atmosphere for several hours, will make the fringes almost invisible. For R_1 = 85%, the visibility is much less sensitive

to a change of A_1, and 85% is therefore a suitable compromise between the conditions for extreme sharpness and good contrast. The fringe visibility is independent of A_2, the absorption coefficient of the back reflecting surface, so that it is preferable to make the back reflecting surface opaque and thus obtain a maximum value of $R(= \sqrt{R_1 R_2})$.

By means of careful evaporation in vacuo silver films can be prepared with uniform thickness, and reflection coefficient R = 94% and transmission coefficient T = 1% in the green. No other evaporated metal gives such a high value of R for T = 1%, and silver is, therefore the most suitable metal for multiple-beam topographical studies.

2. The Technique of Evaporation.

The first requirement for a successful evaporation was a thorough cleansing of the surfaces to be coated. A satisfactory cleansing procedure for the quartz crystal and optical flat consisted of a preliminary washing in soap water to remove gross contamination of grease, followed by a prolonged immersion of the optical flat in hydrogen peroxide and of the quartz crystal in nitric acid. The specimens were then washed in distilled water, and dried by repeatedly rubbing with small pieces of cotton wool. The rubbing was continued until the breath figures, produced by lightly breathing on the surfaces, vanished almost instantaneously. The flat and

crystal were then rapidly transferred to the bell-jar (Fig.4), and the evaporation procedure begun.

The evaporation plant is shown diagrammatically in Fig. 4. It was a commercial type plant manufactured by W. Edwards and Company. The specimens were placed on an aluminium table A, inside a large pyrex bell-jar B. The table was approximately 30cms. above the steel baseplate P. The silver to be evaporated was in the form of a small bead, and was placed in a depression punched in a molybdenum filament F. E_1E_1 were insulated electrodes through which the heating current was conducted to the filament, and E_2E_2 were insulated annular electrodes round the inside of the bell-jar. The three-way valve V_1 allowed the bell-jar to be connected to the rotary pump R, either directly, or through the oil diffusion pump O. V_2 was a high vacuum flap valve between the bell-jar and the diffusion pump.

The evaporation procedure was as follows. With the flap valve V_2 closed and the bell-jar connected directly to the rotary pump, the bell-jar was evacuated to a pressure of approximately 0.1mms. of mercury. A potential of 3,000 volts was then applied to the annular electrodes E_2E_2. This produced a glow discharge, whose function was to give the specimens a final cleansing by ionic bombardment. After several minutes the valve V_1 was turned to the diffusion pump side, and the high vacuum valve V_2 slowly opened. As the pressure fell in

the bell-jar the discharge soon blacked out, and the high tension was switched off. Pumping was continued until a pressure of less than 0.1 micron was attained. This was a sufficiently low pressure to ensure that the mean free path of the silver atoms was considerably greater than their distance of travel to the specimens. Thus accurate contouring of the specimen surfaces by the silver layer was obtained (Tolansky)(37). The silver was fused by passing a current of 120-150 amps through the molybdenum filament, and the shutter S was interposed between the silver and the specimens until the surface impurities on the silver had been evaporated off. The required thickness of the silver layer was estimated visually by viewing through the top of the bell-jar. With experience it was possible to estimate the reflectivity R of the film to within a few % in the range of R_1 80% - 94%.

3. Optical System.

The silvered flat and crystal were supported rigidly in a special mount, which allowed controlled variation of the relative tilt and separation of the interferometer surfaces. The mount was constructed from two flat brass rings separated by three equidistant brass rods. The optical flat was mounted with its silvered surface upwards on the lower ring, and the crystal with its silvered face downwards on the upper ring. A nut screwed on to each rod and pressed against a steel

spring slipped over the rod. The separation of the flat and the crystal surface was adjusted by gently turning long tommy bars passing through holes in the nuts. Other similar mounts were constructed for use with crystals of varying sizes.

The mount was placed on the stage of a Vickers projection microscope, in which the normal illumination system for convergent light had been replaced by a system producing parallel light. The source, source iris and collimating lens have already been described in Section 1 of this chapter. For the production of fringes of equal chromatic order the high-pressure mercury arc was replaced by a white-light carbon-arc source, and the fringes were projected on to the slit of a Hilger constant deviation spectrograph. The mercury line used for the reflected Fizeau system was the green line, λ = 5461Å; and for the transmitted system the yellow doublet lines, 5770Å and 5791Å, were used in addition.

4. Interpretation of Fringe Pictures.

In using Fizeau fringes for the determination of the topography of crystal surfaces, considerable difficulties of interpretation are likely to arise, unless a suitable fringe dispersion is first selected. In the case of quartz it was found that the most suitable dispersion was that for which the fringes were parallel to the geographic contours of the face, i.e. the plane of the flat parallel to a low-index, or close-packed, plane of the crystal. The most convenient way

to obtain this dispersion was to adjust the fringes to be parallel to the edges of the growth sheets. After the general topographical features had been determined by working at this dispersion, individual features were studied in greater detail by using other dispersions and by employing fringes of equal chromatic order.

In Parts III and IV a number of results are quoted of measurements of surface angles to an accuracy of one second of arc. These measurements were taken by one of two interferometric methods - that of Tolansky[37] using multiple-beam Fizeau fringes, and the method of Barakat[43] involving the combined use of multiple-beam Fizeau fringes and fringes of equal chromatic order. The former method has the disadvantage that the measured value of the surface angle is a mean value for the distance encompassed between at least two successive Fizeau fringes. Barakat's method enables the surface angle to be measured at a precise point on the surface. Thus, if it is required to measure the angle over the line of intersection of two vicinal surfaces, and if this angle varies along the line of intersection, it is preferable to use Barakat's method. In practice, however, Tolansky's method is much quicker and more convenient to apply, and was quite adequate for the majority of measurements on quartz.

The multiple-beam methods are at least fifty times more sensitive than the familiar goniometric method for the

measurement of surface angles. It will be seen later (PartIII) that the employment of multiple-beam methods on quartz has led to results of particular interest in the surface angle region which is not accessible to the reflection goniometer.

Chapter IV

ADDITIONAL TECHNIQUES USED FOR TOPOGRAPHICAL STUDIES.

1. Two-beam Interferometry.

This was useful in the preliminary examination of a surface, before deciding whether the surface was suitable for a more detailed examination by multiple-beam interferometry, involving the comparatively long procedure of silvering by evaporation. The unsilvered specimen and flat were placed in the mount used for multiple-beam studies, and the two-beam fringes observed in reflection. Two-beam fringes, have a cosine^2 intensity distribution, and are therefore much less sensitive than multiple-beam fringes in detecting surface detail.

The two-beam method was found to be adequate for the study of certain relatively rough surfaces, in particular the surfaces of some of the synthetic crystals.

2. Microscopy.

Growth sheet edges, or growth fronts, on natural quartz faces can be frequently observed under the microscope. We have seen in Section 1, Chapter III that a knowledge of the shape and position of these growth fronts will not lead to a

complete determination of the surface topography, as the height of the growth fronts varies from one point to another and cannot be determined microscopically. But a knowledge of the form of the growth fronts is essential for the interpretation of the results obtained by the interferometric examination. It is therefore of interest to consider the conditions under which the growth fronts have maximum visibility under the microscope.

Firstly, it was found that the growth fronts were slightly more visible in reflected than in transmitted light. (A Vickers metallurgical microscope was used for the microscopic examination, and the illuminating system could be rapidly interchanged between the reflected and transmitted positions.) The main reason for this was presumably the increase of optical height of the growth fronts, of actual height h, from $(\mu-1)h$ in transmission to $2h$ in reflection - i.e. an increase by a factor of 4.

Secondly, the visibility of the growth fronts on a given face was considerably increased by silvering the face by evaporation. Chemical silvering had a similar effect, and was found to be a safe procedure for microscopic observation, in spite of the complete lack of contouring of the face by the silver film. The increased visibility was due to a reduction of the proportion of parasitic light, scattered from interior surfaces in the microscope. The same

result could have been achieved by the use of bloomed lenses.

Finally, the growth fronts were most visible in bright field illumination with the source iris stopped down to give a narrow pencil of illumination , and with an objective of numerical aperture 0.1, or less. The growth fronts were not visible with an objective of N : A greater than 0.45, unless the aperture was stopped down. The explanation of this effect is as follows.

The height of a unimolecular step on the rhombohedral faces of quartz is 3.3Å[44]. This is too small to be observed in bright field illumination, so that as growth fronts are visible, they must be polymolecular. In fact it will be shown in Part III that they are of the form given in Fig.5. The growth fronts do not consist of vertical cliffs of molecules, but are rather gradually sloping surfaces, making an angle of approximately 1° with the close-packed plane of the growth sheets. As the distance between successive unimolecular steps is of the order of 200Å and therefore considerably less than the wavelength λ, we can replace the growth front by a plane PQ (Fig.5) making an angle of 1° with the adjacent planes AP and QB. In the focal plane F of the objective in Fig.6 the zero, first, second.. order diffracted spectra of AP and QB are represented by 0, $\pm$1, $\pm$2.., and are displaced slightly with respect to the diffracted spectra 0', $\pm$1', $\pm$2'.. of PQ. If the objective collects all the diffracted spectra of AB

the intensity distribution in the image plane I is uniform and no step at P'Q' can be seen. But for an objective of angular semi-aperture α , less than unity, a different proportion of spectra are collected from AP, QB and PQ, and this difference gives rise to a different intensity distribution of A'P' and P'Q' in the image plane. The ratio of the number of spectra collected from AP and PQ is approximately $\frac{\alpha + 2^{\circ}}{\alpha} = 1 + \frac{2^{\circ}}{\alpha}$. This ratio is large when α is small, and hence the visibility of P'Q' increases as α decreases.

3. Phase-Contrast Microscopy.

According to Francon[45] phase-contrast illumination is superior to normal microscopic illumination.for the observation of small steps, and Lyot[46] has detected polish marks only a few Angstroms deep on telescopic lenses by means of a stereoscopic phase-contrast method. In order to use phase-contrast microscopy to its full advantage it is essential to employ a phase plate allowing continuous variation of both the relative amplitude and absorption of the direct and diffracted beams. Such plates have been designed by Nomarski[47] and others. The phase plate used for the present work introduced a fixied phase change of 90°, producing positive phase-contrast, and possessed an absorption coefficient of 80%. The smallest step visible with this equipment was 10Å.

4. Replica Technique.

A final technique required for the topographical studies on quartz was a reliable method for taking a replica of a given surface. Several crystals, which were considered worth further study after examination with a hand lens, were too valuable to be removed from their case in the museum and to be subjected in vacuo to the silvering process. Their surfaces could only be studied by taking replicas.

The principal features required of the replica were:

(a) Accurate reproduction in extension down to $\frac{1}{2}$ micron, the lateral resolving limit of the microscope.
(b) Accurate reproduction in depth down to molecular dimensions.
(c) No overall distortion of the replica.
(d) Stability under vacuum for the silvering process.

Faust and Tolansky[48] have developed a replica technique, which satisfied requirements (a), (b) and (d). The technique consisted of moulding polymethyl methacrylate (perspex), softened by heating to 140°C, against the crystal surface. The perspex was allowed to cool slowly, and then stripped under water. It was not known whether the technique satisfied requirement (c). To test this, a replica of an optically flat surface was prepared, matched against the original flat, and tested for planeness by interference. It was found that distortion invariably occurred, even

after taking great care in the stripping operation. The technique could be used to measure step heights (e.g. heights of growth fronts), but was unreliable for the measurements of surface angles.

The replica techniques used in electron microscopy[49] must satisfy requirements (a) and (d) above, but it is doubtful that they also satisfy (b) and (c). Recently however, new replica techniques have been developed by Brown[50] and Merton[51], and it was decided to study these techniques with reference to the requirements (a) - (d).

Brown's method consists of pouring a few drops of a specially prepared liquid on the crystal surface. The liquid contains a solution of unpolymerised methyl methacrylate in acetone, mixed with a small amount of tributylcitrate to act as a 'stripping agent', benzoin to act as a 'stabiliser', and granulated perspex. A small piece of perspex sheet, 1/8 inch thick, is placed on the liquid and pressed against the face. The solution extruded round the edge of the face is removed, and the remaining solution is polymerised and solidified by irradiation with ultra violet light. With a 125 watt 'Mercra' high-pressure mercury arc, placed six inches above the specimen, polymerisation is completed within an hour. The replica is stripped from the crystal surface after immersion for half an hour in water.

The surface chosen for testing the replica was the rhombohedral face of a Brazilian quartz, which had been previously studied by multiple-beam fringes (Fig.7). The portion shown consists of several conical hills, two wavelengths high, rising from a plane surface. On the left is a sloping step of approximately the same height as the hills. Fig. 8 is the corresponding fringe picture of the perspex replica. The conical hills have been reproduced in depth to an accuracy of 50Å at least, as the smallest kinks in the fringes in Fig. 7 are accurately reproduced in Fig.8. Hopkins and Pearson(52) have shown by means of a Talysurf profilometer that accurate reproduction in depth occurs down to 1 micron, and it can therefore be concluded that requirement (b) is approximately attained. But the fringes in Fig. 8 over the original plane area are non-uniformly spaced, indicating that cylindrical distortion of the replica has occurred, and that (c) is not satisfied.

Several attempts were made to eliminate this distortion. The crystal surface was silvered with an opaque layer several hundred Å thick before being covered with the solution. Distortion was most likely to occur in the stripping process and it was thought that the stripping would be facilitated by immersing the crystal and polymerised replica in acid, in order to dissolve away the silver layer. In addition, the original piece of perspex was backed by a glass plate, 1/8 inch thick, by cementing with a layer of liquid methyl methacrylate, which

was subsequently polymerised. But these modifications only reduced the distortion, without removing it; and it appeared likely that all perspex replicas had this drawback. It is probable that most replica techniques (e.g. those used in electron microscopy) involve the introduction of surface distortion which is normally of no importance, except in the case of interferometric studies.

The replica technique recently developed by Merton[51] and Sayce[54] for the reproduction of diffraction gratings must necessarily be free from surface distortion, which would produce "ghosts" in the diffracted spectra. The technique is a modification of Thorpe's well known method of reproducing gratings, later improved by Wallace[53]. A solution of cellulose acetate in acetone is spread on the grating (or crystal surface) with a straight edge, using wires of suitable thickness as distance pieces. The film is allowed to dry in a dust-free cabinate, and the 'pellicle' of cellulose acetate removed with the aid of tweezers. An optical flat, which has been previously coated with a thin uniform layer of gelatine, is soaked in water, in order to soften the gelatine, and the pellicle is gently placed on the gelatine. The pellicle is rolled with a printers' roller, the gelatine is allowed to dry, and the pellicle is removed, leaving a positive replica of the original surface on the gelatine.

This technique was tried on several quartz

surfaces including the one shown in Fig. 7. Fig. 9 is the multiple-beam picture of the replica, and Figs. 10 and 11 are the photomicrographs of this same area on the original and the replica, respecitvely. Reproduction in extension has been satisfactorily attained (Figs. 10 and 11), but the depth of features on the original surface have been reduced by a factor of approximately two on the replica (Figs. 7,9). This result has been confirmed by Sayce[54]. Several attempts were made to improve the reproduction in depth, e.g. by reducing the concentration of acetate solution, and by evaporating the acetate as slowly as possible by placing the specimen in an atmosphere saturated with acetone. But these attempts were unsuccessful, and indicated that the error in reproduction appeared in the intermediate stage of the process when the gelatine surface received the imprint of the pellicle.

These experiments indicated that the perspex technique met requirements (a), (b) and (d) above, and the gelatine technique requirements (a), (c) and (d). But it was not possible to find a perfect technique satisfying all four requirements. It was decided to use the perspex technique when a replica method was required and to rely only on those interferometric observations which were not affected by the distortion of the replica.

MOS

Part III Chapter 5.

Chapter V.

GENERAL TOPOGRAPHICAL FEATURES OF R FACES.

1. Introduction.

Quartz is a widely distributed mineral, and grows under a wide range of conditions, being a constituent of both igneous and acidic rocks. Synthetic quartz crystals have been grown in the laboratory between temperatures of 20°C and 870°C and between pressures of 1 and 3000 atm. (Kerr and Armstrong[55]).

α-Quartz possesses rhombohedral symmetry and belongs to the trigonal trapezohedral class, 32. X-ray analysis[36] shows that the structure is built up from SiO_4 tetrahedra linked together by oxygen atoms common to adjacent tetrahedra. The linked tetrahedra are arranged spirally, and in a given crystal the spirals are all left- or right-handed corresponding to a laevo-ordextro-rotatory crystal.

The most well-developed faces of natural crystals are those belonging to the $\{10\bar{1}0\}$, $\{10\bar{1}1\}$ and $\{10\bar{1}1\}$ forms. These are the prism, major rhombohedron and minor rhombohedron forms respectively: abbreviated in Miers'[56] notation to m, R and r. They are shown diagrammatically in Fig. 12. The r faces are invariably smaller than the R faces, and the m faces are often horizontally striated. According to Spencer[57] these are the only faces which occur on the majority of natural crystals. They are the only faces which have been studied in the present work.

Previous studies on the surfaces of natural quartz have been carried out by Kalb[5], Tolansky[7], and Griffin[8]. Kalb studied the interfacial angles of a large number of crystals from several different localities by means of the reflection goniometer. The main proportion of his work was confined to the R and r faces, although the m faces and faces of the trapezohedron and scalenohedron forms were also studied. He was primarily interested in the 'vicinal phenomena' of these faces, and in the determination of an accurate value of the axial ratio c/a from the goniometric signals of the vicinal faces. He discovered that the vicinal faces on any given habit face occurred in sets of three, although in certain special cases one or two of the set were absent; and each set constituted the three sides of low growth pyramids. The angles between the vicinal sides of the pyramids were of the order of five minutes of arc.

Tolansky[7] studied the topography of a single R face of a left-handed quartz crystal by means of multiple-beam interferometry. He was able to show, by virtue of the great sensitivity of these fringes, that the vicinal faces were not truly plane, and possessed a slight cylindrical curvature with a radius of curvature of 20 - 60 metres. Further, the angle between adjacent vicinal faces, as measured along their line of intersection, was found to increase in the vicinity of the summit of the growth pyramid. In the cases cited this increase was from approximately three minutes to nine minutes of arc.

Griffin[58] observed a step structure on several rhombohedral faces, which was probably produced by the growth sheet boundaries. He attempted to prove that quartz grows by a dislocation mechanism; But as he was unable to observe unimolecular layers, his evidence for such a mechanism was not convincing.

In the work to be described here, the preliminary observations of Tolansky and Griffin were extended to naturally occurring crystals from at least six different localities; and in addition several synthetic crystals were studied, which had been grown under known conditions of temperature and pressure.

The present chapter contains a description of the general topographical features of the R faces of natural crystals. Most of these results have been obtained by studying crystals from the Herkimer County locality of the U.S.A. Crystals from this locality are generally small and perfectly developed, and therefore lend themselves particularly well to study by multiple-beam interference methods. In addition, they are usually doubly-terminated, so that twice as many rhombohedral faces are available for study, compared with crystals from other localities, which are usually singly-terminated. Observation has shown that the general features of the R faces of Herkimer County crystals are also characteristic of crystals from other localities, and this chapter will accordingly contain references to measurements taken on the latter crystals. In a subsequent chapter

particular features, observed only on isolated crystals from different localities, will be described.

2. Growth by Layer Deposition.

A batch of six untwinned crystals was selected from the large collection of Herkimer County crystals in the Natural History section of the British Museum. These crystals were selected primarily for their suitability for interferometric studies, being free from cracks, which would be liable to extend in the silvering process, and free from re-entrant interfacial angles. Such re-entrant angles occur in twinned crystals. According to Gault[60] the majority of Herkimer County crystals are untwinned and the six crystals could therefore be considered to be a fairly representative selection. The six R and six r faces of each crystal were studied under the microscope and by means of multiple-beam interferometry. The general topographical features of the rhombohedral faces were the same from one crystal to another, and the results can therefore be presented below with reference to the six crystals as a whole.

The major rhombohedral faces of the crystals frequently showed triangular line markings when examined under the microscope. These markings are shown in Fig. 13, which was taken at a low magnification (x20, N.A.= 0.1). The triad axis is vertical in the photograph, and this orientation is adopted in the pictures of rhombohedral faces shown later.

Fig. 14 is a multiple-beam interferogram of the area shown in Fig. 13. The dispersion of the fringes in Fig. 14 has been adjusted to make the fringes approximately parallel to the line markings in Fig. 13. The shape of the triangular features in these two figures is the same, and Fig. 14 may be considered to be derived from Fig. 13 by making only those line markings visible, which are separated in vertical height by intervals of half a wavelength (2730Å).

It was found experimentally that the dispersion of the fringes could be invariably adjusted to make the fringes parallel to the corresponding line-markings on the surface. This showed that, to within the accuracy of measurement of multiple-beam fringes, the markings were parallel to contour lines of the face, and were contained by sheets, which were parallel to one another. A deviation of parallelism as small as one second of arc could have been detected as a corresponding distortion of the triangular fringes.

Examination at other dispersions revealed that the line markings were small surface steps. The height of the steps on any one face was not constant, but was generally of the order of a few hundred Å. As the sheets containing each triangular step were parallel, the sheets consisted of parallel layers of varying height. It is natural to infer that they were polymolecular "growth sheets", and the steps were the boundaries of the growth sheets, or "growth fronts".

The growth fronts were arranged in several concentric groups, and each group gave rise to a three-sided growth pyramid, whose interfacial angles ranged between two and thirty minutes of arc. The highest points on the face were the centres of each concentric group of growth fronts. This indicates that these points were the centres of initiation of growth sheets, which spread at regular intervals from them, and produced low-angle growth pyramids. The vicinal sides of the pyramids were thus produced by the successive series of uniformly spaced stepped growth sheets. This supports Bunn's[8] interpretation of vicinal faces, discussed in Chapter 1.

3. Orientation and Shape of Growth Sheets.

The orientation and shape of the growth sheets is shown by the photomicrograph of the face (e.g. Fig. 13). The growth fronts, however, are frequently too closely spaced to be visible under the microscope over the whole surface, and Fig. 13, in fact, represents a particularly favourable case. In general, it is therefore more convenient to deduce the shape of the growth sheets from the multiple-beam interferogram taken at the geographic dispersion (e.g. Fig. 14).

Fig. 16 is a schematic representation of the shape and orientation of the growth sheets on a right-handed crystal. ABC is the growth front which has spread from the initiating centre O of the growth pyramid. The three sides, AB, BC, CA

are approximately, but not exactly, parallel to the corresponding edges DE, EF, FD of the face. The corresponding diagram for a left-handed crystal (Fig. 17) is obtained from Fig. 16 by reflection of the triangle ABC about a plane normal to FD. In a right-handed crystal CA meets the prism edge at an angle of approximately +7°, and in a left-handed crystal at an angle of -7°. These two cases are illustrated in the photographs, Figs. 18, 19. The symmetry of the growth sheets fails to conform exactly with that of the boundary of the face, owing to the relatively low lattice symmetry of quartz.

The sides CA (Fig. 16) of the growth fronts frequently attain a height of 200Å or more, and can easily be seen with the aid of a x10 magnifying lens, and sometimes with the naked eye. It is therefore possible to determine the hand of the crystal by observing whether the growth fronts CA meet the prism edge of the R face in a positive or negative angle. In a selection of twenty Herkimer County and Brazilian crystals it was found possible to determine the hand of sixteen crystals in this way. The hand was checked independently by etching methods.

It is interesting to compare this method with the two standard methods of determining the hand of a quartz crystal by inspection (Dana (61)). In the first of these

the hand is determined from the position of the general form, the trapezohedron $\{51\bar{6}1\}$, and in the second method from the direction of the striations on the scalenohedral $\{2\bar{1}11\}$ faces (see Figs. 20 and 21). Thus both methods depend upon the development of faces which are absent in the majority of crystals (57), and the growth front method is therefore of more general application than the two standard methods. In the twenty crystals mentioned above, the hand of only five could be determined by the standard methods.

The physical interpretation of the observed triangular shapeof the growth sheets is that the rate of growth outwards from the initiating centre O (Fig. 16) depends on the orientation ψ, and goes through three minima as ψ increases by 2π. The three directions of minimum growth velocity are given by the three directions OP, OQ, OR normal to the sides AB, BC, CA respectively of the growth front. The overall rate of spreading of the growth sheets is determined principally by these three minimum growth rates; just as, in three dimensions, the rate of growth of its habit faces, which are the slowest growing faces, determine the rate of growth of the crystal as a whole. It will be convenient for further reference to denote these three slowest growing directions by the symbols α, β, γ (Figs. 16,17). For a right-handed crystal OQ is greater than OP, so that the rate of growth in the β direction is greater than that in the α direction. The reverse is true for a left-handed crystal.

4. Heights of Growth Fronts.

The heights of the growth fronts were measured from multiple-beam Fizeau interferograms of suitable dispersion. Fig. 22 is an interferogram, taken at the geographic dispersion, which shows an R face consisting of a large growth pyramid, centred on the horizontal prism edge, and two smaller pyramids; and Fig. 23 is an interferogram taken at a suitable dispersion to show the variation of height, H, of the β growth fronts of the large pyramid with their normal distance, p, from the initiating centre. H has been measured as a function of p from Fig. 23, and the results are plotted in Fig. 24. The curve shows that H is initially less than 50Å and increases rapidly with p towards a maximum value H_o = 190Å.

The corresponding H-p curve for the α growth fronts is shown in Fig. 25. This curve was obtained in a more indirect way than Fig. 24, as the α growth fronts were too closely spaced to permit an accurate determination of H by direct measurement of the fringes. Instead H was deduced from the separation of the adjacent growth fronts and from the pyramid gradient, determined from Fig. 22. Again the H-p curve rises steeply from near the origin to a horizontal asymptote, H = Ho.

It was found that the γ growth fronts were, in general, more irregular than the α and β growth fronts, and their height increased with p in a more irregular manner. This is illustrated by the Figures 26 and 27. Fig. 26 shows that

growth fronts have spread downwards in the γ direction from a line of three initiating centres at the upper left of the figure, and Fig. 27 is an interferogram taken at a suitable dispersion to show the variation with p of the height H of these growth fronts. The H-p curve (Fig. 28) has the same general shape as the curves for the α and β growth fronts, but there is a greater scattering of the points about the curve. The origin of the irregularity of the γ growth fronts is probably connected with the fact that these growth fronts travel considerably faster than the α and β growth fronts. (This can be deduced from the different pyramid slopes in the α , β , γ directions.) It has been observed, for instance, by Bunn[8] that the growth fronts on certain crystals become irregular as the growth rate increases.

The general relation between H and p for the R faces of quartz is shown in Fig. 29. For small values of p ($<10^{-2}$cms) H is 40Å or less for Herkimer County crystals, but for crystals from other localities it is often as much as 100Å. In small crystals the curve extends to a point such as P, which corresponds with the edge of the face; but for larger crystals the curve continues beyond P and tends to approach the horizontal asymptote $H = H_0$. H_0 varies between comparatively wide limits - 100 Å to 10,000Å, - but is generally of the order of several hundred Å.U. On the R face of one crystal of Brazilian quartz the growth fronts were of the same height, 110Å, for all values of p. This case was exceptional, and is considered later in Chapter 7.

The form of the H-p curve indicates that the phenomenon of "bunching", or the catching up of growth fronts on one another during growth, is almost universal in quartz. The photograph in Fig. 30 illustrates the phenomenon well. The growth fronts have spread in the α (and β) directions from the lower half of the picture, where they appear in the form of doublets; and in the upper half of the picture the rear components of the doublets have caught up the front components and produced single growth fronts. The behaviour of the growth fronts is made clear in the accompanying profile diagram, Fig. 31.

The approach of H to a maximum value H_o indicates that the bunching process does not continue indefinitely, but stops after the growth fronts have attained a maximum height H_o. We can consider the molecular layers to be initiated in groups containing $n_o = [H_o \div a]$ layers each, where a is the molecular height. The layers in each group travel across the face at slightly different velocities, so that the edges of the faster layers behind catch up the edges of the slower layers in front and produce bunched growth fronts, whose ultimate height is H_o.

The bunching effect is a well-known feature of the growth of several crystals, e.g. diamond. Bunn[8] observed it on certain ionic crystals by noting the increase of visibility of the growth fronts as they spread away from their initiating centres. The origin of the bunching effect is at yet unknown, but a tentative theory for its existence in quartz is given

later in Section 4, Chapter 7.

5. Stepped Nature of Growth Fronts.

The question arises whether the molecular steps in each group of $n(=H_o \div a)$ steps close up to each other completely during the bunching process, and produce a growth front with a sharp vertical edge. To answer this it is necessary to measure the angle χ between the risers of the growth fronts and the upper plane surfaces of the growth sheets. It was found that χ was of the order of 1° of arc. Thus, for a growth pyramid of gradient 5 minutes of arc, the molecular steps were initially 700a apart: The groups of n_o steps then rapidly closed together, so that the successive molecular steps in each group were approximately 60a apart, but no less (Fig. 35).

It was possible to show that χ was a relatively small angle by careful inspection of the growth fronts with the aid of a hand lens. A similar conclusion was obtained by observing that the multiple-beam fringes were invariably continuous over the growth fronts (e.g. Fig. 27).

Accurate values of χ were obtained by interferometric measurement of those growth fronts which were at least one wavelength high and ten wavelengths apart. χ could not be measured accurately on smaller growth fronts, as the direction of the fringes over the fronts could not be accurately determined, owing to diffraction effects near the steps. In the interferograms shown in Figs. 32 and 33 the growth fronts

are parallel to the vertical sides of the picture, and are more than one wavelength high. χ can be measured from these pictures to an accuracy of $\pm$ 10%.

The results of the measurement of χ in the three directions α , β , γ of the R faces of crystals from several different localities are given in the second, third, and fourth columns of table I.

Table I.

Type of Crystal.	χ_α (deg.)	χ_β	χ_γ
Herkimer County I.	1.0	1.4	1.1
Herkimer County II	1.0	1.2	1.0
Brazilian I	1.0	1.3	1.1
Brazilian II	0.9	1.2	–
Synthetic Crystal	0.6 ± 0.2	–	–

The measurements of χ given in each row of the table refer to the values χ_α , χ_β , χ_γ for the α , β , γ growth fronts of the same growth pyramid. The table shows that χ varies slightly with the orientation of the growth front, so that $\chi_\alpha < \chi_\gamma < \chi_\beta$. To within the accuracy of the measurements ($\pm$ 0.1°), the values of χ_α , χ_β , χ_γ were the same for the different natural crystals.

The directional variation of χ can be observed in Fig. 34 without direct measurement by interferometry. This

figure is a photomicrograph of the β and γ growth fronts meeting in the diagonal "vicinal edge", i.e. the edge between the adjacent vicinal faces. Each growth front appears as a bright line at the edge of a broad dark band, and the width of this band gives the lateral extent of the growth front. The band widths are slightly greater for the γ fronts compared with the β fronts of the same height, i.e. $\chi_\gamma < \chi_\beta$.

The low angle type of growth front can be explained by considering the effect of the surface diffusion of adsorbed molecules on the bunching process. There is ample experimental evidence for the existence of surface diffusion in growth from solution (Berg[19], Bunn[8], Humphreys-Owen[20]); and it was assumed in the theories developed in Chapter II that surface diffusion plays a vital role in crystal growth.

It was shown in the last Section that the bunching process in quartz consists of the gradual drawing together during growth of the molecular steps in each group of n($=H_o \div a$) steps. If y is the mean separation of the steps in each group (Fig. 35), and x_s is the mean distance of diffusion of adsorbed molecules, the surface diffusion current to each individual molecular step will be independent of y, provided that $y >> 2x_s$. But as y decreases and approaches the value $2x_s$, a certain proportion of the adsorbed molecules will be able to diffuse to more than one step, so that competition will occur between adjacent steps for the incorporation of the available adsorbed molecules.

The result of this competition will be that each step incorporates on the average fewer adsorbed molecules, and the velocity of each step, except the foremost, will fall. The foremost step, however, still has a relatively large plane area on its lower side from which to 'collect' adsorbed molecules, and its velocity will be hardly affected. Thus when $y \simeq 2x_s$, the spacing of the foremost step and the step which is immediately behind will be adjusted, so that the greater velocity of the step behind, due to the bunching effect, is exactly counterbalanced by its reduced velocity, due to the surface diffusion effect. Similarly, the spacing of all the other steps in the group of n_o steps will be adjusted until each individual step attains the same velocity.

The successive stages in the above argument are illustrated in Fig. 35 (a) - (c). It is interesting to note that the bunching effect alone, operating on a series of molecular steps, will draw the steps together to form a vertical cliff of molecules; and the surface diffusion effect alone, operating on a sharp multimolecular step, will draw the individual molecular steps out to a (theoretically) infinite distance from each other.

The above argument is of general application to crystals which grow by the spreading of multimolecular layers, and such layers should therefore be of the low-angle type. In support of this conclusion Tolansky[62] has observed

low-angle steps on mica; and Verma[63] has observed that multiple-beam fringes were continuous over the multimolecular steps on SiC, indicating that these steps were also of the low-angle type.

It was possible to estimate the difference in velocity of the first and last steps in each group of n_o steps, arising from the bunching effect when $y \gg 2x_s$, by measuring the initial slope of the H - p curve (Fig. 29). The velocity difference was of the order of a few %. Thus, provided that the surface current of adsorbed molecules towards the molecular steps in quartz is not considerably less than the direct solution current, this difference of velocity is counterbalanced by only a small decrease of y below the critical value $y = 2x_s$. We can therefore assume that the steps in each group move together with uniform velocity when $y \cong 2x_s$, and the angle χ between the risers of the growth fronts and the plane of the growth sheets is given by the equation:

$$\chi = \frac{a}{2x_s} \qquad (5.1)$$

where a is the height of a molecular step. Substituting from table I the value of $\chi = 1°$, we obtain $x_s = 30a = 100\text{Å}$.

There is little experimental evidence for the magnitude of x_s for crystals growing from the vapour or solution, but Frank[23] has deduced from the experimental results of Volmer and Schultze[22] that $x_s = 100a$ for iodine crystals growing from the vapour at 0°C; and Cabrera[64] has deduced from

the results of Clancey[65] that $x_s = 120a$ for napthalene molecules at room temperature. The value of 30a for quartz is rather less than the values for I_2 and $C_{10}H_8$, but this is to be expected. For x_s is given by the formula[23]:

$$x_s = a \exp\left[(W_s' - U_s)/2kT\right] \quad (5.2)$$

where W_s' is the evaporation energy from the surface to the vapour and U_s is the activation energy for surface diffusion. Compared with I_2 and $C_{10}H_8$, quartz has a higher temperature of growth T and probably a larger U_s, as it grows from solution and U_s is therefore increased by the solvation effect. Thus, on the whole, 30a appears to be a fair estimate of x_s for quartz.

Table I shows that $\chi_\alpha < \chi_\gamma < \chi_\beta$, and from the above theory, using equation (5.1), this indicates that $(x_s)_\alpha < (x_s)_\gamma < (x_s)_\beta$. It is shown in the next section that the molecular binding energy, ϕ, varies in a similar manner with orientation, i.e. $\phi_\alpha > \phi_\gamma > \phi_\beta$. We can therefore deduce from equation (5.2) that $W_s' - U_s$ increases as ϕ increases, i.e. W_s' increases more rapidly with ϕ than U_s. Burton[23] has shown by direct calculation of W_s' and U_s as a function of ϕ that this is certainly true of face-centred cubic crystals.

6. Curvature of Growth Fronts.

Kalb[5] assumed that the vicinal faces of quartz were truly plane, as the goniometer signal from each vicinal face was sharp and well-defined. However, it can be shown by multiple-beam interferometry that this is only approximately

true, and that there are two respects in which the vicinal faces depart from the condition of being strictly plane:
(a) The vicinal faces possess a cylindrical curvature, with radius of curvature of the order of several metres, which arises from the slight curvature of the boundaries of the growth sheets.

(b) The gradient of the growth pyramids, or the inclination of the vicinal faces to the low-index plane, increases slightly towards the summit of the growth pyramid.

Tolansky[7] observed both these effects; but his observations were confined to a single R face of Brazilian quartz, and he did not attempt to explain his results. In this section the results of the study of the first effect (a) are given, and in the next section the effect (b) is considered. The measurements of the curvature of the growth fronts is of theoretical importance, as according to formula (2.12) the curvature provides a measure of the binding energy of the molecules in the molecular steps which constitute the growth fronts.

The radii of curvature of the growth fronts have been determined as a function of their normal distance p from the initiating centre, for the growth pyramids on several crystals from different localities. The results for the three growth pyramids shown in the interferogram Fig. 22 are given

in the curves Figs. 36 and 37. ϱ denotes the radius of curvature of the close-packed portions of the growth fronts measured in the three directions α, β, γ. ϱ has been determined to an accuracy of $\pm$ 10% in the α and β directions, but to a smaller degree of accuracy in the γ direction. $-(\varrho)_\gamma$ could not be accurately measured as the γ growth fronts were irregular for large p. This irregularity has already been discussed in Section 4. The accuracy of $\pm$ 10% quoted above includes the systematic error which arises from the assumption that the fringe dispersion was exactly the geographic dispersion.

The graphs in Figs. 36, 37 show that the ratio of ϱ/p is constant to within the accuracy of the measurements of ϱ. This was confirmed in the measurements on the other crystals, and the results are given in Table II, columns 2 - 4.

Table II.

Kind of Crystal.		$(\varrho/p)_\alpha$	$(\varrho/p)_\beta$	$(\varrho/p)_\gamma$	$\omega_\alpha/\omega_\beta$	$\omega_\gamma/\omega_\beta$
Herkimer County I	Face 1	35	12	—	1·30	—
		20	8	12	1·35	1·17
		20	8	12	1·35	1·17
	Face 2	35	11	18	1·33	1·15
	Face 3	35	12	22	1·30	1·17
	Face 4	30	10	20	1·32	1·20
Herkimer CountyIII	Face 1	31	10	18	1·33	1·17
	Face 2	32	11	19	1·31	1·16
Brazil II	Face 1	34	12	—	1·29	—
	Face 2	34	12	21	1·29	1·16

Table II continued.

Kind of Crystal.		$(e/p)_\alpha$	$(e/p)_\beta$	$(e/p)_\gamma$	$\omega_\alpha/\omega_\beta$	$\omega_\gamma/\omega_\beta$
Brazil III	Face 1	33	11	–	1·31	–
Madagascar I	Face 1	32	11	24	1·30	1·22
Synthetic 1	Face 1	5·1	3·3	–	1·26	–

The constancy of e/p is explained by the formula (2.12):

$$e/p = 1 + \tfrac{1}{4} \exp\left(\frac{2w}{kT}\right)$$

According to this formula e/p is constant provided that the temperature, T, of growth is constant. In natural quartz it is only possible to observe the growth sheets which were laid down towards the end of growth, and it is therefore not unreasonable to assume that T was constant in this period.

The above formula will not explain, however, the variation of e/p from one growth pyramid to another on the same face (e.g. Herkimer County crystal I, Face 1 in table II). Further, the formula gives:

$$\frac{T_{nat}}{T_{syn}} = \frac{\log\left[4\left(\frac{e}{p}\right)_{syn} - 4\right]}{\log\left[4\left(\frac{e}{p}\right)_{nat} - 4\right]}, \qquad (5.3)$$

where T_{nat}, and T_{syn} are the temperatures of growth of natural and synthetic crystals. Substitution of the values of $(e/p)_{nat}$ and $(e/p)_{syn}$ from table II and the value T_{syn} = 360°C (Part IV) in (5.3) yields the result T_{nat} = 80°C - 130°C. This

estimate of T_{nat} is rather lower than the estimate of Ingerson (66) of T_{nat} = 100°C - 180°C, obtained by a liquid inclusion method.

The only additional factor which can give the anomalous results for face I of Herkimer County crystal I appears to be the supersaturation, σ . If formula (2.12) is modified to the form:

$$\frac{e}{p} = 1 + \tfrac{1}{4}\exp\left[\frac{2w}{kT} f(\sigma)\right] \qquad (5.4)$$

where $f(\sigma)$ is an unknown function of σ , the revised formula can be tested experimentally as follows.

The value of σ varies from one growth pyramid to another of the same crystal, but is constant for the different growth fronts ~~of~~ α , β , γ of the same growth pyramid. Thus the ratios: Since α, β & γ are $\propto$ to e/p

$$\log\left[4\left(\frac{e}{p}\right)_\alpha - 4\right] : \log\left[4\left(\frac{e}{p}\right)_\beta - 4\right] \qquad (5.5)$$

and

$$\log\left[4\left(\frac{e}{p}\right)_\gamma - 4\right] : \log\left[4\left(\frac{e}{p}\right)_\beta - 4\right] \qquad (5.6)$$

are, from formula (5.4), equal to:

$$\frac{w_\alpha}{w_\beta} \quad \text{and} \quad \frac{w_\gamma}{w_\beta} ,$$

where w_α , w_β , w_γ are the energies of formation of Frenkel kinks in the α , β , γ step orientations. The ratios (5.5) and (5.6) should therefore be constant, and the figures in

columns 5 and 6 of table II show that this is approximately true. The figures in these columns give:

$$\omega_\alpha : \omega_\beta : \omega_\gamma = 1.31 : 1 : 1.17 \qquad (5.7)$$

For a face-centred cubic crystal $\omega = \frac{\varphi}{2}$, where φ is the molecular binding energy[23]. For quartz we can write:

$$\omega = b\,\frac{\varphi}{2} \qquad (5.8)$$

where b is a constant, which is only slightly less than unity as quartz is a relatively close-packed structure[56]. Combining (5.7) and (5.8) we obtain:

$$\varphi_\alpha : \varphi_\beta : \varphi_\gamma = 1.31 : 1 : 1.17 \qquad (5.9)$$

Thus the molecules are more tightly bound along the α orientation than along the β and γ orientations. This is in accordance with the covalent nature of the binding in quartz.

An independent estimate of the ratio $\varphi_\alpha : \varphi_\beta$ is obtained in the next section, and found to agree satisfactorily with the value given in (5.9). Further, it is shown in the next chapter, devoted to the r faces of natural quartz, that the ratio of the mean binding energies of the R and r faces, calculated from (5.4) and the measurements of e/p, is approximately equal to the ratio calculated directly from the lattice structure[67].

7. Profile of the Growth Pyramids.

The increase of gradient of the growth pyramids towards the pyramid summit can be seen directly in the interferogram,

Fig. 27. The position of the summits of the pyramids on this face are shown by the interferogram Fig. 26, taken at the geographic dispersion. In Fig. 27 the vertical fringe which is second from the right is straight in the lower half of the picture, indicating that the pyramid gradient is uniform here; but the change in direction of the fringe near the pyramid summit indicates an increasing gradient. A similar effect is shown in Fig. 23, in which the pyramid summit lies on the horizontal prism edge.

The pyramid gradient can be measured most conveniently by means of the multiple-beam interferogram taken at the geographic dispersion, e.g. Fig. 38. The fringes give the positions of growth fronts, which are separated in vertical height by intervals of 2730Å $\left(\frac{\lambda}{2}\right)$, and therefore the local gradient is inversely proportioned to the horizontal distance between successive fringes. In Fig. 39 the profile of the pyramid in Fig. 38 in the α direction has been obtained by plotting the number, n, of the fringe, counted from the initiating centre O, against its normal distance, p, from O. The pyramid gradient θ, is constant ($= \theta_0$) for $p > p_0$, where $p_0 = 0.25$cms.; and $\theta > \theta_0$ for $p < p_0$.

The general shape of the n - p curve was similar to Fig. 39 for crystals from several different localities. Thus the n - p curve for the large pyramid in Fig. 22 is as shown in Fig. 40.

Now θ is determined by two factors:

(a) The velocity, v, of the growth fronts as they spread across the face.

(b) The rate, I, at which the growth sheets are initiated at the centre O.

Thus the gradient is steep if I is large and v is relatively small; for I small and v relatively large the vicinal sides of the pyramid make a smaller angle with the close-packed R plane. As θ is constant for $p \geq p_o$, both v and I are constant for the growth sheets whose boundaries are greater than a distance p_o from O. The increase of θ for $p < p_o$ must be due either to an increase of I or a decrease of v, or both. We expect, however, on theoretical grounds v to be reduced near O; for it is here that the growth fronts have their greatest curvature (as e/p is constant), and the rate of evaporation of molecules from them is therefore relatively large. The formula giving the dependence of growth front velocity, v_r, on its radius of curvature, r, has been quoted in chapter 2:

$$v_r = v_\infty \left(1 - \frac{r_o}{r}\right) \qquad (2.11)$$

where v_∞ is the velocity of the straight step and r_o the size of the critical nucleus, i.e. the smallest two-dimensional nucleus which tends to grow rather than to shrink. For polygonal growth fronts, r is replaced by the normal distance, p, of the growth front from the initiating centre.

(2.11) gives the dependence of v on p. But in order to calculate the pyramid gradient, θ, we must also find the dependence of I (initiation rate) on p. We have seen that I is constant for $p > p_o$, and let us assume that it is also constant for $p < p_o$, except at the end of growth (p=0) when it suddenly falls to zero. This is rather a drastic assumption, which at best can only be approximately true. But it is the simplest assumption which can be made, and it is interesting to work out its consequences.

From (2.11) we have:

$$v_r = \frac{dp}{dt} = v_\infty \left(1 - \frac{r_o}{p}\right) \quad ; \qquad (5.10)$$

and from the assumption that I is constant for $p > 0$:

$$\frac{y}{t} \propto I = \text{const.} \qquad (5.11)$$

where y is the vertical height of the growth sheets below the pyramid summit, and the time t is reckoned from the point of initiation of the growth sheet.

Combining (5.10) and (5.11):

$$\frac{dp}{dy} = C\left(1 - \frac{r_o}{p}\right),$$

where C is a constant; and integrating:

$$p + r_o \log (p - r_o) = Cy + \text{const.} \qquad (5.12)$$

This is the theoretical equation of the pyramid profile in terms of the rectangular coordinates p and y. The theoretical curve is shown in Fig. 40 and has two asymptotes: $y = \theta_o p$ and $p = r_o$. The first asymptote corresponds with the observed fact

that θ = constant ($= \theta_0$) for large p.

In comparing the observed and theoretical pyramid profiles it is convenient to use the differential form of (5.12):

$$\frac{dp}{dy} = \frac{1}{\theta_0}\left(1 - \frac{r_0}{p}\right) \qquad (5.13)$$

The variables $\frac{dp}{dy}$ and p can be measured directly from the measured p-y curve (e.g. Fig. 39); and if the theory is correct, the function $\left[1 - \theta_0 \frac{dp}{dy}\right]^{-1}$ plotted against p will give a straight line, which passes through the origin. This graph has been plotted for the α and β slopes of twenty growth pyramids on crystals from several different localities. It was not plotted for the γ slopes, owing to the irregularity of the Υ growth fronts.

The graph of $1 - \theta_0 \frac{dp}{dy}$ $\left[= f\left(\frac{dp}{dy}\right)\right]$ against p for the α slope of Fig. 39 is shown in Fig. 41: to within the accuracy of the measurements it is a straight line passing through the origin. The slope of the line is equal to $\frac{1}{r_0}$, from equation (5.13); and this gives the value $r_0 = (0.9 \pm 0.1) \times 10^{-2}$ cms.

The results obtained for the other growth pyramids are summarised in Fig. 42. In eight cases the $f\left(\frac{dp}{dy}\right) - p$ graph was a straight line for the whole range in which p could be measured. These pyramids, including the one shown in Fig. 38, will be denoted Class I pyramids. In the majority of the remaining cases (Class II pyramids) the graph was linear over

a certain portion only, corresponding to the higher values of p; and in two cases (Class III) the graph was entirely non-linear.

These results indicate that the initiation rate, I, fell to zero more suddenly for Class I than for Classes II and III, so that the theory for the shape of the pyramid profile in terms of p and y is substantially correct, except for small values of p. In particular, formula (2.11) gives a satisfactory relation between the velocity of a step and its radius of curvature.

In table III the values of r_o are tabulated, as measured from the $f\left(\frac{dp}{dy}\right) - p$ graphs of the growth pyramids of Class I.

Table III

Kind of Crystal		$(r_o)_\alpha$ (cms)	$(r_o)_\beta$ (cms)	$(r_o)_\alpha : (r_o)_\beta$
Herkimer County I	Face 1	3.3×10^{-3}	2.7×10^{-3}	1.22
	Face 2	0.9×10^{-2}	—	—
	Face 3	3.1×10^{-3}	2.5×10^{-3}	1.24
Herkimer County II	Face 1	2.0×10^{-4}	—	—
	Face 2	7.0×10^{-3}	5.5×10^{-3}	1.27
Herkimer County III	Face 1	6.2×10^{-3}	4.0×10^{-3}	1.55
Brazilian I	Face 1	1.8×10^{-3}	1.4×10^{-3}	1.32
Brazilian II	Face 1	1.1×10^{-4}	0.8×10^{-4}	1.38
Arkansas I	Face 1	6.2×10^{-3}	4.5×10^{-3}	1.38

$(r_o)_\alpha$ and $(r_o)_\beta$ refer to the distances from the edge to the centre of the critical nucleus in the α and β directions (Fig. 42). If growth takes place by a dislocation, rather than a nucleation, mechanism, $(r_o)_\alpha$ and $(r_o)_\beta$ are defined alternatively as the minimum distances of a screw dislocation from the α, β face edges, for which growth will take place.

In the fourth column of table III the ratio $(r_o)_\alpha : (r_o)_\beta$ is tabulated. The figures give the average value: $(r_o)_\alpha : (r_o)_\beta = 1.34$. From formula (2.6):

$$r_o = \frac{\alpha \phi}{kT \ln \alpha}$$

this ratio is equal to $\varphi_\alpha / \varphi_\beta$, where φ_α, φ_β are the molecular binding energies in the α, β orientations. We have already deduced in Section 6 that $\varphi_\alpha / \varphi_\beta = 1.31$, so that the two values are in good agreement.

In chapter VII the value of r_o is deduced for the growth pyramid of one crystal (Brazilian crystal A) by the method indicated in this section, and an independent, but less accurate, estimate is obtained by another method. The two values are of the same order.

8. Localisation of Initiating Centres.

The summits of the growth pyramids are the positions at which new growth sheets are initiated. If the same initiating

centres are active throughout the growth of the whole crystal, they will probably be clustered round the centre of the finally developed faces. No such clustering was observed on natural quartz crystals, and it therefore appeared that the initiating centres were individually active for only relatively short periods in the history of growth of the crystal. It is shown in Part IV that this was certainly true for synthetic quartz crystals.

For this reason it was difficult to arrive at any general conclusions concerning the localisation of the initiating centres. But two isolated observations, (a) and (b), can be mentioned -

(a) The initiating centres had a distinct tendency to develop along an edge (Figs. 22, 44) or at a corner (Fig. 26) of the face. This was also characteristic of the r faces of natural crystals and the R faces of synthetic crystals.

This result cannot be explained by either the two-dimensional nucleation theory or the dislocation theory, for both predict nucleation at the centres, rather than the edges and corners, of the face. Thus according to Kossel[68] the energy of formation of a two-dimensional nucleus is least at the centre of the face, and according to Frank[69] dislocation lines are under tension and tend to emerge normal to the face i.e. towards the face centre. A possible explanation of the edge and corner nucleation in quartz is obtained by considering

the effect of adsorbed impurities on the growth process. These adsorbed molecules will either be pushed along the face by the expanding growth sheets, or grown over, by the sheets and incorporated in the lattice as impurity. In the former case the foreign molecules will be pushed to the edge of the face, and there becomes trapped by the sheets expanding from the adjacent face. In this trapped position they can behave as nuclei for the inception of new layers. There is the further possibility that the molecules are pushed along the edge to the corner of the face, and in this case corner nucleation will occur

(b) The initiating centres were frequently localised in straight lines (Figs. 26, 45). The orientation of these straight lines with respect to a fixed direction (e.g. prism edge) was found to vary over a wide range of angle; but in several cases the line had an orientation in the relatively narrow range 38°- 42° from the prism edge (e.g. Fig. 26).

This time the phenomenon can be interpreted on the basis of the dislocation theory, for groups of dislocations are associated with 'lineage' and 'mosaic' boundaries, and so will often occur in straight lines. Griffin(70) has shown experimentally that linear arrays of screw dislocations occur in natural beryl. The interpretation assumes the existence of screw dislocations in the quartz lattice. Evidence for this is given in a later chapter (chapter 7).

The 38°- 42° range in quartz can be explained if we

consider the effect on growth of the partial cleavage parallel to the $(10\bar{1}1)$ planes. Tolansky and Bardsley[71] have induced limited slip in this place by means of piezo-electric stress, and it therefore seems possible that it can also be produced during growth by the stresses which are associated with the growth process itself. Evidence for the occurrence of slip during growth is given in chapter 7, and also in Fig. 46, which is a multiple-beam picture of the natural prism face of a Herkimer County crystal. The fringes show that slip has taken place in several narrow zones, (marked by arrows), and the direction of the slip is parallel to the line of intersection of the face with a major rhombohedral plane. According to the dislocation theory limited slip parallel to these planes will give rise to a linear array of screw dislocations on the R face, and the direction of the array is at 41° to the prism edge.

MOS

Part III Chaps 6, 7. 8

and Part IV Chaps 9, 10.

Chapter VI.

GENERAL TOPOGRAPHICAL FEATURES OF r FACES.

1. Introduction.

The general topography of the minor rhombohedral faces is very similar to that of the R faces. It can again be described in terms of low growth pyramids, which are produced by the successive spreading of triangular layers from a small number of initiating centres. The properties of these growth layers and pyramids will be described in a similar way as was adopted for the R faces; but the description will be much more brief, as the general principles underlying the growth process (layer deposition, bunching etc.) apply in exactly the same way. Only differences in behaviour of the two kinds of rhombohedral face will be explained.

2. Geometry of Growth Fronts.

Figs. 47 and 48 are multiple-beam interferograms of the minor rhombohedral faces of two right-handed Herkimer County crystals. The dispersion is the normal geographic dispersion, so that the fringes have the same shape as the growth fronts. The growth fronts are triangular, but are more irregular and possess a greater curvature than the growth fronts on the R faces.

An interferogram (geographic dispersion) of a left-handed crystal is shown in Fig. 49. The orientation of the growth fronts with respect to the face edges is approximately

the same for right-handed as for left-handed crystals, and, unlike in the case of the R faces, the hand cannot be determined from the growth sheet orientation. Nevertheless, comparison of Figs. 47 and 49 shows immediately that the hand can be determined from the direction of the vicinal edge running upwards from the summit of the growth pyramid. This method of determining the hand of an r face was first noted by Kalb(5).

It was shown in the preceding chapter that the Burton formula:

$$e/p = 1 + \tfrac{1}{4} \exp\left(\frac{2w}{kT}\right)$$

fails to give a reliable value of ϕ or T from the measurement of e/p, but that it will give an indication of the relative change of the binding energy, ϕ, with orientation. It was concluded that the formula must be applied in the modified form:

$$e/p = 1 + \tfrac{1}{4} \exp\left[\frac{\phi}{kT} f(\sigma)\right], \quad (5.4)$$

where $f(\sigma)$ is an unknown function of the supersaturation,, The ratios $(e/p)_{\alpha'}$, $(e/p)_{\beta'}$, $(e/p)_{\gamma'}$, were measured on several crystals in the three directions α', β', γ' (Fig. 47a) of minimum growth rate, and the results are tabulated in table IV.

Table IV

Type of Crystal.		$(e/p)_{\alpha'}$	$(e/p)_{\beta'}$	$(e/p)_{\gamma'}$	$\phi_R : \phi_r$
Herkimer County I	Face 1	18	14	4	1·18
	Face 2	15	13	5	1·17
	Face 3	18	—	4	—

Table IV continued.

Type of Crystal.		$(e/p)_\alpha$,	$(e/p)_\beta$,	$(e/p)_{\beta'}$,	$\phi_R : \phi_r$
Herkimer County III	Face 1	18	–	–	
Brazilian II	Face 1	17	14	6	1·22
	Face 2	18	14	4	1·24
Brazilian III	Face 1	10	–	3·5	–

Comparison with table I shows that the e/p values are considerably less for the r faces compared with the R faces. This can be interpreted by the above formula (5.4) as indicating that

$$\phi_R > \phi_r$$

where ϕ_R, ϕ_r are the mean molecular binding energies of the molecules in the R, r planes.

In order to estimate the ratio $\phi_R : \phi_r$ from formula (5.4) it is necessary to determine the average values of for a number of growth pyramids on the R and r faces of the same crystal; and to assume that the unknown term $f(\sigma)$ is, on the average, the same for all the growth pyramids. The value of $\phi_R : \phi_r$ calculated in this way is given in column 5 of table IV, and leads to the result:

$$\frac{\phi_R}{\phi_r} = 1.20$$

An independent method of calculating $\phi_R : \phi_r$ has been indicated by Saksena[67]. Saksena calculated the cleavage energies of the R, r planes by finding the number of Si-O bonds per unit area which cross these planes. His results are given

in the following table, which is quoted from his original paper*.

Table V.

Type of plane.	Equation of Plane.		Number of Bonds cut per unit area.
r (Inverse Rhombohedron)	$x + \frac{y}{\sqrt{3}} + \frac{z}{1.1}$	= 3.3	$5/1.4a^2$
		2.8	$3/1.4a^2$
		1.85	$3/1.4a^2$
R (Primary Rhombohedron)	$x + \frac{y}{\sqrt{3}} - \frac{z}{1.1}$	= 2.8	$1/1.4a^2$
		1.85	$7/1.4a^2$
		1.38	$7/1.4a^2$

The table shows that the number of bonds cut per unit area have any one of three values, corresponding to three different positions of the intersecting plane with respect to the atoms in the unit cell. Saksena was concerned in calculating the cleavage energies of the R, r planes and assumed that this was given by the smallest number in column 3, thus leading to

$$\frac{\text{Cleavage Energy R plane}}{\text{Cleavage Energy r plane}} = \frac{1}{3}.$$

For our present purpose, however, we require the binding energy, rather than the cleavage energy, of the R, r planes, and the binding energy is more likely to be given by the average number in column 3. On this assumption Saksena's figures give:

$$\frac{\phi_R}{\phi_r} = 1.35$$

This is only in fair agreement with the value of 1.20 quoted

above from the measurements of ϱ/ρ, but the discrepancy is hardly surprising in view of the approximations made in both determinations.

It is well known that the R faces of quartz are in general, more developed than the r faces (Fig. 12). Saksena (loc.cit.) has attempted to explain this on the basis of the (calculated) smaller surface energy per unit area of the R faces, compared with the r faces. This conclusion, however, is incorrect as the habit of quartz, and of crystals in general, is determined by the relative rates of growth of the different faces, and not by equilibrium considerations. This principle was clearly stated by Willard Gibbs[72] as long ago as 1878. Thus the greater development of the R faces of quartz indicates that they grow at a slower rate than the r faces. Recalling formulae (2.5) and (2.10), which give the dependence of growth rate on the binding energy ϕ for growth from two-dimensional nuclei (2.5) or dislocations (2.10) and remembering that the molecular steps on the R, r faces are of equal height, we obtain:

$$\phi_R > \phi_r$$

This is the same result as obtained previously from the measurements of ϱ/ρ.

3. Other Properties of Growth Fronts.

The bunching effect on the r faces is shown by the interferograms, Figs. 50 and 51. Fig. 50 is taken at the normal geographic dispersion and shows the shape of the growth pyramid,

and Fig. 51 is taken at a suitable dispersion to show the increase of height of the growth fronts in the α' and β' directions, as they recede from the pyramid summit.

Examination of several other Herkimer County crystals revealed that the bunching was generally more severe than indicated by Fig. 51. Thus in Figs. 49 and 52 the growth fronts shortly after initiation are only several molecules high, but on moving away from the initiating centre they close together to form high and irregularly shaped bunched growth fronts. The growth fronts on the R faces are only rarely as high and irregular in outline as those shown in these two figures.

Examination of Fig. 52 shows that the irregularity of the growth fronts appears to be connected with the inhibiting action of the edge of the face on the spreading of the layers. The growth fronts have been delayed at certain points along the face edge on the left, and the layers have subsequently surrounded these points and formed shallow depressions. A similar example of this effect is shown along the face edge on the left of Fig. 47.

An explanation of the effect is that impurity molecules are pushed to the edge of the face by the expanding layers and become trapped there. They can then cause a delay in the rate of spreading of the growth layers either directly, or indirectly by giving rise to lattice imperfections at the face edge. It is odd, however, that no evidence for this kind of behaviour was

discovered on the numerous R faces studied, apart from the indirect evidence from initiation of growth sheets at the face edge, (Section 8, Chapter 5). In particular the R faces adjacent to the r faces in Figs. 47 and 52 showed no trace of the effect.

Another phenomenon observed on the r faces was 'kinking' of the growth fronts along the vicinal edge between the β' and γ' directions. This is illustrated in Figs. 47 and 50. In other cases (e.g. Fig. 48) the growth fronts were quite smooth along this vicinal edge. The equilibrium shape of the growth fronts is determined by the condition of minimum free energy per unit length. Hence, although the origin of the kinking is unknown, its presence shows that the shape of the growth front is determined by kinetic, rather than equilibrium, considerations.

Owing to the general irregularity of the growth fronts it was not possible to make precise measurements of the angle between the risers and upper plane surfaces of the growth sheets. Nevertheless, the multiple-beam fringes were continuous over the growth fronts and χ appeared to be of the same order as for the R faces. If the theory given in Chapter 5 for explaining the low value of χ is correct, this indicates that the mean distances of diffusion of adsorbed molecules on the R and r faces are of the same order.

4. Properties of Growth Pyramids.

It was found that the pyramid gradient increased in the neighbourhood of the pyramid summit, in the same way as for the R faces. Measurements indicated that in general the equation of the pyramid profile in terms of the rectangular co-ordinates p and y (Fig. 41) was approximately the theoretical equation:

$$p + r_0 \log (p - r_0) = Cy + \text{const.} \qquad (5.12)$$

where r_0 (the radius of the critical nucleus) was of the order of 3×10^{-3}cms. It was not possible, however, to check the theoretical equation to the same degree of accuracy as for the R faces, owing to the greater irregularity of the growth fronts.

In a few cases the equation (5.12) was entirely disobeyed, and one such case is illustrated in Fig. 53. The summit of one of the growth pyramids on this face appears to be located at the lower left-hand corner of the face. The gradient of this pyramid is exceptionally small in the neighbourhood of its summit, and <u>increases</u> further away from the summit. The pyramid is so flat near the face corner that the multiple-beam fringes have in part spread out to form sensitive-tint fringes. This was the most plane area of the numerous rhombohedral faces examined in the course of this work.

The phenomenon of edge nucleation, or the localisation of pyramid summits along the face edge, is shown in Fig. 54. This phenomenon was previously observed on the major rhombohedral faces (Chapter V), and the same arguments for its occurrence apply as were given in that chapter.

Chapter VII.

TOPOGRAPHICAL FEATURES OF SELECTED CRYSTALS.

1. Circular Growth Sheets.

In the previous two chapters the general topographical features of the rhombohedral faces of natural crystals have been described. The present chapter is concerned with a description of particular topographical features shown only by a few selected crystals.

Examination of over thirty Herkimer County crystals showed that the growth sheets on the rhombohedral faces were invariably orientated, i.e. triangular. This was also true of the crystals from the other localities, with the exception of the Brazilian crystals, which occasionally possessed circular growth sheets. Thus Fig. 55 is a Fizeau picture showing the presence of numerous pyramids of approximately circular symmetry on the R face of a Brazilian quartz. These circular pyramids, or growth cones, have previously been observed by Griffin[59] on the R faces of quartz. We can infer that the growth sheets are circular, although the individual growth fronts could not be resolved under the microscope. Growth cones have been observed on several crystals, and were distinguished by the following features:

(i) The gradient of the cones was considerably larger than the gradient of the orientated growth pyramids of other crystals.

(ii) The cones were sometimes surmounted by a sharp protuberance easily visible under the microscope (Fig. 10; also Griffin,[59]) This was quite different from the gradual increase of gradient of orientated growth pyramids near the pyramid summit. The latter was not visible under the microscope, and could only be detected by interferometry.

In a large aggregate of crystals embedded in the same matrix growth cones had developed on the R and r faces of all the crystals. This indicated that the condition for circular symmetry was connected with the external conditions of growth (e.g. temperature and supersaturation).

As the circular growth fronts could not be resolved under the microscope little direct information concerning their behaviour could be obtained. It will be seen in Part IV, however, that circular growth sheets develop on synthetic crystals grown under certain known conditions, and the circular growth fronts are occasionally visible under the microscope. Further discussion of this type of behaviour will therefore be deferred until Part IV.

2. Brazilian Crystal A.

Molecular steps were not observed on quartz, and the failure to do so was probably connected with the following reasons:

(a) The steps were too small (3Å) to be detected with the available phase-contrast equipment.

(b) Owing to the bunching of the steps into groups, the distance between adjacent steps in a group (200Å) was too small to allow of lateral resolution under the microscope.

Nevertheless, the growth fronts on the R face of one crystal (Brazilian A) were all of uniform height (110Å), and it was possible in this case to trace the polymolecular growth fronts round the initiating centre and to determine whether the fronts were of closed or spiral form. Fig. 56 is a photomicrograph of the growth fronts in the α direction. They are slightly irregular; and as the direction of decreasing slope is vertically downwards in the photograph, careful inspection indicates that the irregularity is probably due to deposition of (foreign) material along the steps after growth had stopped. The growth fronts were uniformly spaced, so that the natural face behaved as an echelon grating. Two diffracted spectra could be observed with white light, and from the angular positions of these spectra an approximate height of the growth fronts of 100 - 150Å was calculated. More accurate measurement by Fizeau fringes (Fig. 57) and fringes of equal chromatic order (Fig. 58) gave $H = 110Å \pm 5Å$. This latter value was calculated from the measurement of the surface angle between the adjacent vicinal faces.

Fig. 59 is a photomicrograph of the growth fronts near the summit of the growth pyramid. The photograph is not good, as the irregularity of the growth fronts is particularly marked in this region, but careful tracing of the growth fronts round the initiating centre reveals that they are in the form of a spiral with two separate branches. The accompanying diagram, Fig. 60, has been drawn from Fig. 59, and illustrates the behaviour more clearly.

The spiral growth front indicates that growth has taken place from a group of screw dislocations with combined Burgers vector[73], normal to the face, equal to 220Å. Similar multimolecular growth spirals have been observed by Forty[30] on cadmium iodide.

An estimate of r_0, the size of the critical nucleus, can be obtained from formula (2.18): page 24

$$r_0 = \frac{a}{4\pi\theta} \cdot \frac{S}{\left(1 + \frac{L}{2\pi r_0}\right)},$$

giving the relation between r_0 and the pyramid gradient, θ, for the case of growth from S dislocations in a line of length L. Substituting Sa = 220Å, $\theta = 1.6 \times 10^{-3}$ rad. and $L \leqslant 2.10^{-4}$cms. from Fig. 59 gives:

$$0.8 \times 10^{-4}\text{cms} < r_0 < 1.1 \times 10^{-4}\text{cms}.$$

An independent estimate of r_0 was obtained from the pyramid profile by the method given in Section 7 of Chapter V. This estimate was $r_0 = (1.1 \pm 0.2) \times 10^{-4}$cms. The two values

of r_o are therefore in satisfactory agreement, and it is important to note that only one of the estimates depends upon the assumption of a dislocation mechanism of growth. The dislocation theory therefore not only account for the spiral nature of the growth fronts, but also accounts for the observed pyramid gradient, θ (given by formula (2.18) with r_o, L and Sa known).

A rough estimate of the supersaturation, σ , of growth for Brazilian crystal A can be obtained by applying the formula (2.6):

$$r_o = \frac{a\phi}{kT \ln \alpha} = \frac{a\phi}{kT\sigma} \text{ , for } \sigma \text{ small.}$$

Substituting $\frac{\phi}{kT} = 4$, a = 3.3Å and $r_o = 10^{-4}$cms. gives $\sigma = \frac{1}{10^4}$. This is a very small value for the supersaturation, but it must be remembered that it is the value which prevails at the end of growth, and is therefore probably near the critical value at which growth stops.

It has only been possible to obtain conclusive evidence of growth from screw dislocations in the case of this single crystal. If we assume, however, that all natural crystals grow by a similar mechanism, the bunching effect can be tentatively explained as follows.

The main factor of the bunching process on the R faces are:

(i) The growth fronts shortly after initiation are in general less than 50Å high.

(ii) These growth fronts spread across the face at slightly different velocities, so that the faster ones catch up the slower ones in front and produce bunched steps.

(iii) The bunching process ceases after the steps have attained a maximum height H_o, which is generally of the order of a few hundred Å.U.

(iii) indicates that the molecular layers are initiated in groups, each group containing $n_o = H_o \div a$ layers. Thus the initiation of fresh molecular layers appears to be a periodic process, and this rules out the possibility of bunching arising from the deposition of a uniform layer of impurity over the face during growth.

The periodic initiation of layers follows naturally from the dislocation theory, applied to growth from a large number of screw dislocations, all of the same hand. In Fig. 62 a group of five dislocations of the same hand is represented by A, B, C... and their associated molecular steps by AA', BB', CC'... The growth process consists of a rotation of the molecular steps round the central dislocation group and is thus a periodic process. The successive groups of five steps which are produced at each successive rotation are represented by A", B", C"..., A"', B"', C"'... The dislocations A, B, C... will be in general non-uniformly spaced, so that the steps within each group will also be non-uniformly spaced, although the groups themselves will be equally spaced apart. As the

molecular layers spread across the face the differences in spacing within each group will lead to difference in step velocity within the group, the reason being that more solute will diffuse through the solution to the rear steps of relatively closely spaced steps than to the front steps. Thus in Fig. 62 the steps will bunch together into groups of five (Fig. 62b). In the general case the steps will bunch together into groups of n' molecular steps, where n' is the number of dislocations at the initiating centre, which 'cooperate' with one another, i.e. are separated from one another by distances of less than 2 r_o.

3. Brazilian Crystal B.

This was an exceptionally large and well-developed crystal and the face of particular interest was a major rhombohedral face, approximately 50 sq. cms. in area. Fig. 63a is a photograph of a small area of this face, showing the α and β growth fronts which have spread from an initiating centre below the figure. The α fronts are continuous, but the β fronts are discontinuous along the diagonal black line. The corresponding two-beam interferogram, Fig. 63b, shows that this line is a step on the surface, whose height varies between 0 and 950Å. The line makes an angle of 40° with the prism edge of the face and is therefore within 1° of the line of intersection of the face with an adjacent R plane.

It is well known that the R planes of quartz are

planes of partial cleavage [74], and we can conclude that the diagonal straight line in Fig. 63a is a slip line. Moreover, the slip line terminates on the surface at both ends. The termination of the line at the lower end is shown more clearly in the photograph Fig. 63c. The termination at the upper end has led to several growth fronts terminating on the surface. The points on the surface where the slip line terminates, and the points where the slip step changes height, must mark the points of emergence of screw dislocations.

It appears that the slip occurred towards the end of growth, as otherwise the slip step would have been filled in by the expanding sheets. Fig. 63a shows that cross-linking of the growth fronts has taken place in the direction shown by the arrow, as a result of slip.

If limited slip had taken place an appreciable time before the end of growth, the line of screw dislocations along the slip direction would have acted as initiating centres for further growth. This is the explanation of linear occurrence of initiating centres in a direction at 40° to the prism edge, which was previously given in Section 8, Chapter V.

The growth fronts in Figs.63a and c are approximately 3200Å high, i.e. they are several times higher than the slip step, although they appear to be less visible. The reason for this reduced visibility is that the growth fronts are of the

low-angle type (see Section 5, Chapter V), whereas the slip line is presumably an abrupt step.

The two crystals, Brazilian A and B, are the only natural crystals for which direct evidence for the existence of screw dislocations has been obtained.

4. Arkansas Crystal A.

A minor rhombohedral face of this crystal showed an interesting phenomenon, which has also been observed on several other crystals. Under the naked eye the face had a rippled appearance, giving the impression of the presence of growth fronts, at least a wavelength high. Microscopic observation showed, however, that these 'growth fronts' were actually groups of growth fronts, with approximately twenty fronts in each group.

Fig. 64 is a photomicrograph of the r face, showing the growth fronts which have spread from the pyramid summit on the right. Near the summit the individual growth fronts can only just be detected, whereas the groups of growth fronts are clearly visible. This region, marked A in Fig. 64, corresponds to the multiple-beam picture Fig. 66. The growth front direction in Fig. 66 is approximately vertical, and the picture shows the division of the growth fronts, which are individually less than 100Å high, into three separate groups. Further away from the pyramid summit in Fig. 64 the individual

growth fronts are more visible, and the corresponding interferogram Fig. 65 shows that the growth fronts are now at least 200Å high. The pyramid profile, shown in Fig. 67, has a rippled or undulating form.

It appears that there were two independent periodic processes in operation during the growth of this face. The first (bunching process) gave rise to the generation of molecular growth layers in groups, and the layers in each group subsequently bunched together into growth fronts approximately 200Å high. The second, of longer period, gave rise to a grouping of the bunched growth fronts, so that the combined height of the groups of growth fronts was of the order of one wavelength. This second process led to the undulating nature of the pyramid profile. It is possible that it was connected with a periodic variation of the supersaturation at the initiating centre.

Chapter VIII

PRISM FACES AND FACES OF TWINNED CRYSTALS.

The prism faces of natural crystals are usually less well-developed than the rhombohedral faces, and are not very suitable for study with sensitive interference techniques. Furthermore, the faces are frequently striated in a direction perpendicular to the triad axis, and a heavily striated face is too rough for detailed study.

An interferometric survey of five prism faces of a crystal from the Rhone Glacier was undertaken by Griffin(59). Griffin observed bunching of steps; and also what he termed surface "buckling", i.e. a variation of height of the bunched steps along their length, leading to a buckling of the surface.

Buckling has been observed on a Madagascar crystal, the step height varying between 500Å and 1200Å in a linear distance of 5mms. The presence of buckling indicates that the successive planes of growth layers are not strictly parallel. It was shown in Part 2, Chapter V that there was no evidence for a similar distortion of the growth layers on the rhombohedral faces. Thus the more perfect development of the rhombohedral faces may be connected with the absence of layer distortion.

Investigation of several prism faces of Brazilian and Madagascar crystals revealed that the growth fronts had the shape of a parallelogram (Fig. 68). The two opposite sides

AB and CD, perpendicular to the triad axis, were considerably longer than the other two sides. These facts are illustrated by the photomicrograph, Fig. 69, of a Madagascar crystal. The upper horizontal line is the boundary between the adjacent prism faces and the lower horizontal line is a Dauphine twin boundary. Growth sheets have spread from these two boundaries, and formed numerous tetrahedral growth pyramids centred on the boundaries. This face appeared to be striated when viewed with the naked eye.

The elongation of the growth fronts in a direction perpendicular to the triad axis indicates that the growth rate on the prism face is greater in a direction perpendicular than parallel to this axis. This differential growth rate leads to a relatively steep gradient in the triad axis direction (Fig. 68.). Thus the long, steep ridges, or striations, which can be seen by eye are the opposite sides of tetrahedral growth pyramids, and arise as a result of the different growth rate parallel and perpendicular to the triad axis.

Fig. 70 is a photograph of the tetrahedral pyramids on a second crystal. This face was more severely striated than the one shown in Fig. 69, and again indicated that the striations were due to the development of tetrahedral growth pyramids.

It is generally believed however, that the prism striations on quartz arise instead from an "oscillatory development" of adjacent prism and rhombohedral faces. This is the

"oscillatory combination theory" (Dake, Fleener and Wilson[75]). This theory requires the angle of inclination between the side of the striation and the prism plane to be 38°, whereas interferometric measurement showed that it was at most 7° for the face shown in Fig. 69. Further, observations on synthetic crystals showed that the growth fronts on the prism faces were in general circular, and that no striations could be seen. There appears to be no reason why the symmetry of the growth sheets should affect the development of striations according to the oscillatory-combination theory.

Thus, although there is considerable evidence[75] for the oscillatory development of rhombohedral and prism faces on some crystals, it appears that this is not the correct reason for the development of striations on well-developed crystals. It can be concluded that striations occur in most natural crystals as a result of the development of tetrahedral growth pyramids, and that occasionally the striated appearance is accentuated by the oscillatory development of adjacent faces.

Observations on twinned R and r surfaces (Dauphine and Brazilian twins) showed that the separate twinned portions grew independently from separate centres of initiation. The growth sheets from one twinned portion spread to the twin boundary but no further. It has been suggested by Miers[57] that there is a small rotation of the lattice of one twinned

portion with respect to the lattice of the neighbouring portion, but no evidence for this was obtained from the several twinned crystals examined. Thus it was found that when the multiple-beam fringes were adjusted parallel to the growth fronts of one twinned portion of the rhombohedral face, they were also parallel to the growth fronts on the remainder of the face.

Localisation of initiating centres along the twin boundary was frequent (Figs. 71, 72). This is a well-known feature of the growth of several twinned crystals (e.g. fluorite). The twin boundary is a favourable position for initiation of growth sheets as (a) the binding energy is smaller at the boundary step, and (b) impurities tend to be trapped at the boundary.

Chapter IX.

SEEDS WITH SMALL AMOUNT OF SYNTHETIC GROWTH.

1. Introduction.

The first successful attempts to grow large synthetic quartz crystals were reported by Spezia[76] at the beginning of this century. Spezia used a silver-lined bomb containing a solution of sodium metasilicate. In the upper part of the bomb he placed a silver basket containing fragments of broken quartz, and just below this he suspended the seed crystals of natural quartz. The temperature was 330°C in the upper part of the bomb, and fell to 200°C in the lower part. The quartz fragments were dissolved at the higher temperature, and re-deposited on the seed crystals at a slightly lower temperature. The rate of growth was of the order of 1cm. in 100 days.

During the 1939 - 45 war Nacken in Germany developed a different technique employing vitreous silica as the nutrient material. In the neighbourhood of the critical point of water vitreous silica is about ten times more soluble in water than α - quartz. Thus it is possible to obtain growth under isothermal conditions by producing a solution which is undersaturated with respect to the vitreous silica and supersaturated with respect to the seeds of natural quartz. In this method the rate of growth is at first rapid; but then decreases and eventually falls to zero, owing to crystallisation of vitreous

silica in situ. For this reason the temperature-gradient method of Spezia is now generally preferred; and further progress in growing synthetic quartz has been reported by Van Praagh[77], and by workers at the G.E.C. Laboratories, England[78] and the Bell Telephone Laboratories, U.S.A.[79], who have developed Spezia's original technique.

The surface topography of several synthetic crystals grown at the G.E.C. Laboratories by the temperature-gradient method has been studied interferometrically. The crystals examined were of two types:

(a) Natural seed crystals with a small amount (several wavelengths) of synthetic growth.
(b) Seed crystals with several cms. of synthetic growth.

The results on the (a) crystals will be described in this chapter, and on the (b) crystals in Chapter X.

2. Surface Topography and Thickness of Synthetic Growth.

Six (a) crystals were investigated. They possessed different average thicknesses of synthetic growth from a small fraction of a wavelength to approximately ten wavelengths. The seeds were thin layers cut parallel to the major rhombohedral face, and were ground on both sides.

Fig. 73 is a multiple-beam interferogram of the seed with the smallest amount of synthetic growth. Several

isolated nuclei of synthetic growth have developed on the original ground surface, which is represented by the broad striated fringes. The small triangular markings are etch pits, which were probably formed at the end of growth. The fringes are not at the geographic dispersion and therefore do not give the true shape of the synthetic nuclei, or pyramids.

The next stage of growth is represented by Fig. 74, which is an interferogram taken in transmitted light of a seed with an average thickness of synthetic growth of half a wavelength (2500Å). The isolated nuclei in Fig. 73 have developed into pyramids several wavelengths high, and growth has taken place in addition from numerous smaller nuclei over the remainder of the face. The existence of these smaller nuclei is revealed by the orientation of the background fringes. The fringes are approximately orientated in three directions, corresponding to the direction of the three sides of the growth pyramids.

Fig. 75 is a photomicrograph of a crystal with slightly more synthetic growth. One pyramid has spread over a relatively large area of the face, and growth sheets edges can be detected on this pyramid. The outlines of the pyramids and of the growth sheets are not of the same shape, indicating that the original ground surface of the seed was not exactly parallel to the $(10\bar{1}1)$ lattice plane.

It appears from Figs. 73 - 75 that two types of growth pyramids develop in the intitial stages of synthetic growth. Type A pyramids are developed first and grow faster than the type B pyramids, which are more numerous and develop later. As growth proceeds the A pyramids spread over the whole face and cover the B pyramids, which are thus rendered inactive. Figs. 76 and 77 are the photomicrograph (with oblique illumination) and corresponding transmission multiple-beam interferogram of a crystal with an average thickness of synthetic growth of 1.5 microns. The A pyramids have extended over the whole face, and there is now no trace of the pyramids of type B.

Interferometric observations can shed no further light on the distinction between the A and B pyramids, and for the present one can only speculate on the reason for this distinction. It is possible that the A pyramids developed from screw dislocations, whereas the B pyramids grew by two-dimensional nucleation. This suggestion accounts for the development of the A pyramids first and also for their more rapid growth, as the activation energy for growth from a two-dimensional nucleus is considerably larger than that for growth from a screw dislocation (Chapter II).

It will be shown in the next chapter that seed crystals with several cms. of synthetic growth grow from a relatively small number of nuclei - of the order of 10/sq.cm. Thus in the growth of synthetic crystals, the density of

growth nuclei is high (10^4/sq.cm.) in the early stages of growth, but rapidly falls as the B pyramids become inactive, and falls even further until eventually growth continues from only a small proportion of the original A pyramids. A factor, which will lead to this progressive de-activation of growth nuclei, is illustrated by the diagram, Fig. 78 a, b. Imagine two growth pyramids P and Q (Fig. 78a) shown in profile and whose gradients are θ_P and θ_Q. Let S_P and S_Q be the summits of the pyramids. In general the supersaturation will vary over the surface and the growth sheets will spread at different velocities from S_P and S_Q. Let us suppose that the growth sheets from S_P spread faster than those from S_Q, so that eventually the boundary of pyramid P reaches the position S_Q (Fig. 78b). When this occurs, growth cannot continue from Q unless $\theta_P = \theta_Q$. If $\theta_P = \theta_Q$ molecular steps cannot spread from Q as their radius of curvature will be smaller than the radius of the critical nucleus, r_o.

Fig. 79 is a photomicrograph of the R face of a crystal with 0.02mms. of synthetic growth. The synthetic layer was deposited at a comparatively large growth rate, and the synthetic surface is less well-developed than that shown, for instance, in Fig. 76. In Fig. 79, a radial structure can be seen, which has spread from the summit of each growth pyramid. As the pyramid summits are the initiating centres for growth, this radial structure appears to be the two-dimensional counterpart of the lineage structure postulated by Buerger: according

to Buerger[80] many crystals develop a lineage structure, which radiates outwards from the nucleus of growth.

Chapter X.

LARGE SYNTHETIC CRYSTALS.

The second type (B) of synthetic crystal studied were those which possessed a considerable thickness, of the order of several mms. of synthetic growth. The major rhombohedral faces of these crystals were studied by two-beam and multiple-beam interferometry. Several photographs shown in this chapter were taken on replicas of the R faces, using the ultraviolet perspex technique described in Chapter IV. The r and m faces of these crystals were in general severely etched, and the growth features were almost obliterated. Consequently the R faces only were examined.

Fig. 80 is a photomicrograph, taken with oblique illumination, and Fig. 81 a two-beam interferogram of typical areas on an R face. The growth pyramids have approximately circular symmetry, i.e. they are growth cones, and at the summit of the cone there is a distinct protuberance. In addition to the large growth cones there are a much greater number of small cones, which can easily be seen in Fig. 80. They lead to the rippled appearance of the fringes in Fig. 81.

The presence of growth cones indicates that the growth sheets are circular. It is only rarely that the growth fronts can be observed under the microscope. Photographs of the growth fronts are shown in Figs. 82 - 84, and in each case

the circular fronts appear to spread from an initiating centre which lies close to the face edge.

It is difficult to account for the development of circular sheets on these crystals in contrast to the orientated sheets on the synthetic crystals of type A, as both kinds of crystal grew at different concentrations but at approximately the same temperature, 360°C. According to Burton, Frank and Cabrera[23] the growth sheets will be circular if $x_s > x_o$, where x_s is the mean distance of diffusion of adsorbed molecules and x_o the mean distance between Frenkel kinks; and polygonal if $x_s < x_o$: We expect x_s and x_o to vary with temperature, but to be independent of the supersaturation. A possible explanation of this difficulty is that the surface diffusion current in the growth of the B crystals was relatively unimportant compared with the direct diffusion current through the solution. In this case, even if $x_s < x_o$, we will expect the growth sheets to be circular.

The steep rise in gradient of the growth cones in the neighbourhood of their summit indicates that the ratio:

$$\frac{\text{rate of initiation of growth sheets}}{\text{rate of spreading of growth sheets}}$$

increases suddenly towards the end of growth. The supersaturation of the solution rises at the end of growth, when the heating current is switched off and the solution begins to cool. According to the dislocation theory of growth[23] the above ratio is proportional to the supersaturation, and the theory

will therefore account for the observed nature of the summits of the growth cones.

A similar explanation will apply to the development of protuberances on the summits of the growth cones of natural crystals (Section 1, Chapter VII). Natural crystals will cease growing either when the solution is exhausted, or when the metastable limit for growth is attained. If the temperature of growth suddenly falls, the supersaturation will rise and the pyramid gradient increase, until the metastable limit is reached.

An attempt was made to verify the prediction of the dislocation theory that the gradient of the growth pyramids is proportional to the supersaturation. The gradients of the pyramids on six crystals grown at different supersaturations were measured, and the results indicated that the gradient increased with supersaturation. It was not possible to obtain a precise relationship between gradient and supersaturation, as (a) the calculations of the supersaturation were only approximate, and (b) the gradient of the individual growth pyramids on the same face were not the same, and it was therefore necessary to take a mean value. Furthermore, it is possible that the supersaturation varied over the surface of the growing crystal, in spite of the efficient stirring provided by convection currents induced by the temperature gradient.

As growth fronts could rarely be detected on the faces of the synthetic crystals, they must be in general of

smaller height than the growth fronts on natural crystals. Thus, if bunching occurs, the ultimate height H_0 of the growth fronts on the synthetic B crystals is less than that on natural crystals. This is to be expected on the theory of bunching given in Section 2, Chapter VII. The supersaturation for the growth of the B crystals was of the order of 3%, and therefore considerably higher than the value of 1/10% previously estimated on natural crystals. Thus the radius of the critical nucleus, r_0 ($= a\phi/kT\sigma$) is smaller for the B crystals; and the corresponding number of screw dislocations, which are within a distance $2\pi r_0$ of each other and can co-operate with one another and produce a bunched growth front, is therefore less.

Fig. 85 is a two-beam interferogram of the face shown in Fig. 84. It shows that the circular growth fronts in Fig. 84 are several wavelengths high and of the low-angle type. The angle χ between the risers of the growth fronts is of the order of 10^{-2} radians of arc. Applying the formula (5.1):

$$\chi = \frac{a}{2x_s},$$

we obtain $x_s = 50a$. This is rather higher than the value $x_s = 30a$, which was previously estimated for several natural crystals.

Several steps in Fig. 84 appear to terminate on the surface and this is confirmed by Fig. 85. In several cases circular pits are located at the points of termination of these steps. These points must represent the points of emergence

of screw dislocations of exceptionally large ($\sim 10^4$ Å) Burgers vector.

A large growth cone is shown in the interferogram, Fig. 86, together with numerous smaller cones. A similar development of small growth cones has already been noted in Fig. 80. The height of the small cones in Fig. 86 is a few wavelengths, and this is the same height as the protuberance at the summit of the large pyramid. It therefore appears that the protuberance and the small cones were developed simultaneously at the end of growth, after the supersaturation began to rise. Thus, although growth initially takes place from a large number of nuclei and most of these subsequently become inactive, the density of growth nuclei rises again if the supersaturation of the solution is increased.

A final point of interest on the synthetic B crystals is illustrated by the two-beam interferograms Figs. 87 and 88. Steps have developed on these faces parallel and close to the edges of the face. The presence of these steps indicates that the growth fronts have been partly held up along lines parallel to the face edges. These lines may have originally marked the position of the face edges, and in this case the obstruction to the spreading of the sheets could have arisen from the presence of impurities trapped along the face edge. The holding up of sheets has been so severe in Fig. 87 that the edges fall away in a concave surface, which can easily be observed with the aid of a magnifying lens.

ACKNOWLEDGEMENTS.

I should like to express my deep thanks to Professor S. Tolansky, F.R.S., for his continual guidance and encouragement in the course of this work.

I am indebted to the Director of the Research Laboratories of The General Electric Company for the loan of several synthetic quartz crystals; the Keeper of Minerals, British Museum, for the loan of natural specimens; and the Ministry of Supply for the provision of a Maintenance Grant.

Finally, I must thank Dr. G. Van Praagh and my colleagues at the Physics Department, Royal Holloway College, for valuable discussions.

References.

1.	Pfaff.	Sitzungsber. d. Physik Med. Soc. zu Erlangen	10	59	(1878)
2.	Brauns.	Neues Jahrbuch	1	138	(1887)
3.	Miers.	Proc. Roy. Soc.,	71	439	(1903)
		Phil. Trans. Roy. Soc. A.	202	459	(1904)
4.	Hedges.	J. Chem. Soc.	1	791	(1926)
5.	Kalb	Z. Krist.	73	266	(1930)
		Z. Krist.	86	439	(1933)
		Z. Krist.	89	400	(1934)
6.	Schubnikow and Brunowsky.	Z. Krist.	77	337	(1931)
7.	Tolansky.	Proc. Roy. Soc. A.	184	41	(1945)
8.	Bunn and Emmett.	Disc. Far. Soc.	5	119	(1949)
9.	R. Marcelin.	Ann. Physique.	10	185	(1918)
10.	Kowarski.	J. Chim. Physique.	32	303, 395, 469	(1935)
11.	A. Marcelin and Boudin.	Compt. rend.	191	31	(1930)
12.	Tolansky and Wilcock.	Nature.	157	583	(1946)
13.	J.W. Gibbs.	Collected Works Vol. I. (New York: Longmans, Green and Co.)		325	(1928)
14.	Volmer.	Physik. Z.	22	646	(1931)
15.	Kaischew and Stranski.	Physik. Z.	36	393	(1935)
16.	Becker and Doring.	Ann. Physik.	24	719	(1935)
17.	Buckley.	Crystal Growth (New York: John Wiley).		243	(1951)

18.	Stranski.	Z. Phys. Chem.	136	259	(1928)
19.	Berg.	Proc.Roy.Soc. A.	164	79	(1938)
20.	Humphreys-Owen.	Proc.Roy.Soc. A.	197	218	(1949)
21.	Burton, Cabrera and Frank.	Nature.	163	398	(1949)
22.	Volmer and Schultze.	Z. Phys.Chem.A.	156	1	(1931)
23.	Burton, Cabrera and Frank.	Phil. Trans. Roy.Soc. A.	243	299	(1951)
24.	Frenkel.	J. Physics, U.S.S.R.	9	392	(1945)
25.	Griffin.	Phil. Mag. 7	41	196	(1950)
26.	Verma.	Nature.	167	939	(1951)
		Phil. Mag. 7	42	1005	(1951)
27.	Amelinckx.	Nature.	167	939	(1951)
28.	Dawson and Vand.	Nature.	167	476	(1951)
		Proc. Roy.Soc. A.	206	555	(1951)
29.	Menzies and Sloat.	Nature.	123	348	(1929)
30.	Forty.	Phil. Mag. 7	42	670	(1951)
31.	Frank.	Advances in Physics	1	No.1. 91	(1952)
32.	Haward.	Trans. Far. Soc.	35	1401	(1939)
33.	Cockroft.	Proc.Roy.Soc. A.	119	293	(1928)
34.	Volmer and Estermann.	Z. Physik.	7	13	(1921)
35.	Mott.	Nature.	165	295	(1950)
36.	Frenkel	Z. Physik.	26	117	(1924)

37.	Tolansky.	Multiple-beam Interferometry (Oxford: Clarendon Press).			(1948)
38.	Tolansky.	Phil. Mag.	35	120	(1944)
		Phil. Mag.	36	225	(1945)
39.	Brossel.	Proc. Phys. Soc.	59	224	(1947)
40.	Tolansky and Barakat.	Proc. Phys. Soc. B.	63	545	(1950)
41.	Holden.	Proc. Phys. Soc. B.	62	405	(1949)
42.	Bruce.	Australian Journal of Scientific Research.	4. No.2.	117	(1951)
43.	Barakat.	Nature.	16	603	(1949)
44.	Bragg and Gibbs.	Proc. Roy. Soc. A.	109	405	(1925)
45.	Francon.	Le Contraste de Phase en Optique et en Microscopie. (Paris)			(1950)
46.	Lyot and Francon.	Rev. d'Optique.	27	397	(1948)
47.	Francon and Nomarski.	Rev. d'Optique.	29	619	(1950)
48.	Faust and Tolansky.	Proc. Phys. Soc.	59	951	(1947)
49.	Drummond.	The Practice of Electron Microscopy (London: Microscopical Society).			(1950)
51.	Merton.	Proc. Roy. Soc. A.	201	187	(1950)
52.	Hopkins and Pearson.	J. Iron and Steel Inst.	159	67	(1948)
53.	Wallace.	Jour. Astrophysics.	22	123	(1905)
54.	Sayce and Dew.	Proc. Roy. Soc. A.	207	278	(1951)
55.	Kerr and Armstrong.	Bull. Geol. Soc. Amer.	54	Suppl. I.	(1943)
56					
57.	Spencer.	Encyclopædia Britannica.	18	830	(1945)

58.	Griffin.	Ph.D. Thesis (London University).		(1950)
59.	Miers.	Mineralogy. (London: Macmillan).	375	(1902)
60.	Gault.	Amer. Mineralogist. 34	142	(1949)
61.	Dana.	Descriptive Mineralogy (New York: John Wiley)	185	(1906)
62.	Tolansky.	Private Communication.		(1952)
63.	Verma.	Private Communication.		(1952)
64.	Cabrera.	Nature. 167	766	(1951)
65.	Clancey.	Nature. 166	275	(1950)
66.	Ingerson.	Am. Min. 32	375	(1947)
	Peach.	Journ.Geol. Chicago. 59	32	(1951)
67.	Saksena and Srivastava.	Proc. Ind. Acad.Ac. 29	189	(1949)
68.	Kossel	Nach. Ges. Wiss. Gottingen Jahresber. math.-physik. Klasse.	135	(1927)
69.	Frank.	Disc. Far. Soc. 5	76	(1949)
70.	Griffin.	Phil. Mag. 42	1337	(1951)
71.	Tolansky and Bardsley.	Proc.Phys. Soc.B. 64	224	(1951)
72.	J.W. Gibbs.	Collected Works, Vol.I. (New York: Longmans, Green and Co.).	footnote p 325	(1928)
73.	Burgers.	Proc. Kon. Ned. Acad. Wet. 42	293	(1939)
	Cottrell.	Progress in Metal Physics, I. (London: Butterworths Scientific Publications)	Chapter 2	(1949)
74.	Nomoto.	Nature. 164	359	(1949)

75.	Dake, Fleener and Wilson.	Quartz Family Minerals. (New York: McGraw Hill)		69	(1938)
76.	Spezia.	Acad. Sci. Torino. Atti.	40	254	(1905)
			41	158	(1905)
			44	95	(1908)
77.	Van Praagh	Disc. Far. Soc.	5	338	(1949)
78.	Brown, Kell, Thomas, Wooster N. and Wooster W.A.	Nature.	167	940	(1951)
79.	Walker and Buehler.	Industrial and Engineering Chem.	42	1369	(1950)
80.	Buerger.	Am. Mineral.	17	177	(1932)

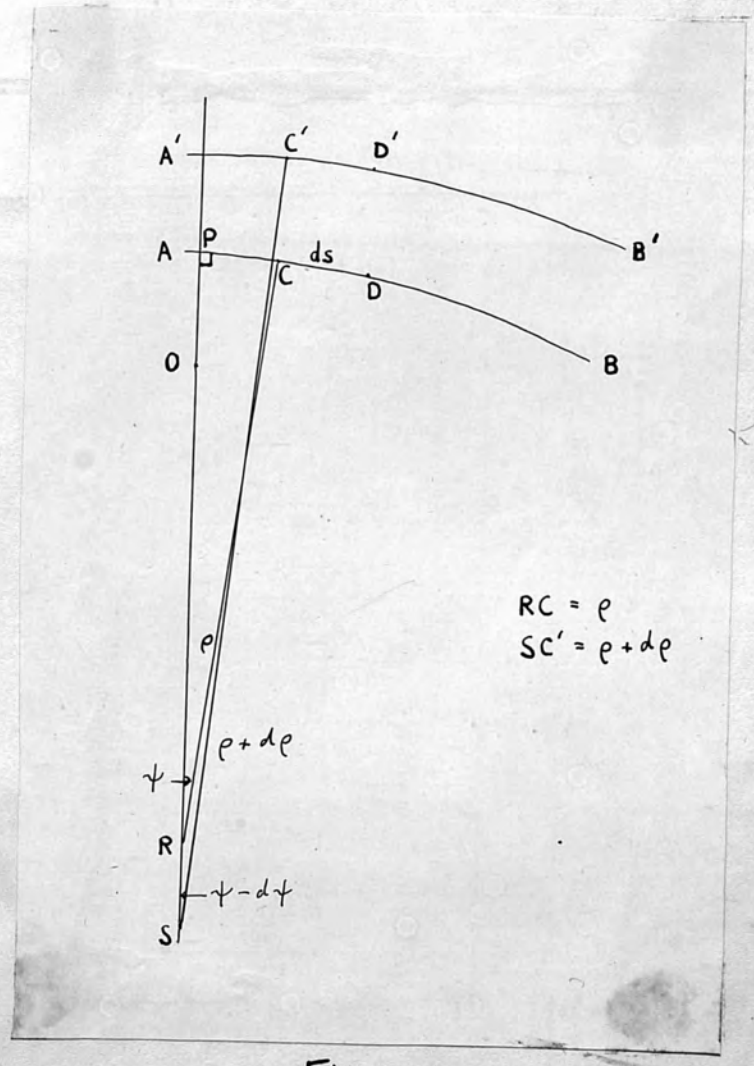

Fig. 3.

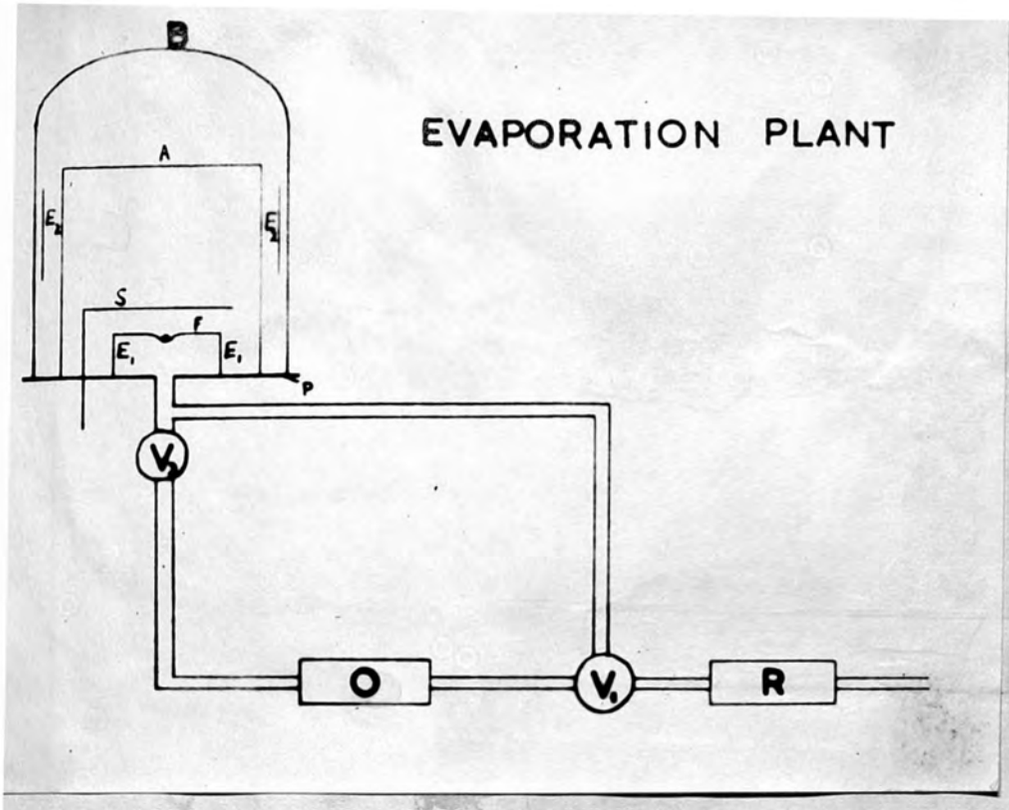

Fig. 4.

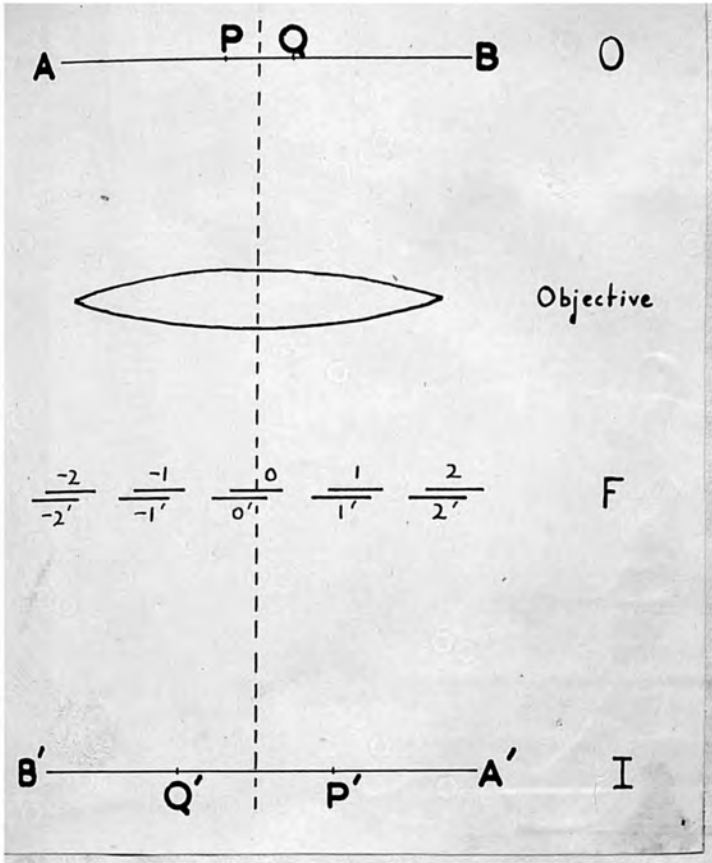

Fig. 5.

Fig. 7

Fig. 6.

Fig 8

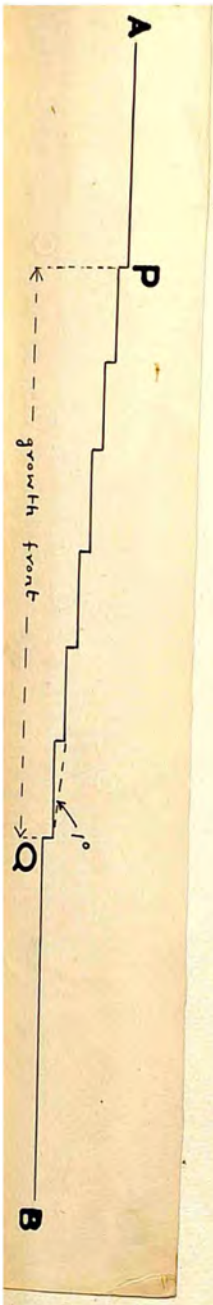

Fig. 7.

Fig. 8.

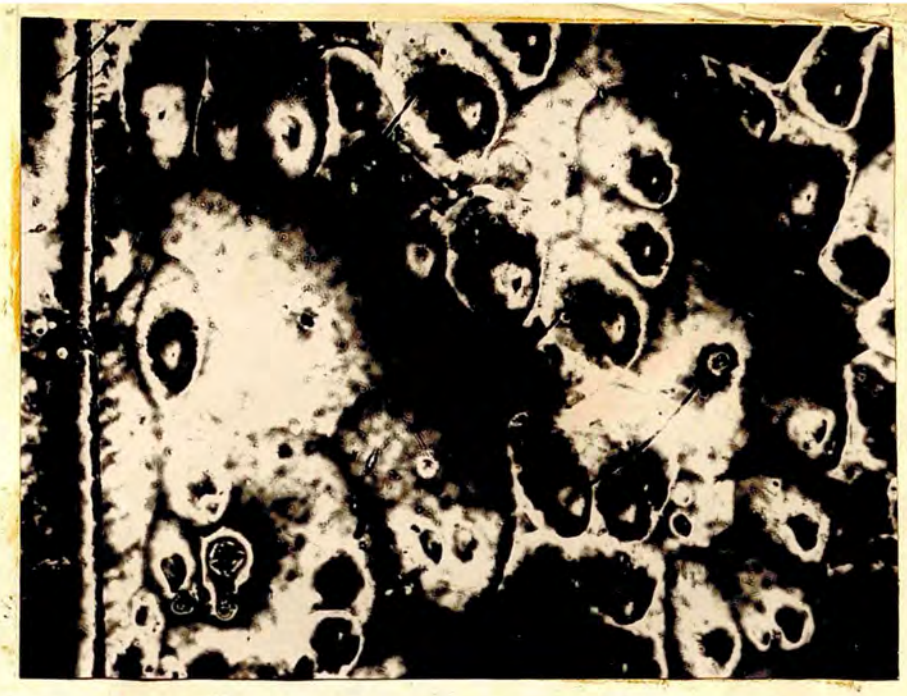

Fig. 9.

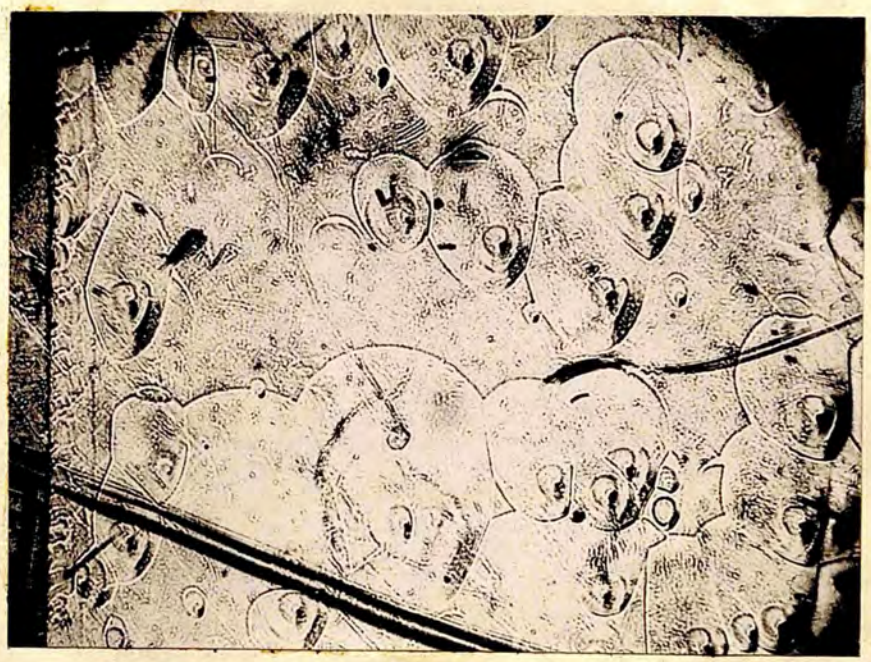

Fig. 10.

Fig. 11.

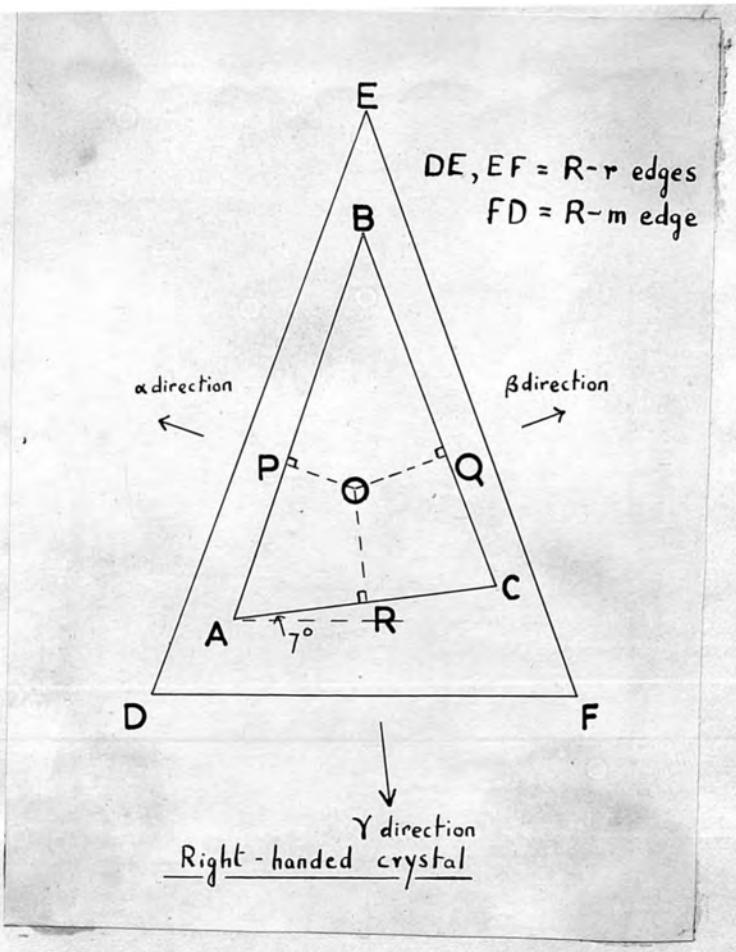
E
DE, EF = R-r edges
FD = R-m edge
B
α direction
β direction
P
Q
T
C
A
7°
R
D
F
γ direction
Right-handed crystal

Fig. 16.

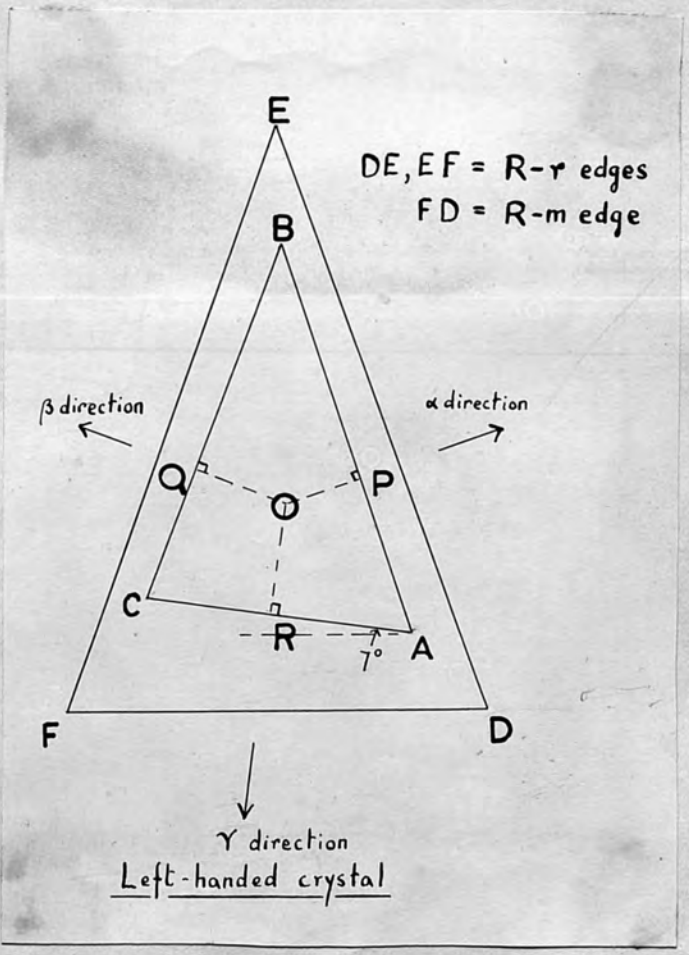
E
DE, EF = R-r edges
FD = R-m edge
B
β direction
α direction
Q
P
T
C
R
7°
A
F
D
γ direction
Left-handed crystal

Fig. 17.

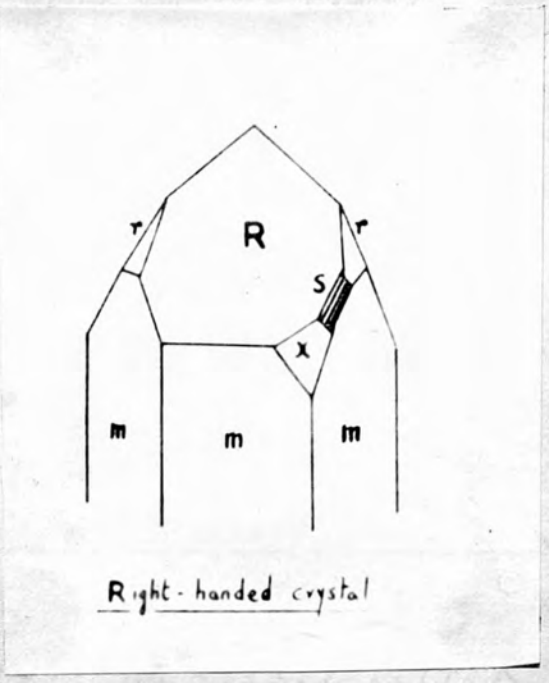
r
R
r
S
x
m
m
m
Right-handed crystal

Fig. 20.

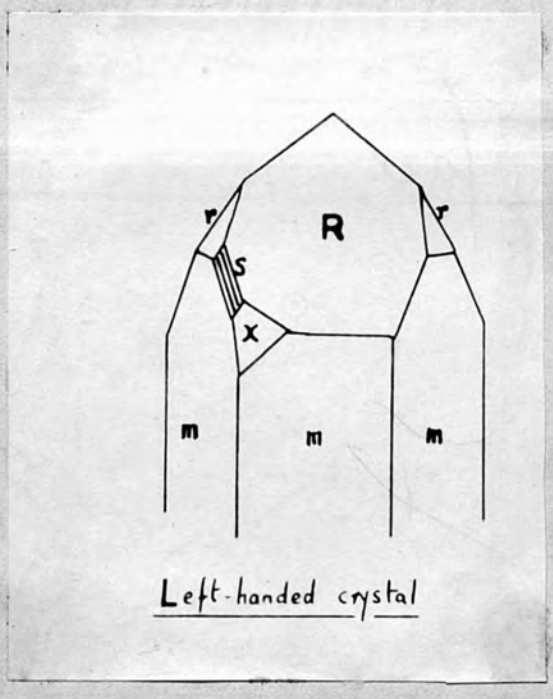
r
R
r
S
x
m
m
m
Left-handed crystal

Fig. 21.

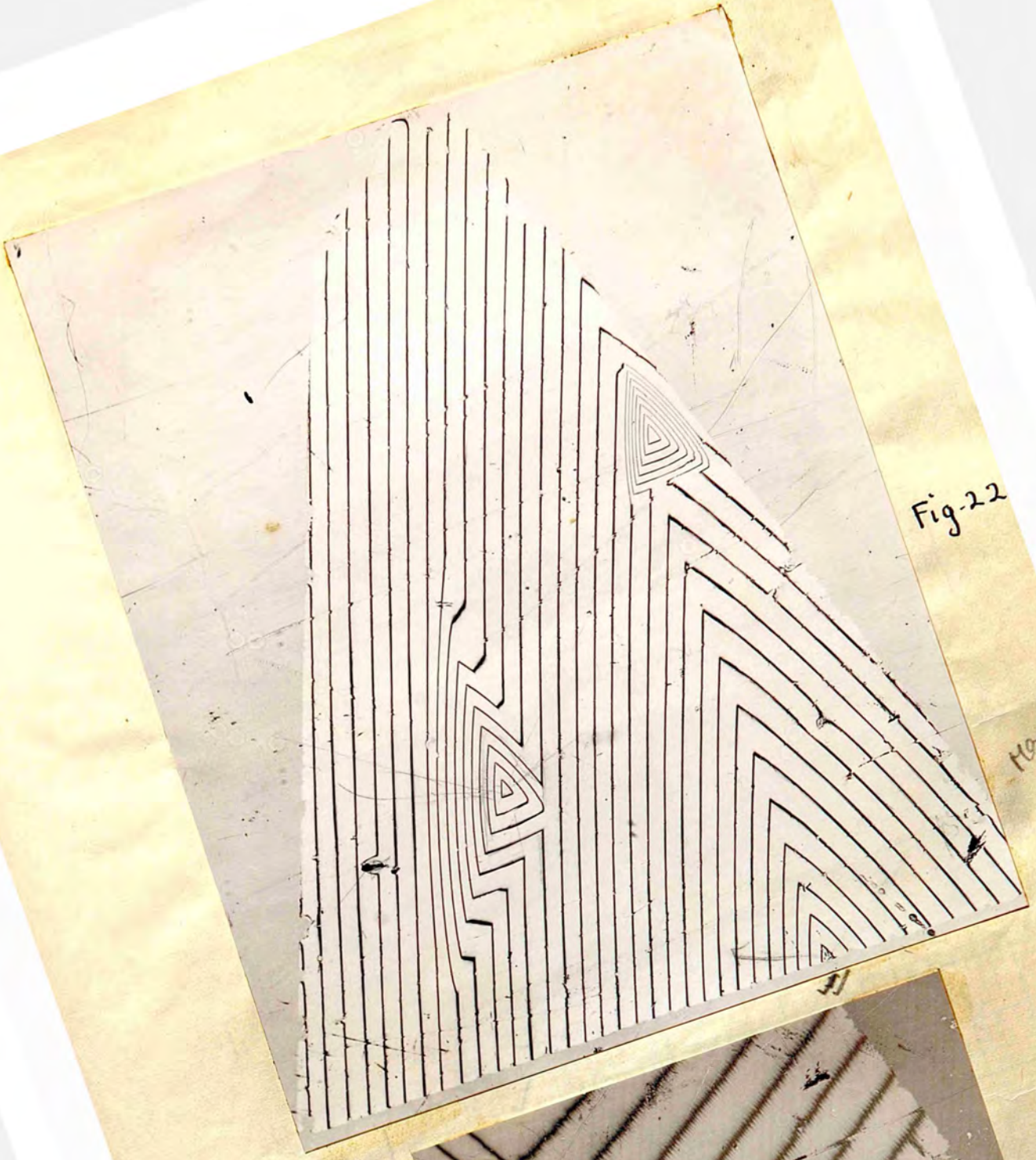

Fig-22

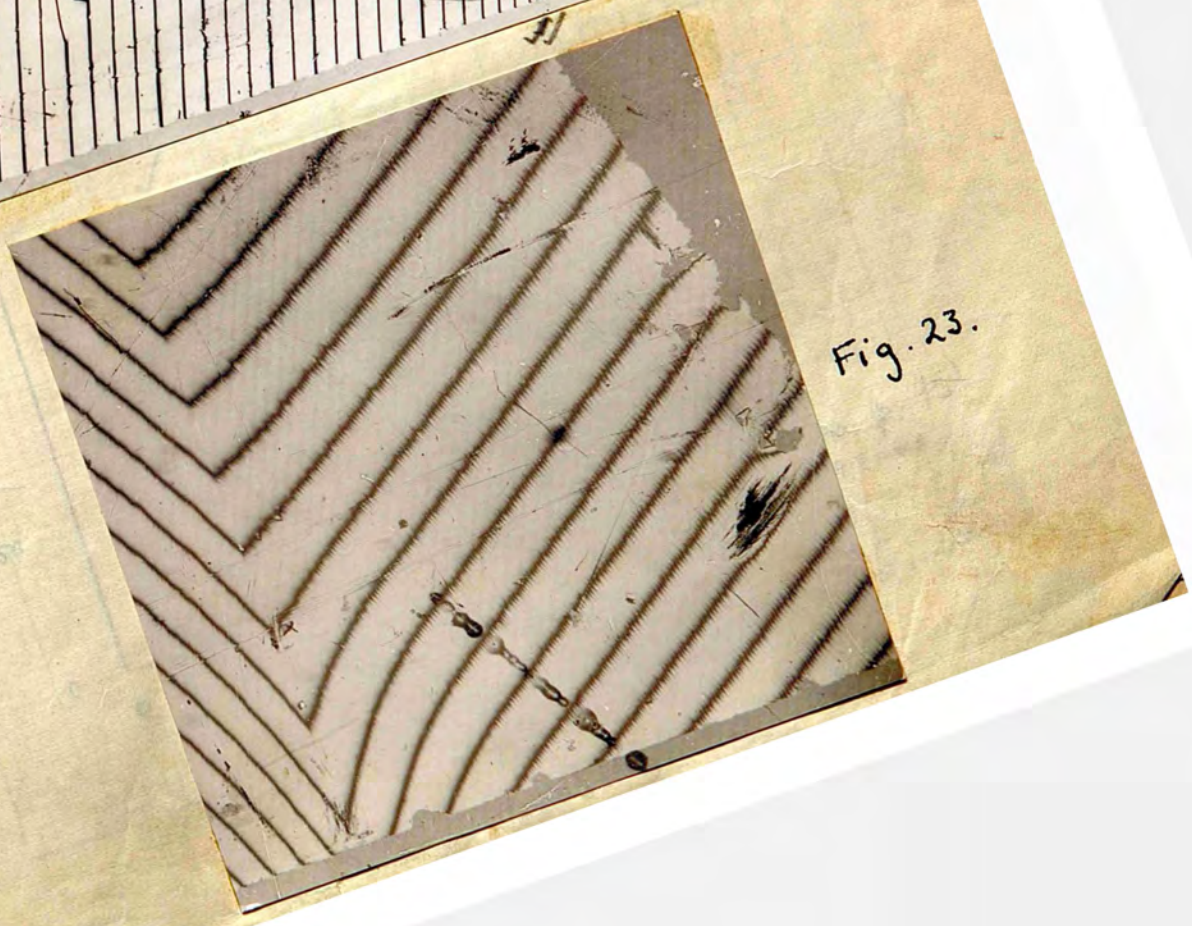

Fig. 23.

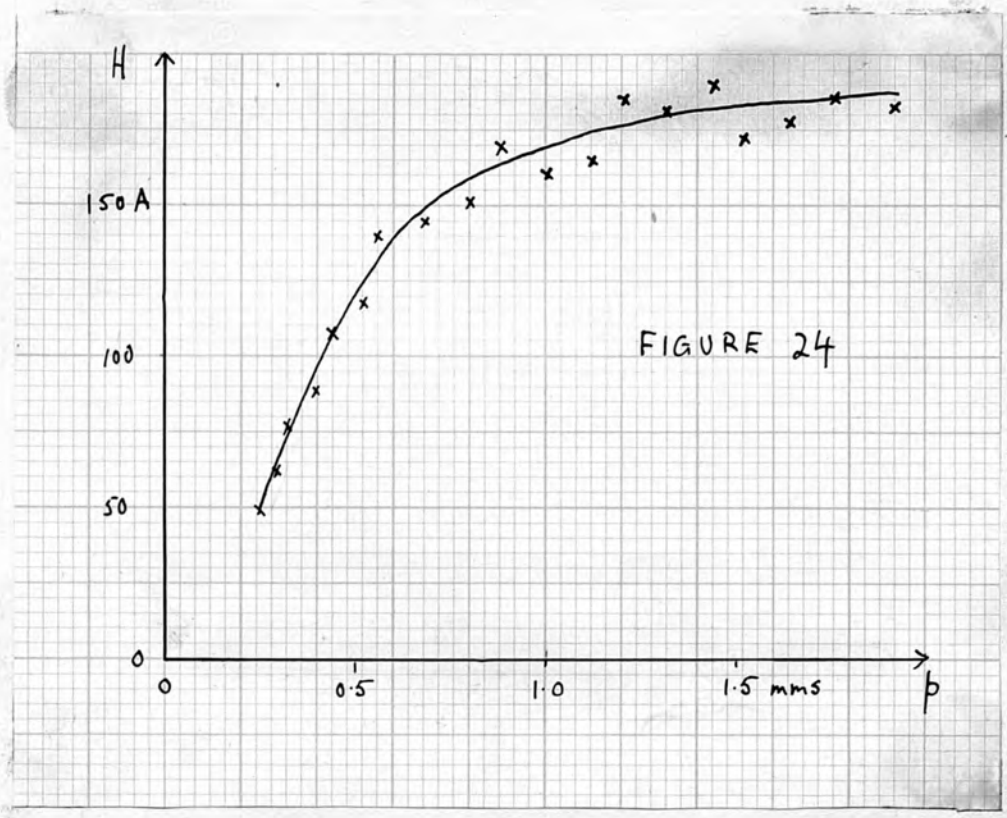

FIGURE 24

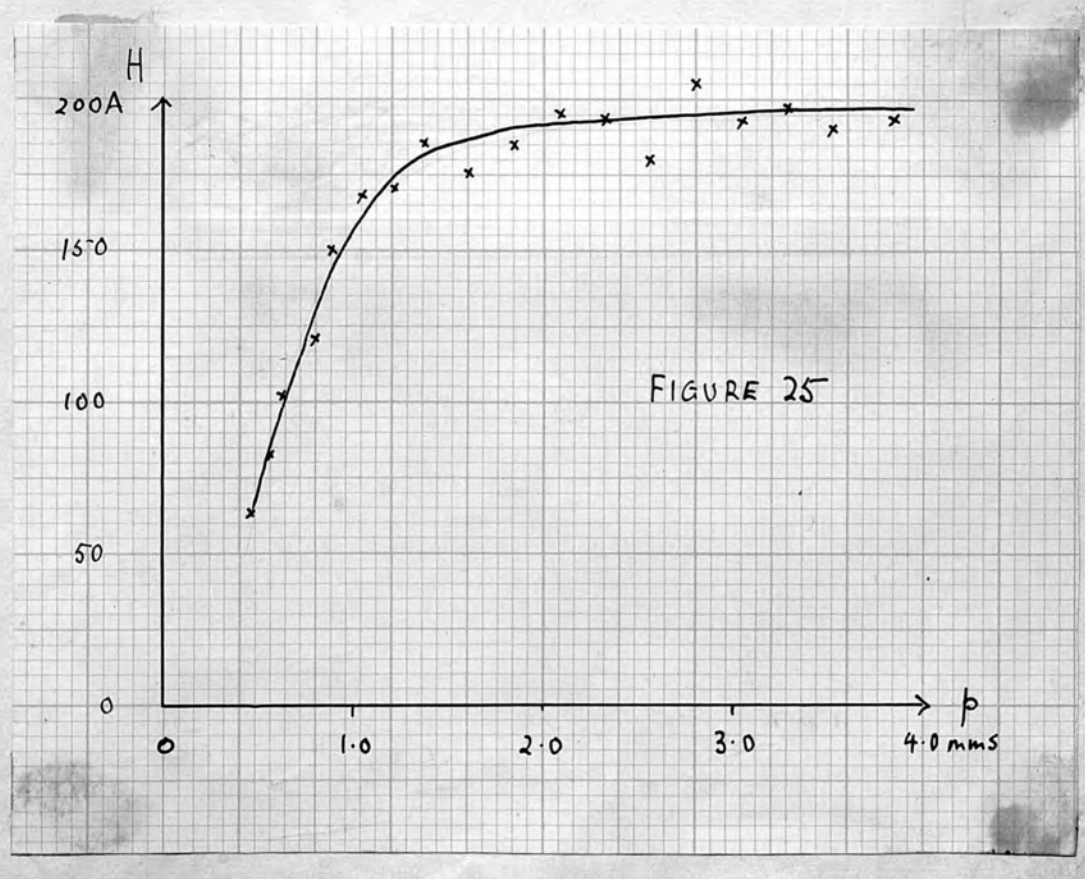

FIGURE 25

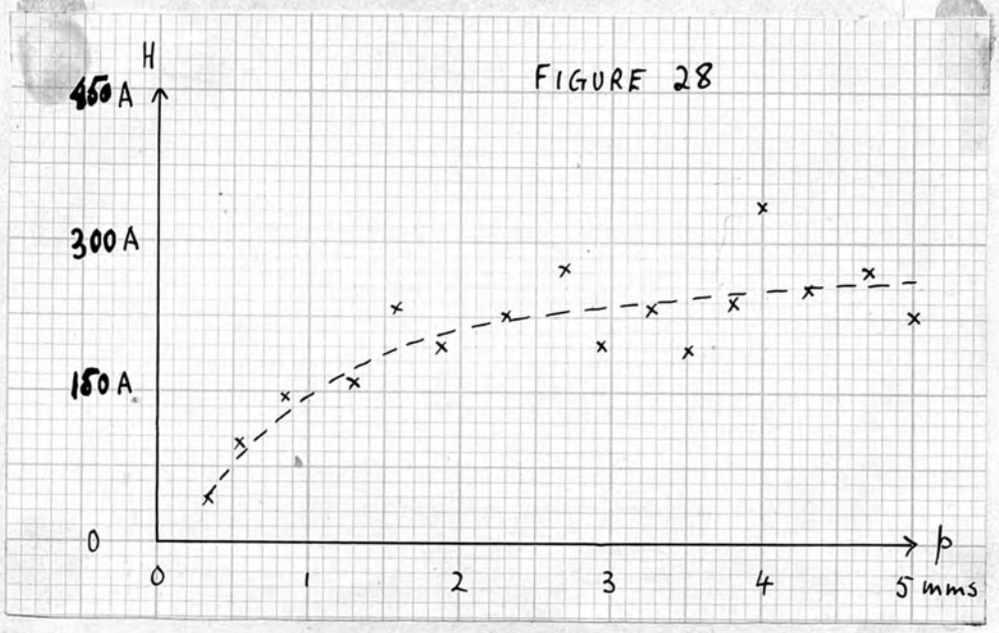

FIGURE 28

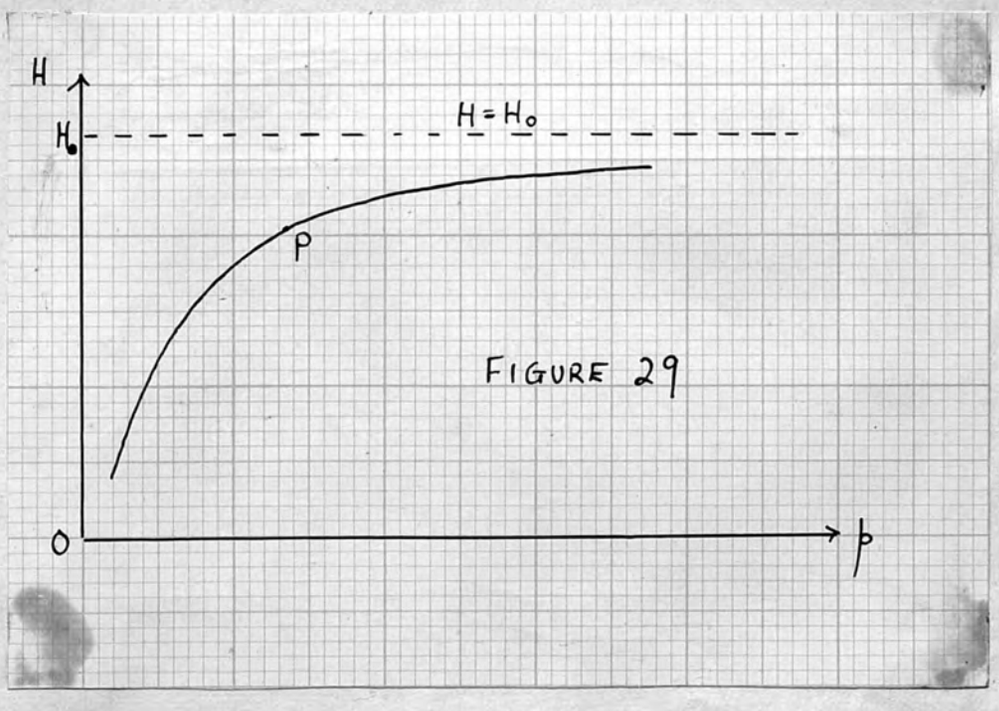

FIGURE 29

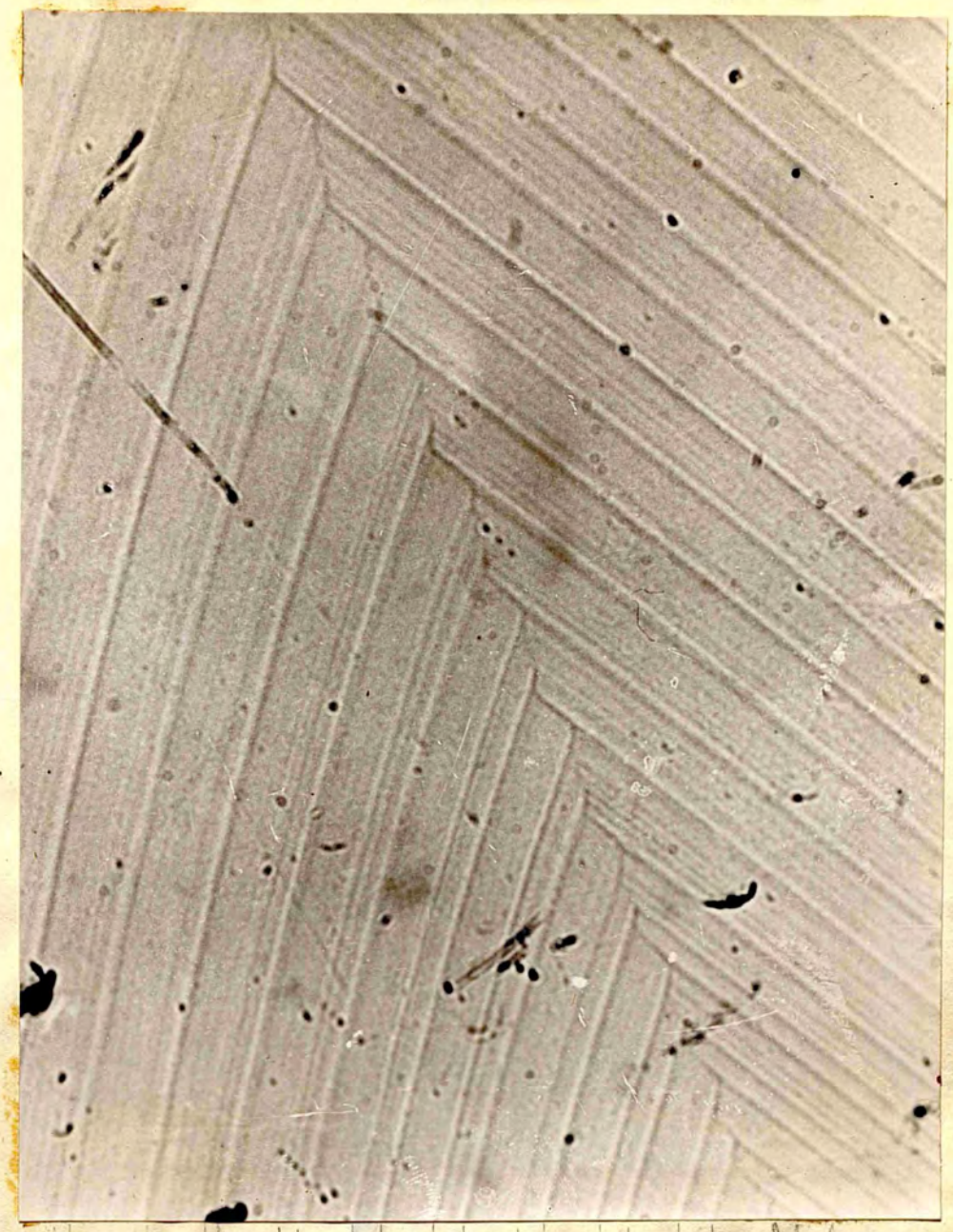

Fig. 30.

Fig. 31.

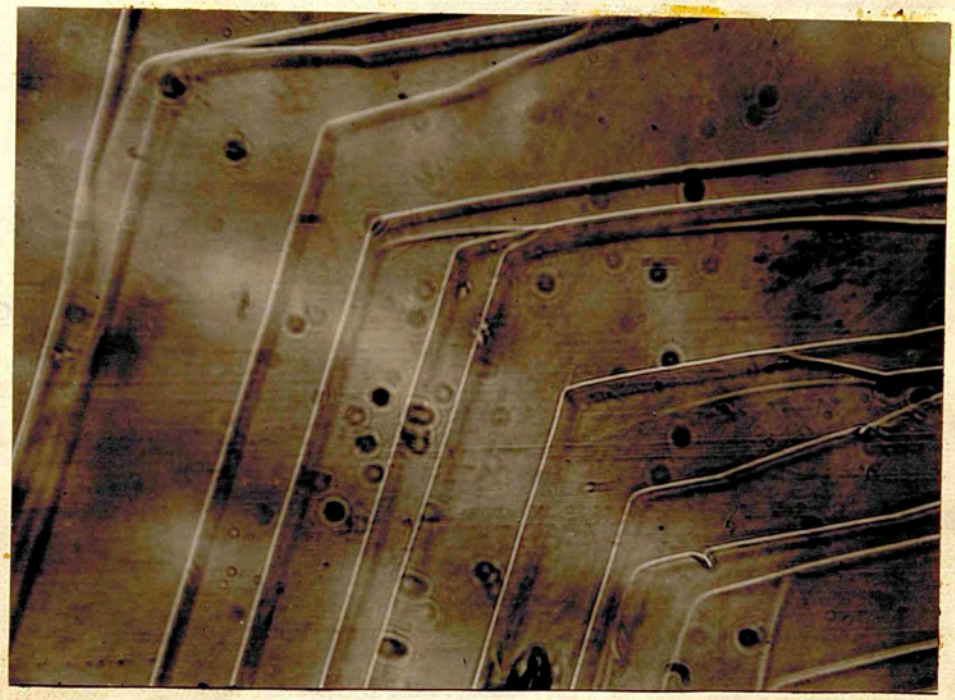

Fig. 34.

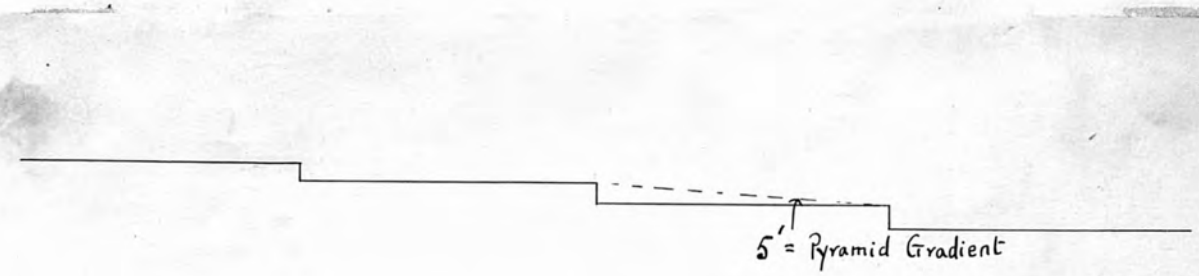

(a) Molecular Steps shortly after Initiation.

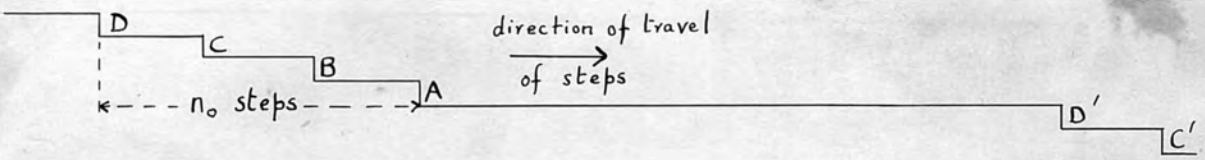

(b) Bunching begins. Steps break up into Groups containing n_o steps each.

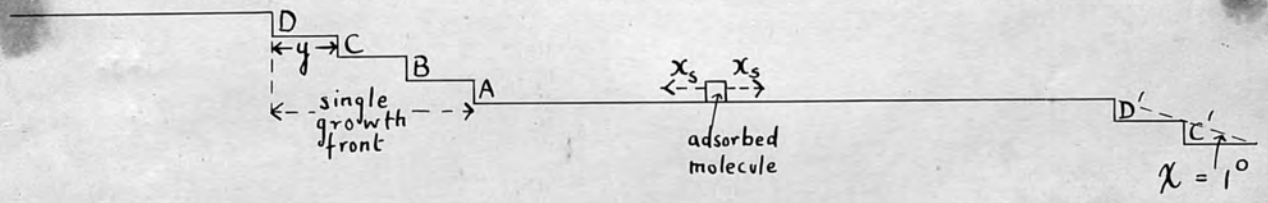

(c) $y \simeq 2x_s$. Velocities of B, C, D... fall to that of A.

Fig. 35.

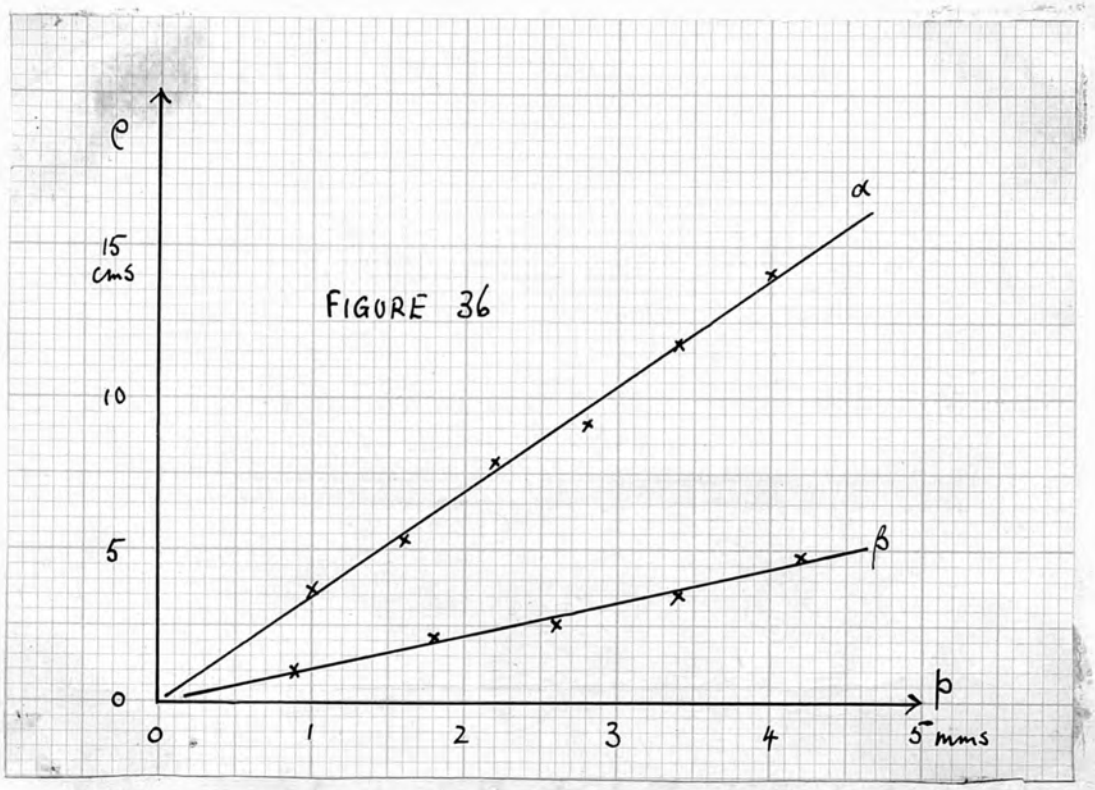

FIGURE 36

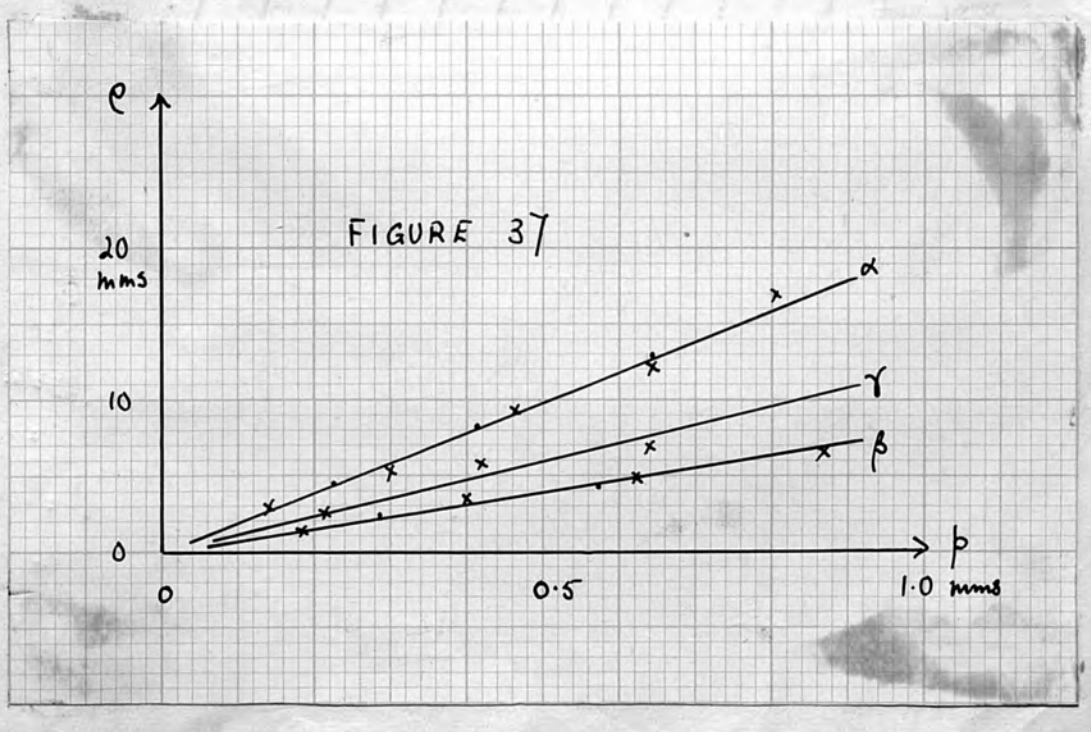

FIGURE 37

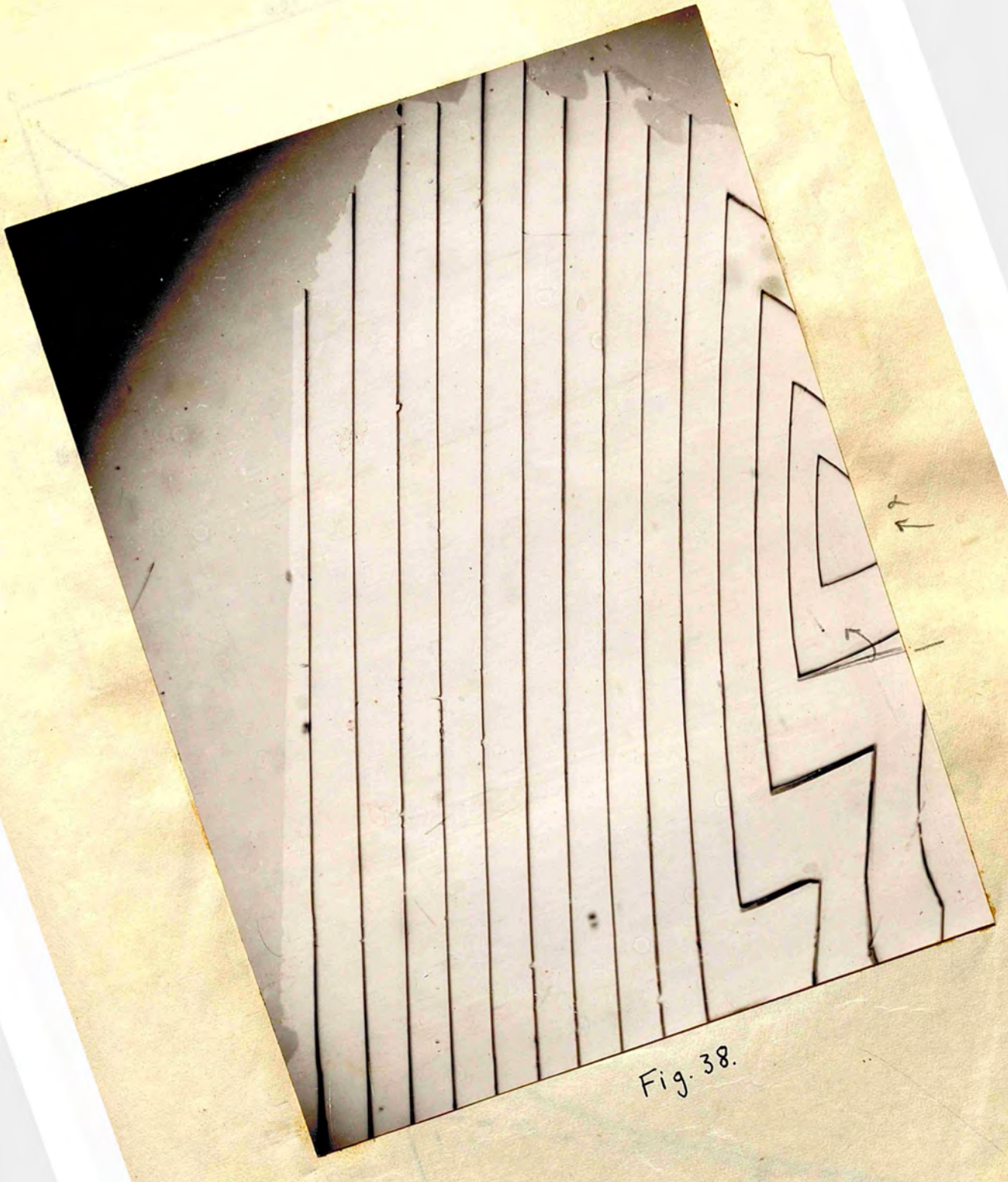

Fig. 38.

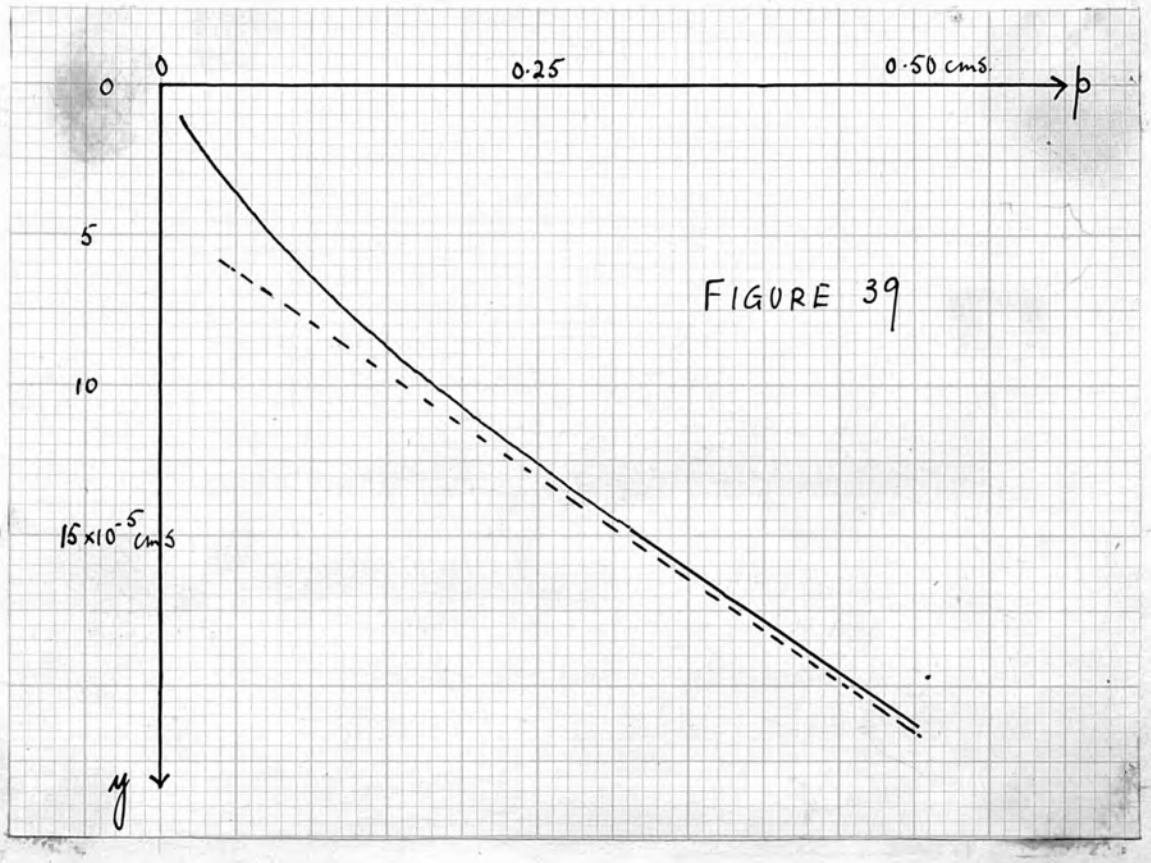

FIGURE 39

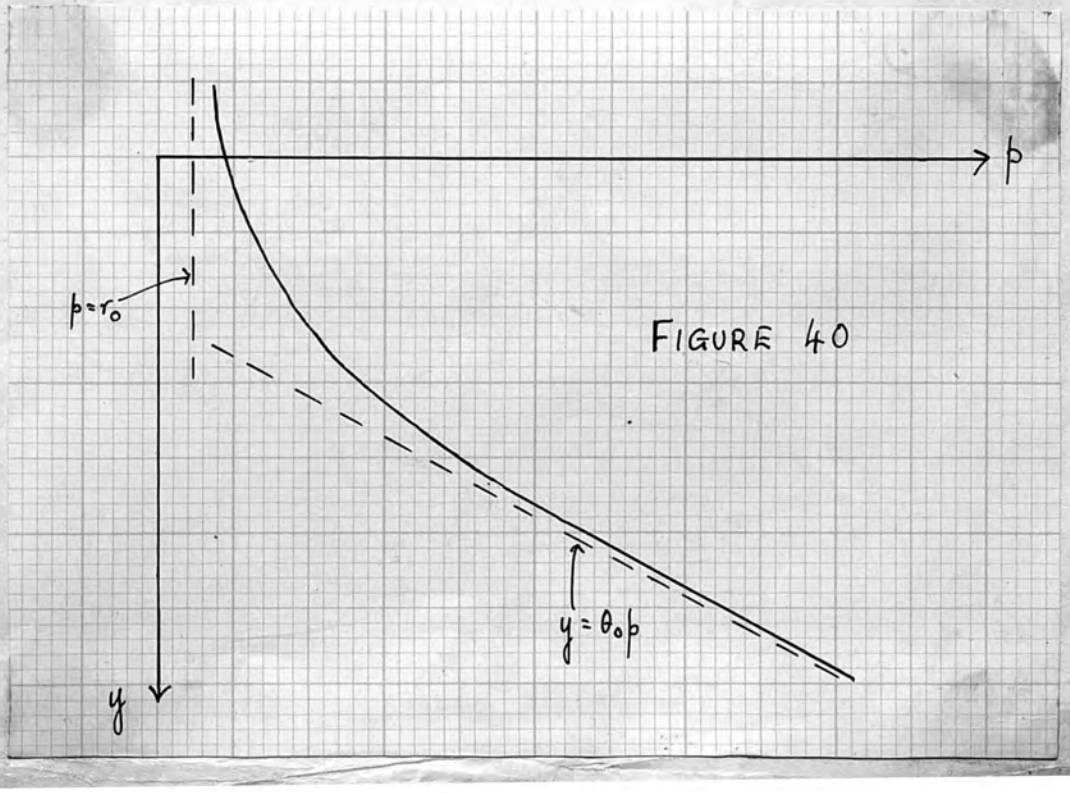

FIGURE 40

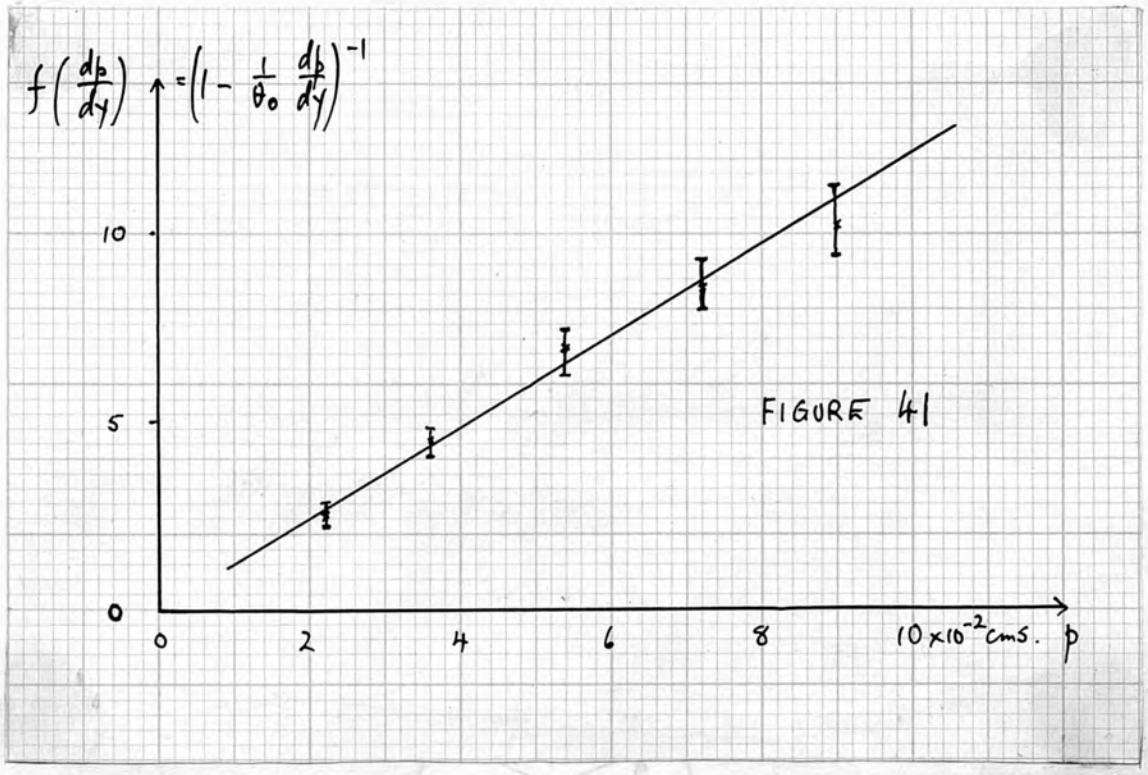

FIGURE 41

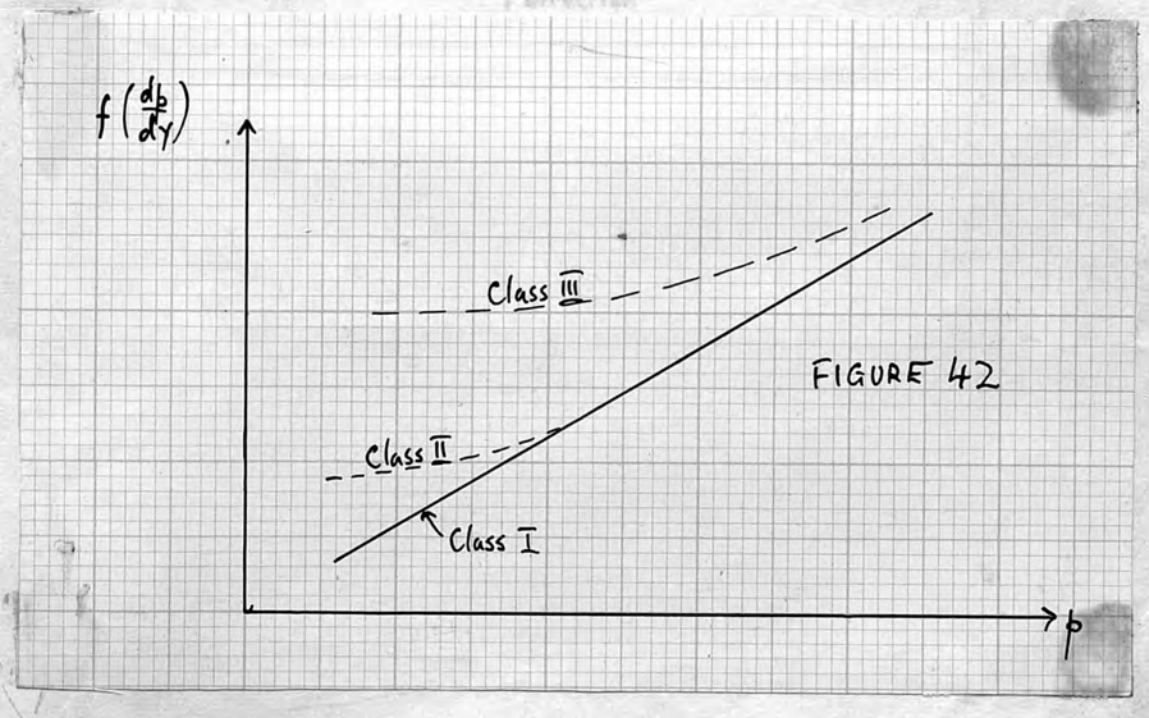

FIGURE 42

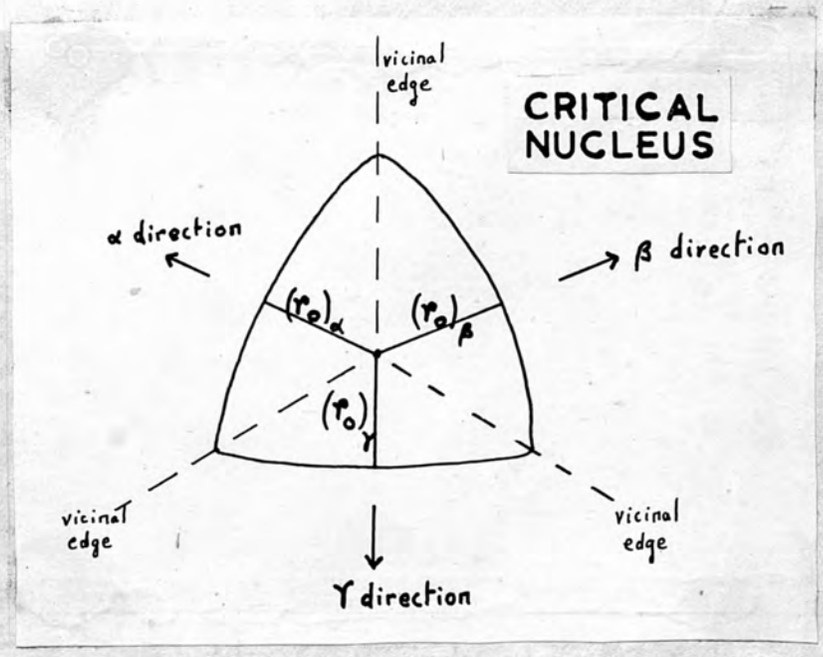
vicinal edge
CRITICAL NUCLEUS
α direction
β direction
$(r_o)_\alpha$
$(r_o)_\beta$
$(r_o)_\gamma$
vicinal edge
vicinal edge
γ direction

Fig. 43.

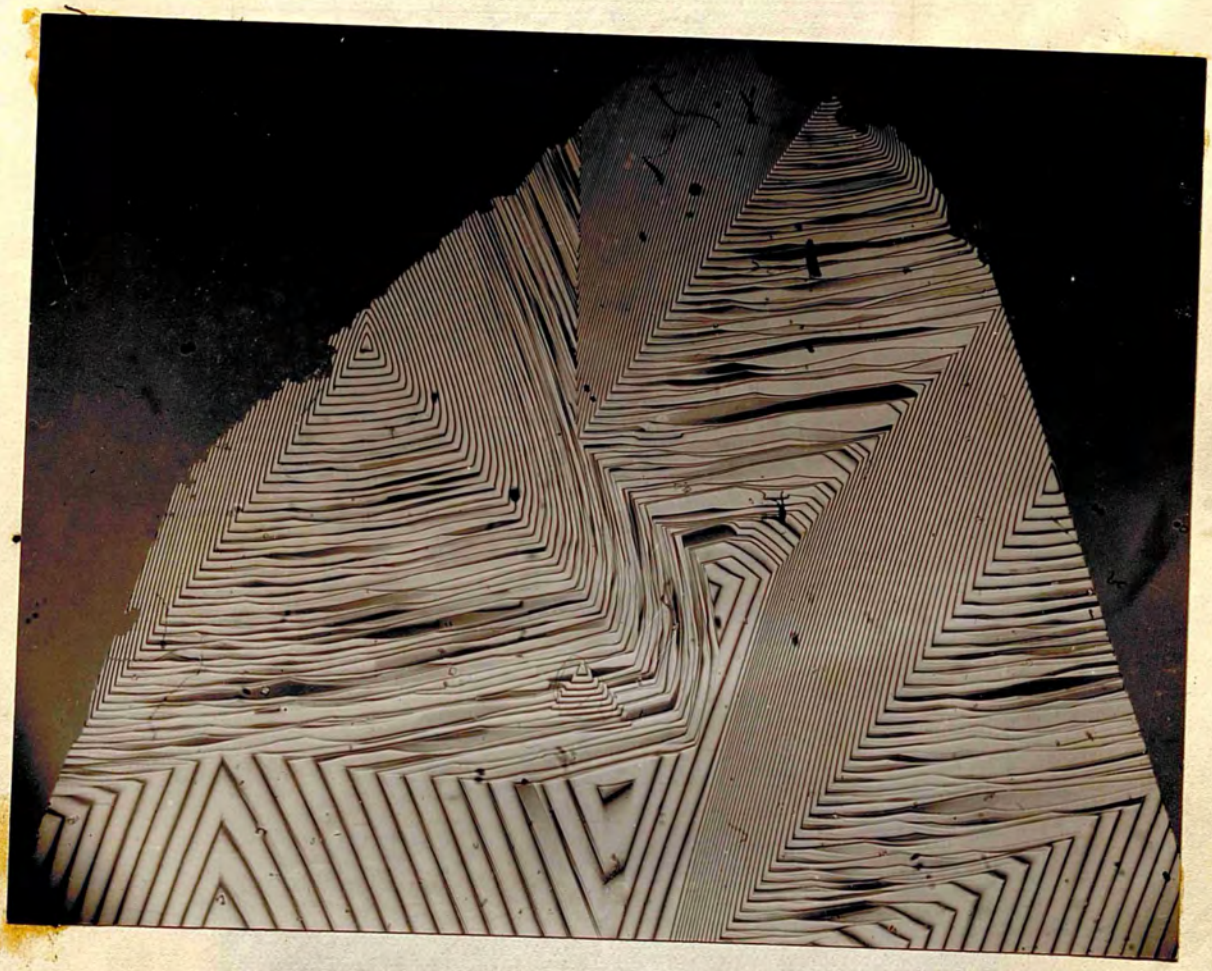

Fig. 44.

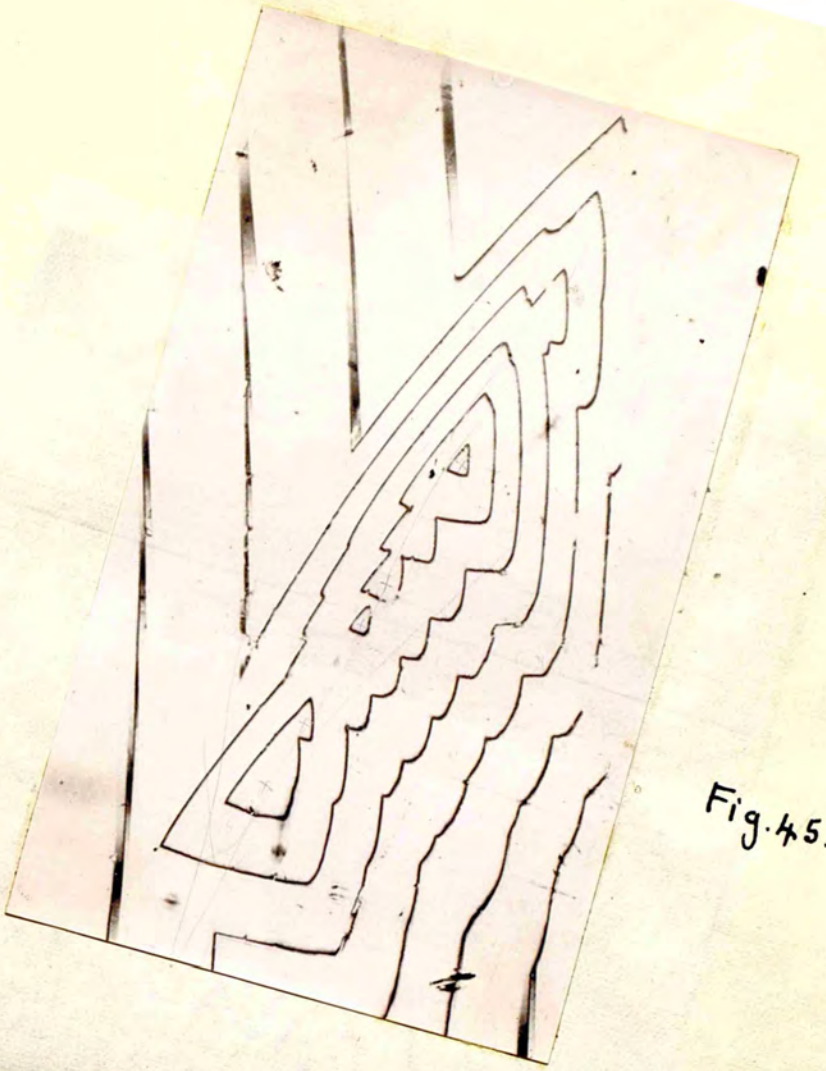

Fig. 45.

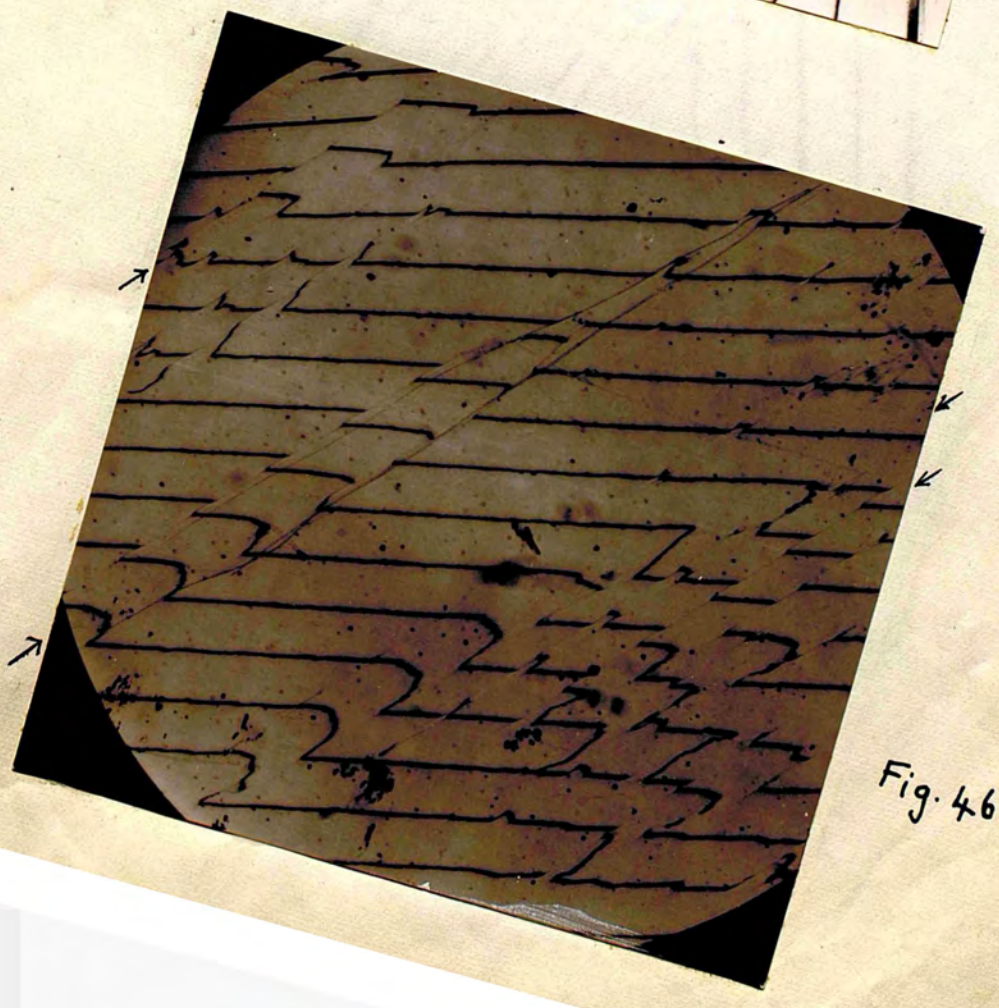

Fig. 46.

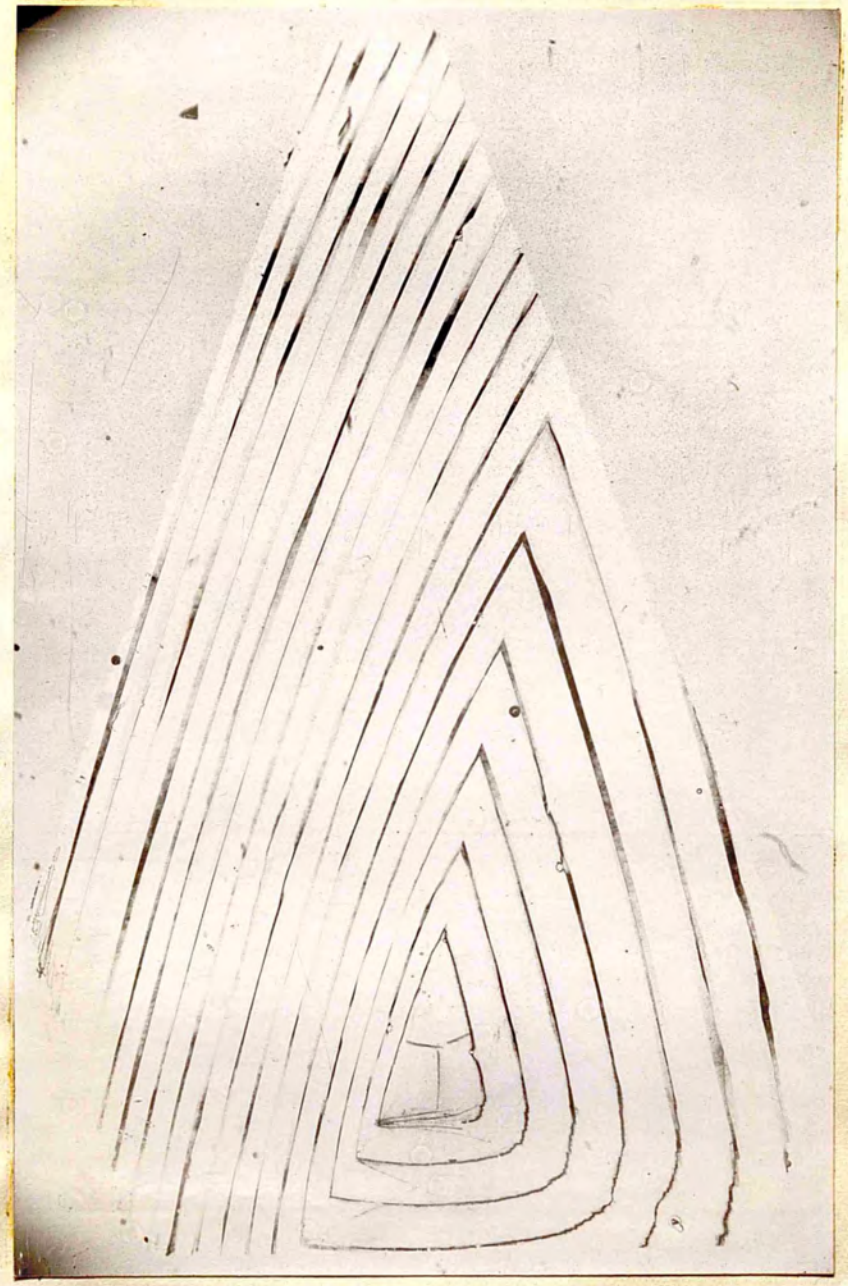

Fig. 50.

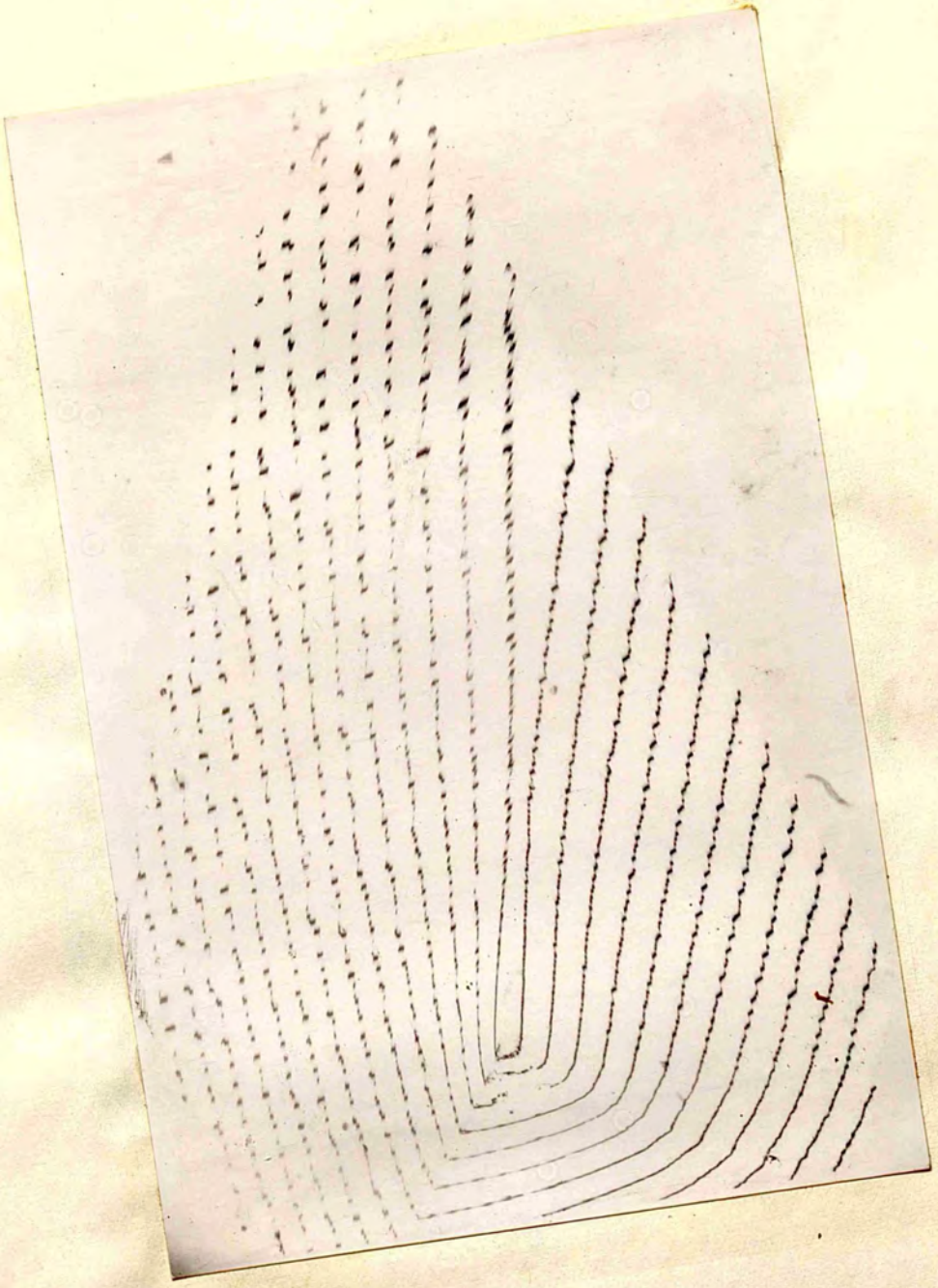

Fig. 51.

Fig. 52.

Fig. 55.

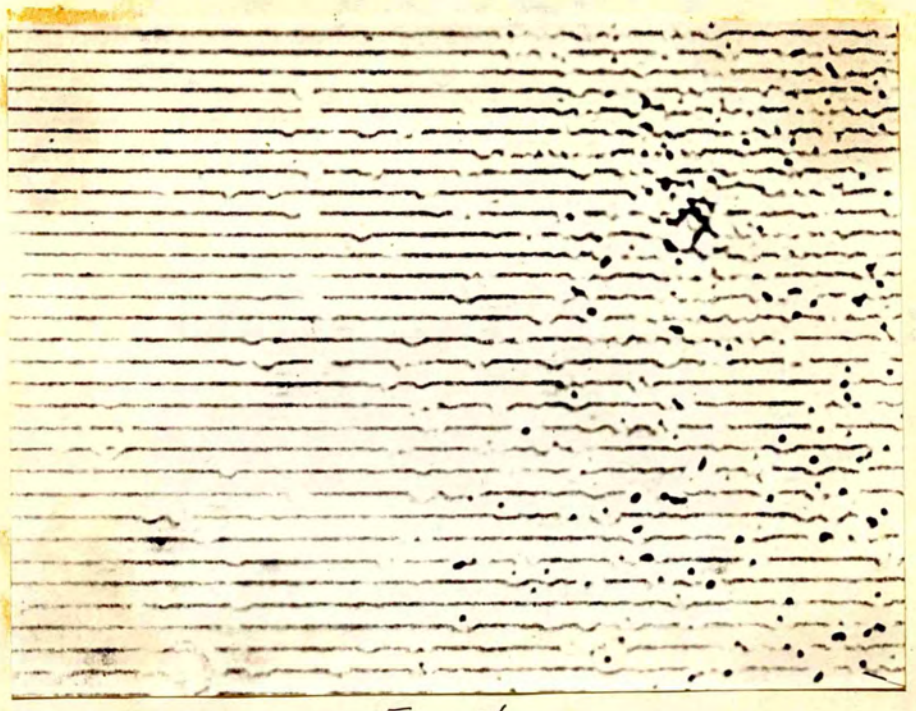

Fig. 56.

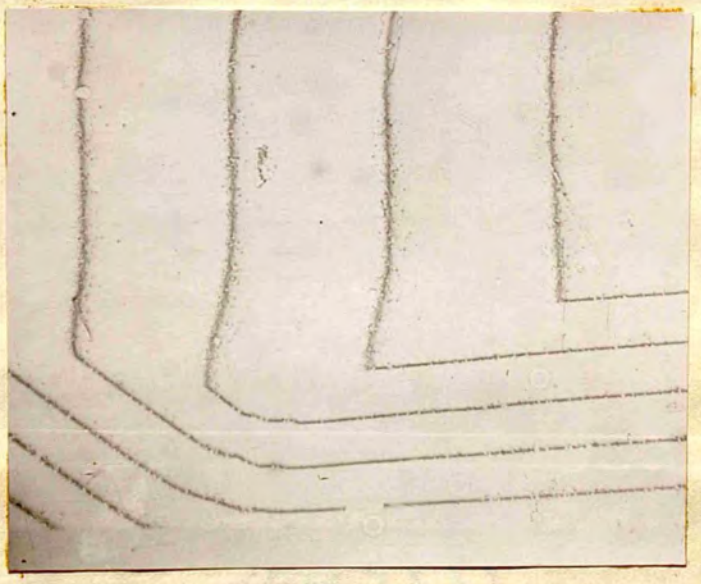

Fig. 57.

Fig. 58.

Fig. 59.

Fig. 60.

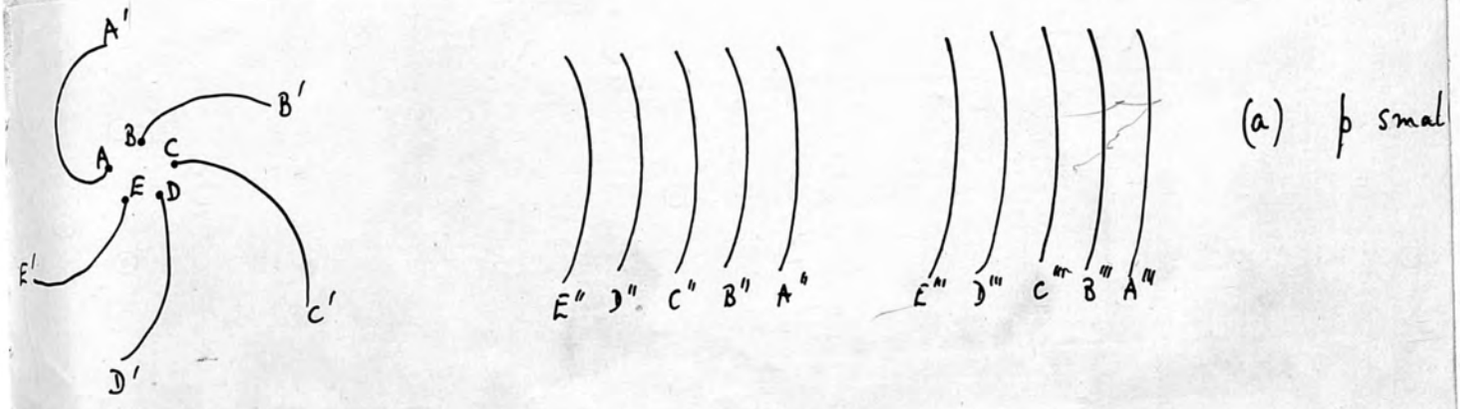

FIGURE 62

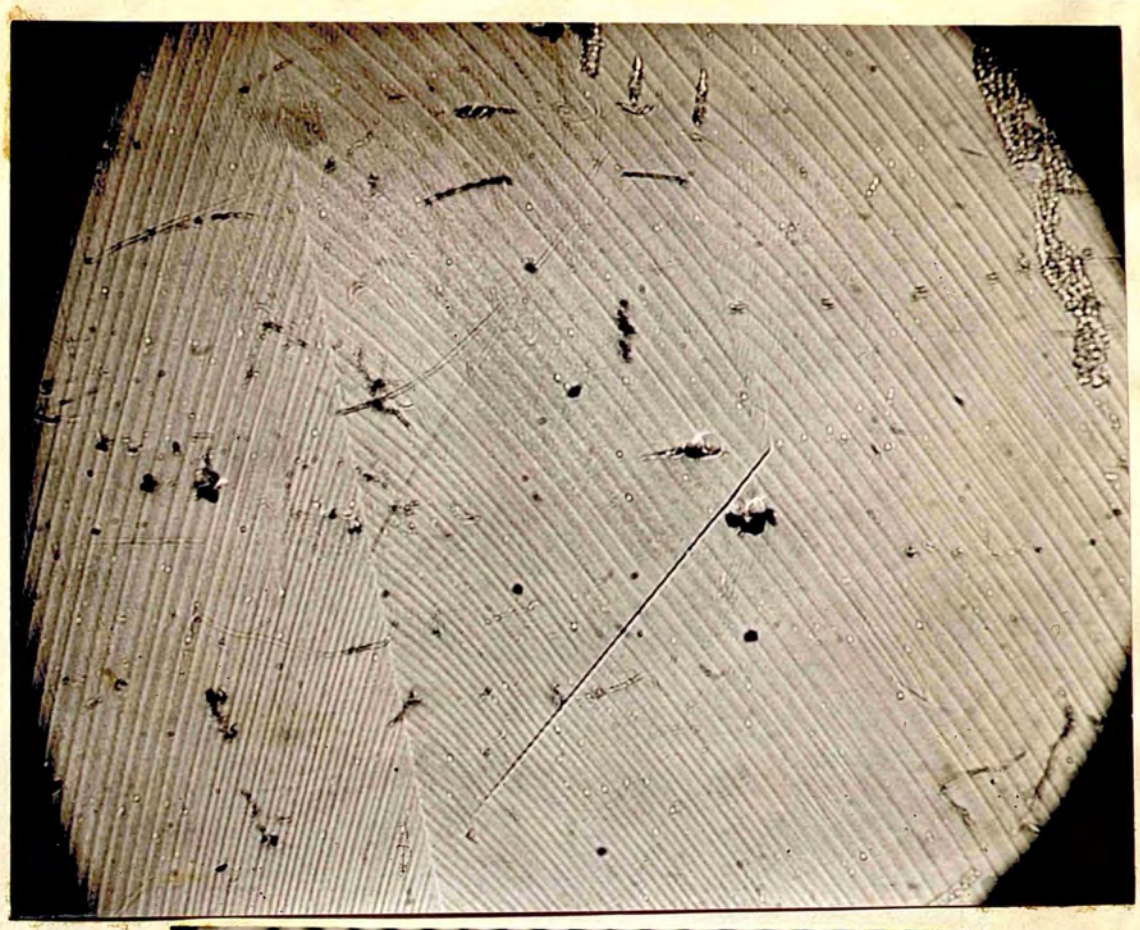

Fig. 63(a)

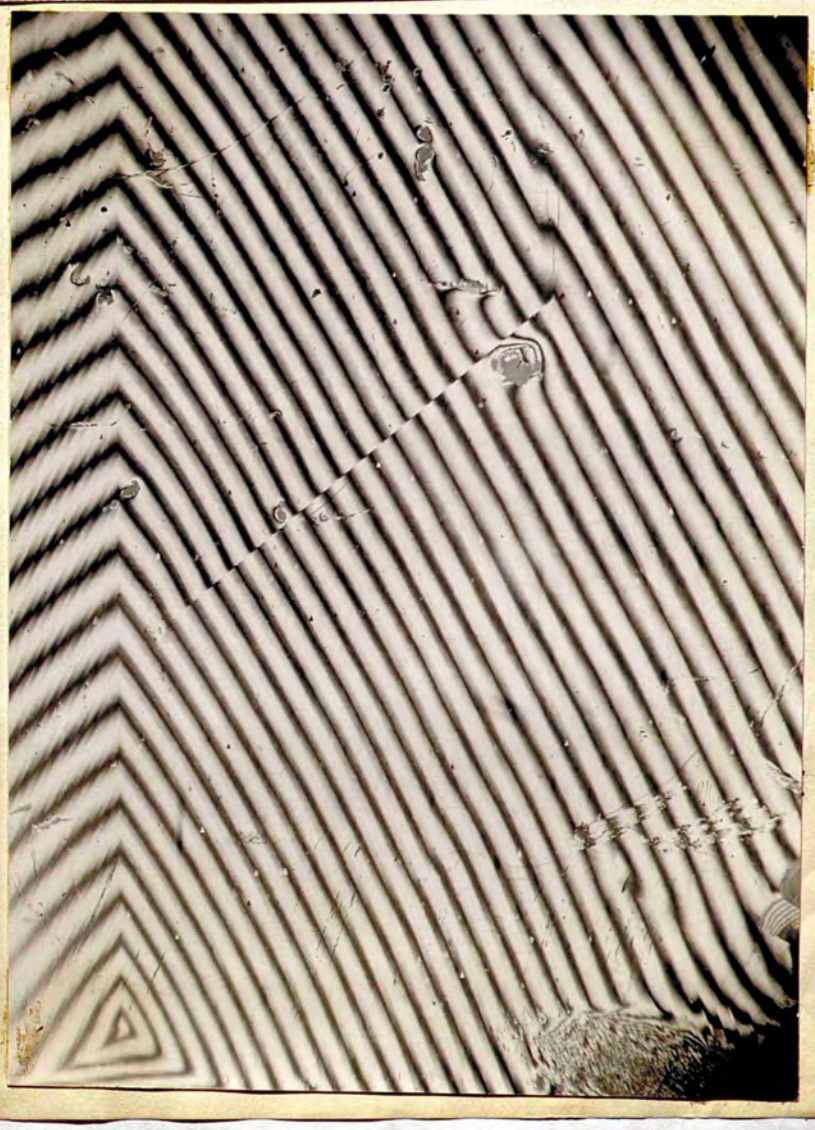

Fig. 63(b)

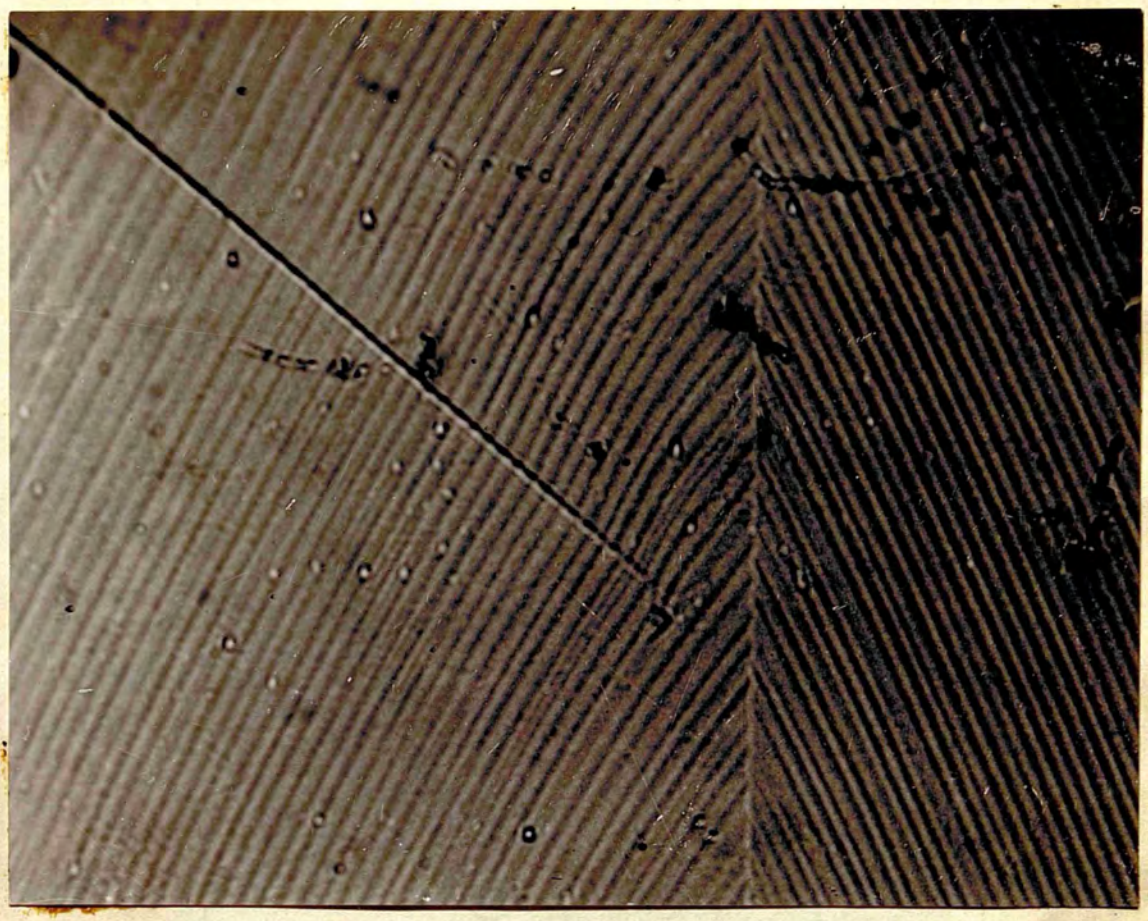

Fig. 63. (c)

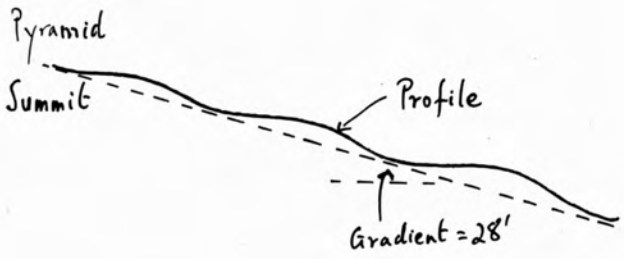

FIGURE 67

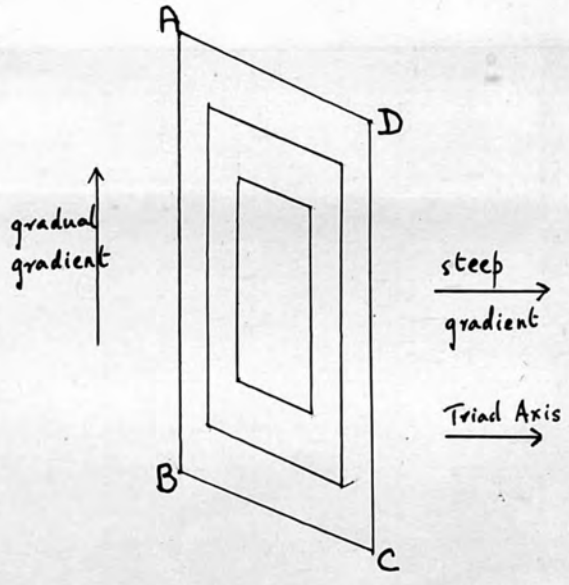

FIGURE 68

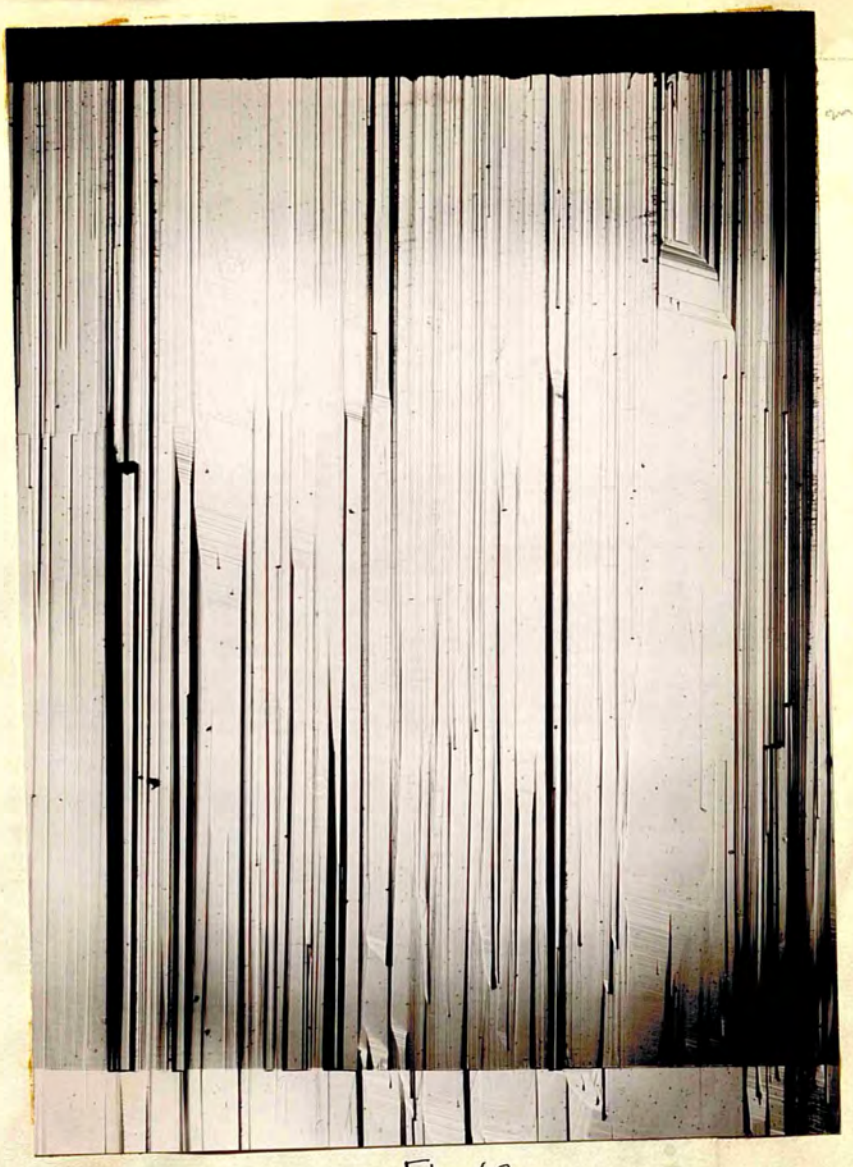

Fig. 69.

Fig. 70.

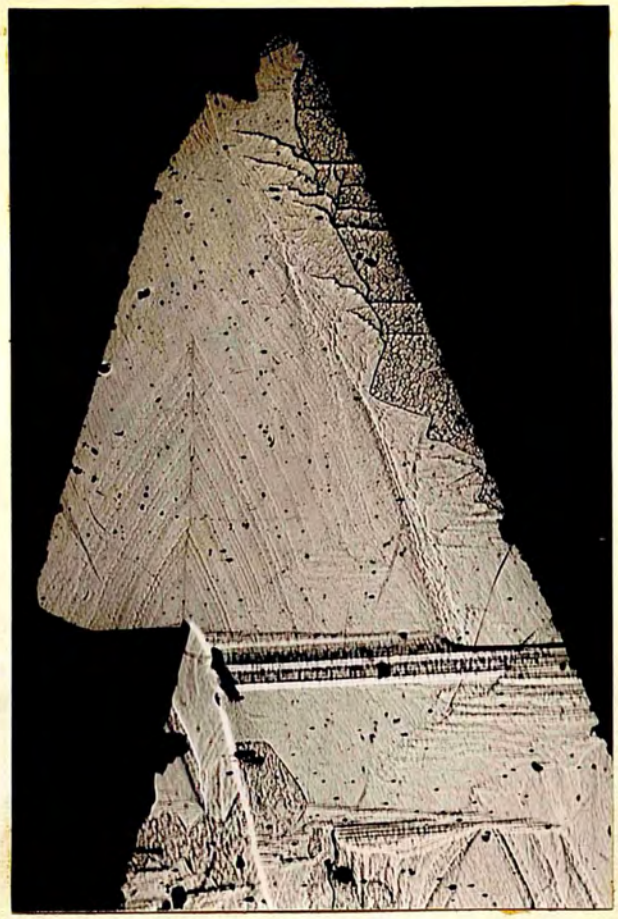

Fig. 71.

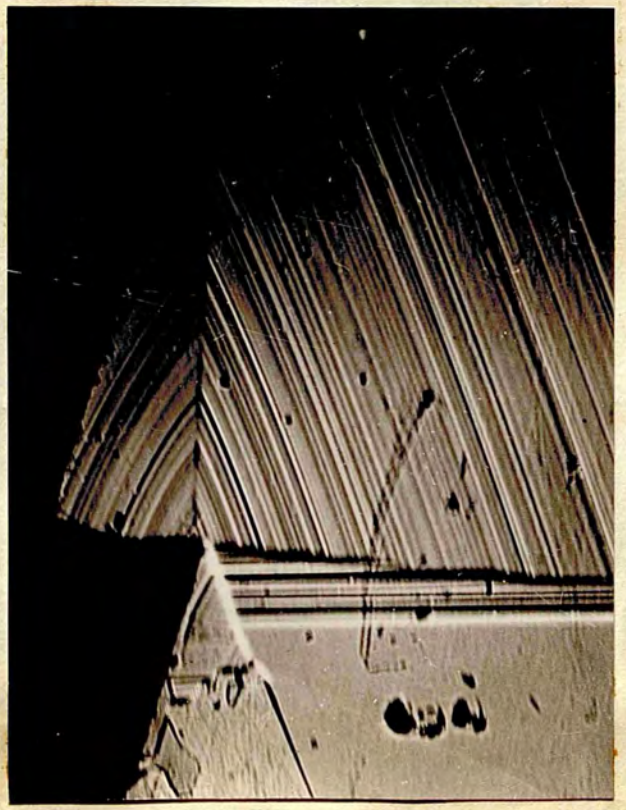

Fig. 72.

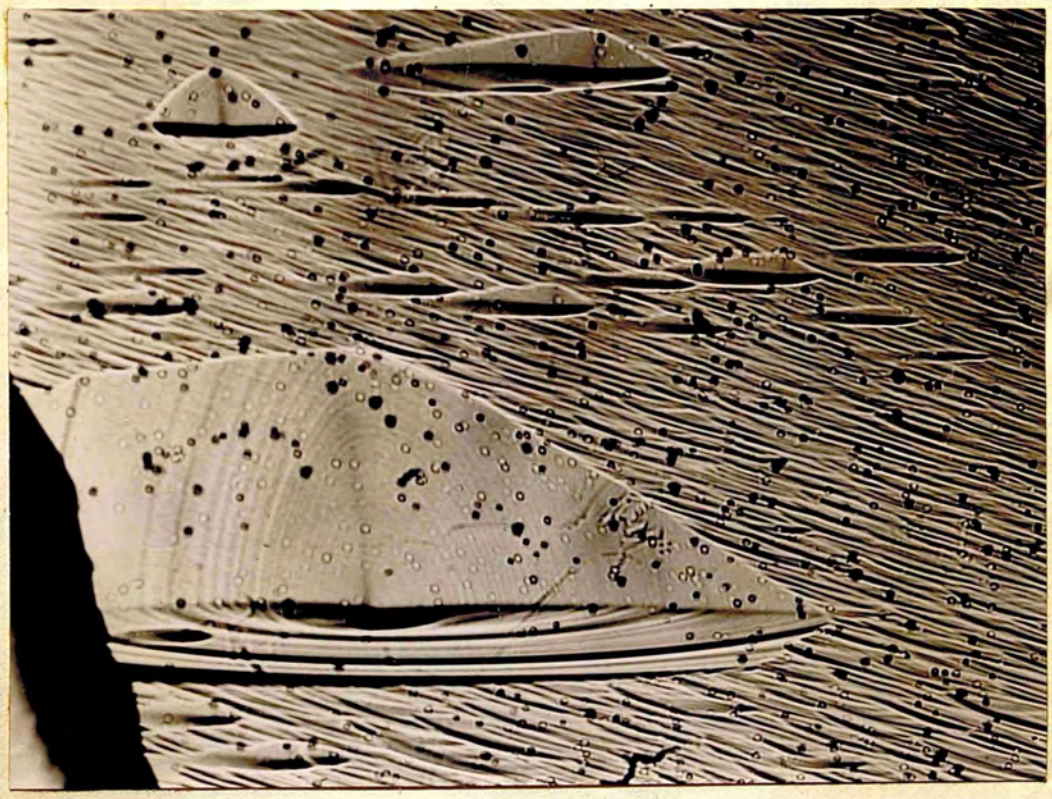

Fig. 75.

FIGURE 78 (a)

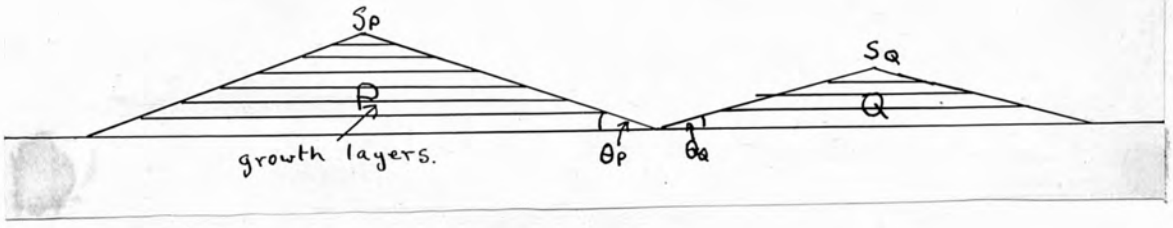

FIGURE 78. (b)

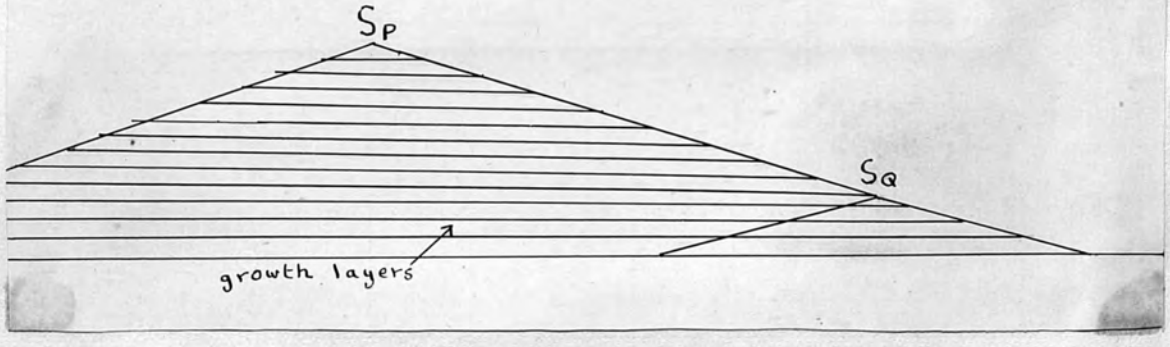

Fig. 79.

Fig. 80.

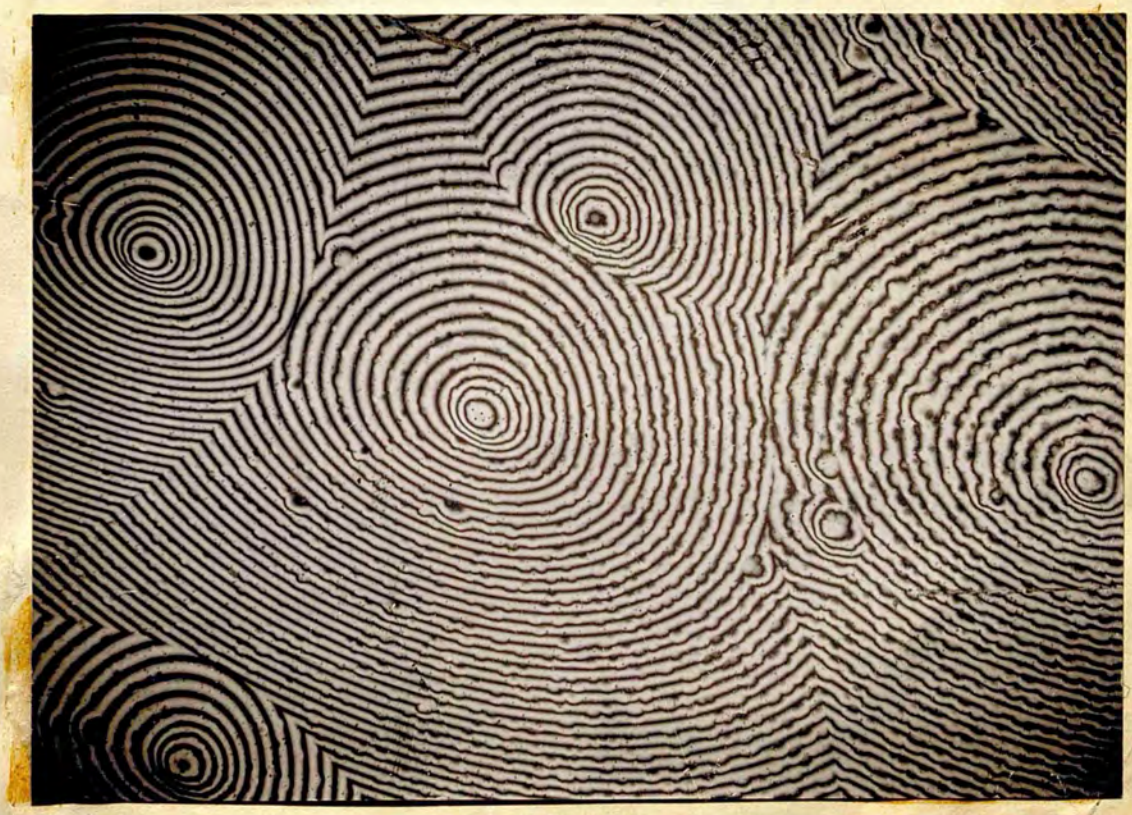

Fig. 81.

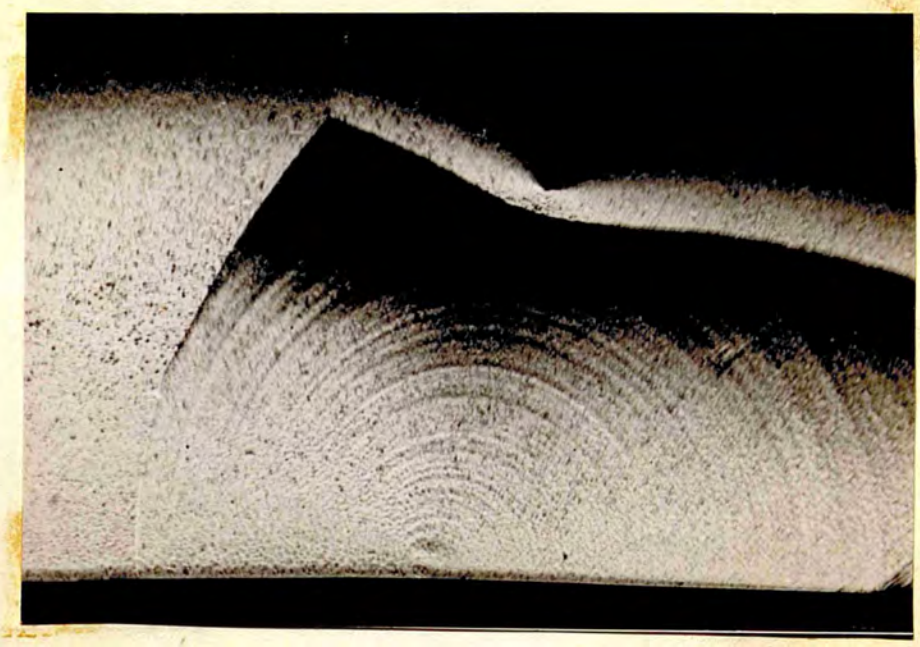

Fig. 82.

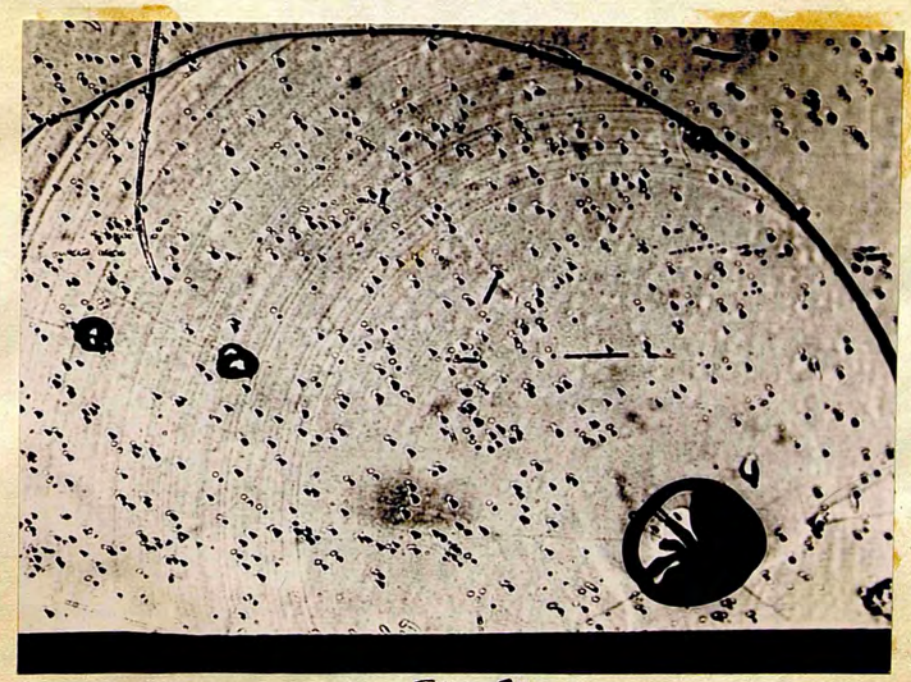

Fig. 83.

Fig. 84.

Fig. 85.

Fig. 86.

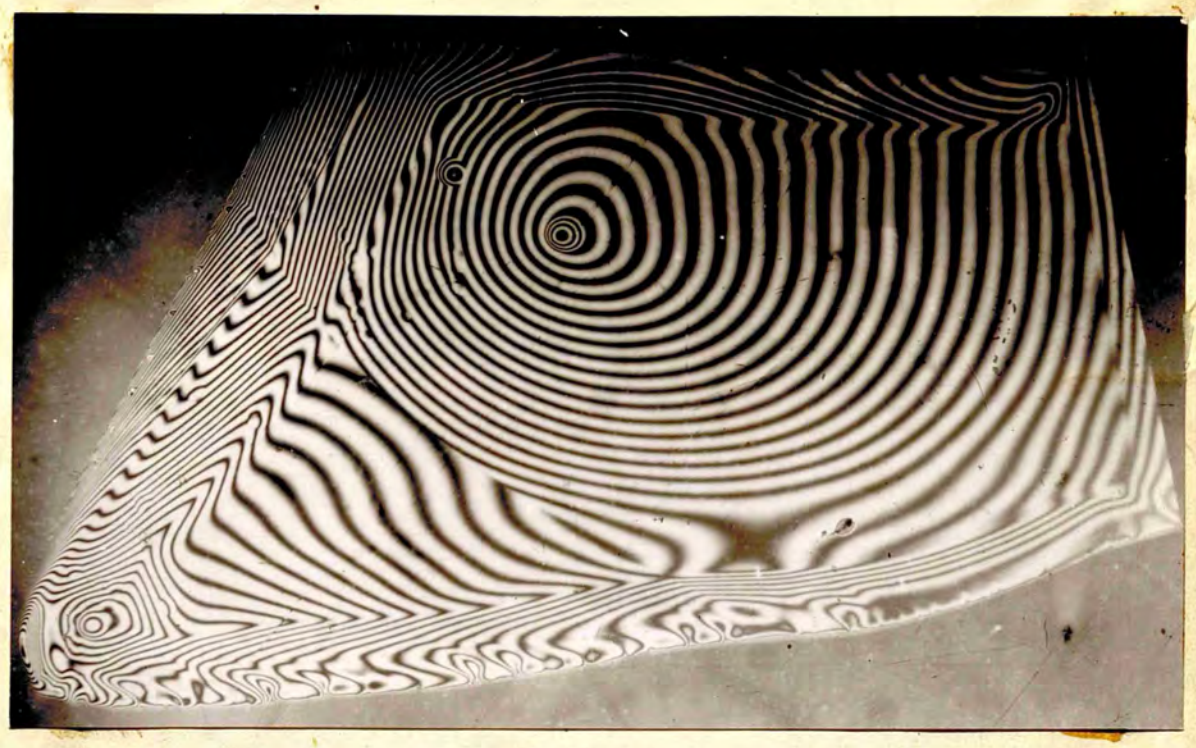

Fig. 87.

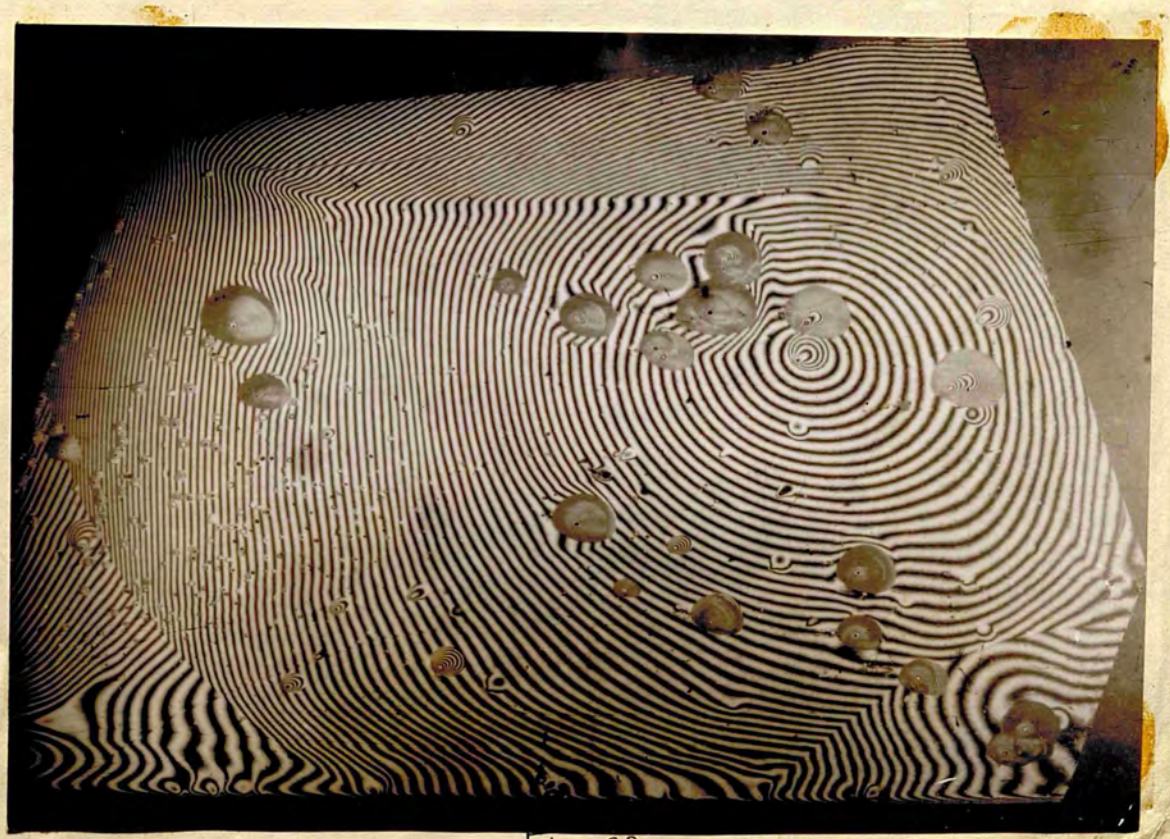

Fig. 88.

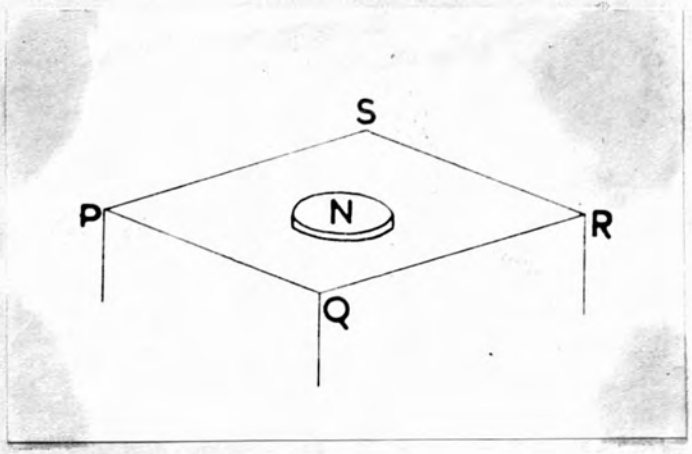

Fig. 1.

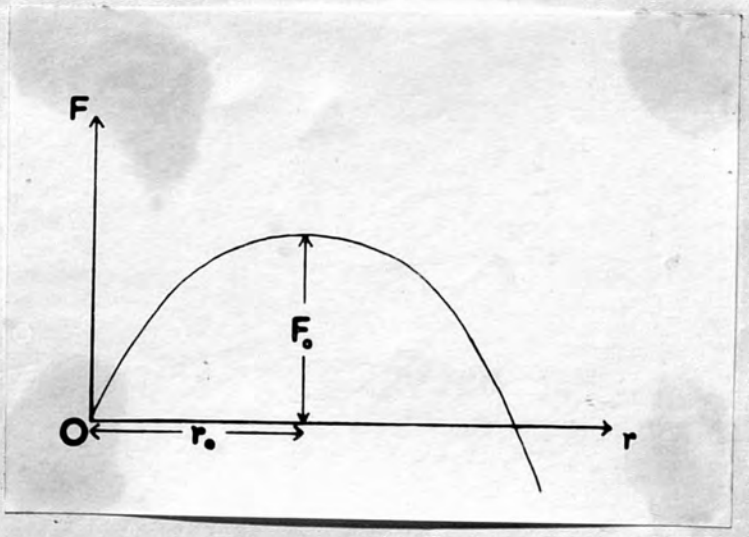

Fig. 2.